NOVEL SYNCHROTRON-BASED ANALYSES OF METAL PATHOLOGY IN FRIEDREICH'S ATAXIA

A Thesis Submitted to the College of
Graduate Studies and Research
in Partial Fulfillment of the Requirements for

the

Degree of Doctor of Philosophy

in the

Department of Anatomy and Cell Biology
University of Saskatchewan
Saskatoon

By

Bogdan Florin Gh. Popescu

Permission to Use

In presenting this thesis in partial fulfillment of the requirements for a Postgraduate degree from the University of Saskatchewan, I agree that the Libraries of this University may make it freely available for inspection. I further agree that permission for copying of this thesis in any manner, in whole or in part, for scholarly purposes may be granted by the professor or professors who supervised my thesis work or, in their absence, by the Head of the Department or the Dean of the College in which my thesis work was done. It is understood that any copying or publication or use of this thesis or parts thereof for financial gain shall not be allowed without my written permission. It is also understood that due recognition shall be given to me and to the University of Saskatchewan in any scholarly use which may be made of any material in my thesis.

Requests for permission to copy or to make other use of material in this thesis in whole or part should be addressed to:

Head of the Department of Anatomy and Cell Biology
107 Wiggins Road
University of Saskatchewan
Health Sciences Bld.
Saskatoon, Saskatchewan S7N 5E5

Abstract

Friedreich's ataxia (FRDA) is a progressive spinocerebellar ataxia (SCA) inherited as an autosomal recessive trait. The neurodegeneration, cardiomyopathy, diabetes mellitus and skeletal deformities characteristic to FRDA result from a deficiency in the mitochondrial protein frataxin. Frataxin chaperones iron to heme and iron-sulfur clusters and its deficiency causes mitochondrial iron accumulation and oxidative stress.

To address the effect of frataxin deficiency on mitochondrial iron chemistry, mitochondria were isolated from FRDA and control fibroblasts. X-ray absorption spectroscopy showed that ferrihydrite was the predominant form of iron in both. Near edge analysis showed that the ferrihydrite in the FRDA mitochondria resembled the highly organized ferrihydrite of ferritin. Western blotting confirmed that FRDA mitochondria had 3-fold more holoferritin containing stainable iron. I conclude that mitochondria from FRDA fibroblasts mineralize excess iron as ferrihydrite within mitochondrial ferritin.

To address how cellular iron dysregulation affected metal distribution in brain and spinal cord, a new synchrotron imaging technique, rapid-scanning x-ray fluorescence (RS-XRF) was employed and validated. Brain structures were readily identified by their unique metal content and distribution. This showed that RS-XRF could be used to reveal metal pathologies associated with diseases of metal metabolism such as FRDA. Since human FRDA tissues were not available for a detailed study, RS-XRF was employed to study the distribution of metals in normal cerebellum, a major site of FRDA-associated neurodegeneration, and to localize and quantify metals in the brain and spinal cord from a patient with a SCA of unknown aetiology. The motivation for this work is the prospect of future systematic studies on metal pathology in neurodegenerative diseases with direct application to FRDA. Novel findings arising from this work were the metal segmentation of the dentate nucleus, the high copper content of the olivary region and the different metal content of lesions at different stages of neurodegeneration. My results suggest that not only iron, but also copper and zinc may play a role in the physiopathology of neurodegeneration. Therefore, all three metals should be investigated in FRDA and other SCA of both known and unknown aetiologies to identify possible new therapeutic targets.

Acknowledgements

I would like to first and foremost thank my supervisor, Dr. Helen Nichol for taking me on as her graduate student, for all the help, guidance, encouragement and support she provided during my degree. You have been a great mentor and I could not have had a better supervisor. I will be forever grateful for all the opportunities you have given me, opportunities that I have never imagined.

To the members of my advisory committee, Dr. Dean Chapman, Dr. Troy Harkness, Dr. Patrick Krone and Dr. Vikram Misra, thank you for your encouragement, guidance, criticism and help.

To Dr. Graham George, Dr. Ingrid Pickering and Dr. Roger Prince, thank you for your advice and patience while training me in synchrotron data collection and analysis. It has been my honour to work with such prominent scientitists.

To Akela Hanson, Richard McCrea, Ni Ao, Stephanie Roach and Justin Tse, I could not have had better colleagues. To Darren Nesbitt and Karen Yuen, thank you for all your help.

I am indebted to Dr. Uwe Bergmann and Martin George of the SSRL for support with RS-XRF technology, to Dr. Sam Webb and Dr. Konstantin Ignatyev for the beamline support at SSRL, to Dr. Grazia Isaya (Mayo Clinic) for the human frataxin protein and the antibodies, to Dr. Paolo Arosio (University of Milan) for the recombinant mitochondrial ferritin and to Dr. Christopher Robinson (Department of Pathology and Laboratory Medicine, University of Saskatchewan) for the help with the α synuclein immunohistochemistry and the silver staining.

To my father…

TABLE OF CONTENTS

LIST OF TABLES

LIST OF FIGURES

LIST OF ABBREVIATIONS

º	degree
ATP	adenosine triphosphate
C	Celsius
CCS	cosmic calf serum
cm^2	square cenimeter
CO_2	carbon dioxide
CV	cresyl violet
DMSO	dimethyl sulfoxide
DNA	deoxyribonucleic acid
eV	electron volt
ED	embryonic day
EDTA	ethylenediaminetetraacetic acid
FAD	flavin adenine dinucleotide
FRDA	Friedreich's ataxia
GAA	guanosine adenosine adenosine
GeV	gigaelectron volt
H	hematoxylin
H_2O_2	hydrogen peroxide
HDACI	histone deacetylase inhibitors
HE	hematoxylin and eosin
HMF	'heavy' mitochondrial fraction
i-fxn	frataxin intermediate
IRE	iron regulatory element
IRP	iron regulatory protein
ISC	iron sulfur cluster
IscU	scaffold protein
IscC	cysteine desulfurase
kDa	kilodalton

keV	kiloelectron volt
LAMP	lysosomal associated membrane protein
LFB	luxol fast blue
M	molar
m-fxn	mature frataxin
MDa	megadalton
MEM	Eagle's minimal essential medium
ml	milliliter
mm	millimetre
mM	millimolar
mRNA	messenger ribonucleic acid
ms	millisecond
mtDNA	mitochondrial deoxyribonucleic acid
MtFt	mitochondrial ferritin
NADH	reduced nicotinamide adenine dinucleotide
NFR	nuclear fast red
p-fxn	frataxin precursor
PAGE	polyacrylamide gel electrophoresis
PAS	periodic acid-Schiff
PB	phosphate buffer
PBSS	Puck's balanced salt solution
PD	Parkinson's disease
PMI	post mortem interval collection time
PTA	phosphotungstic acid
R·R·Y	purine·purine·pyrimidine
ROS	reactive oxygen species
RPM	rotations per minute
RS-XRF	rapid scanning X-ray fluorescence
s	second
SCA	spinocerebellar ataxia
SDS	sodium dodecyl sulphate

SOD	superoxide dismutase
SSRL	Stanford Synchrotron Radiation Lightsource
TBS	Tris-buffered saline
TEM	transmission electron microscopy
TfR	transferrin receptor
TIBC	total iron binding capacity
TTC	thymidine thymidine cytosine
UTR	untranslated region
V	volt
WT	wild type
XAS	X-ray absorption spectroscopy
XRF	X-ray fluorescence
Yfh1p	yeast frataxin orthologue
yfh1Δ	frataxin knockout yeast
µg	microgram
µl	microliter
µm	micrometer

CHAPTER I

General Introduction, Hypothesis and Objectives

1.1 History

In 1863, Nikolaus Friedreich, a German doctor, described a nonsyphilitic hereditary type of locomotor ataxia occurring as a familial disease in young patients. Locomotor ataxias had already been described by Duchenne as the prominent feature of tabes dorsalis (degeneration of the posterior columns of the spinal cord associated with neurosyphilis). Thus, the separation of Friedreich's ataxia from the general group of locomotor ataxias was first greeted with skepticism. While Charcot considered that Friedreich's patients suffered from multiple sclerosis, Gowers was the first neurologist to accept the new disease entity (Greenfield 1954; Berciano et al. 2000; Pearce 2004). Two years after Friedreich's death, Charcot himself demonstrated that a young man suffering from ataxia did not have syphilis and recognized hereditary ataxia. Following that, Duchenne affirmed the existence of the new disease and in 1882, Brousse attached Friedreich's name to the new entity (Greenfield 1954; Berciano et al. 2000; Pearce 2004).

1.2 Clinical and Pathological Features

Friedreich's ataxia (FRDA) is a progressive neurodegenerative disease inherited as an autosomal recessive trait that affects 1:50,000 Caucasians (Campuzano et al. 1996). This is a typical example of a progressive spinocerebellar ataxia and is characterized by neurodegeneration, cardiomyopathy, diabetes mellitus and skeletal deformities.

1.2.1 Neuroanatomy Overview

Before reviewing the clinical and pathological features characteristic to FRDA, a short overview of the neuroanatomy and especially of the major structures and pathways affected in FRDA is appropriate.

The somatosensory information (bodily sensations of pain, temperature, touch, vibration and limb and joint position sense, also called proprioception) travels from peripheral receptors to the spinal cord and brain through sensory nerves. The cell bodies of sensory neurons are located in the dorsal root ganglion and have one process that brings sensory information from the periphery and a second process that conveys this information to the central nervous system through the dorsal nerve roots. The proprioception, vibration and fine, discriminative touch sensory modalities are carried

through large diameter, myelinated axons. They enter the dorsal columns of the white matter of the spinal cord and ascend towards the medulla forming the dorsal column – medial lemniscal pathway. The somatosensation from the lower limbs and lower half of the body travels medially in the posterior columns forming the gracile fascicle. The somatic sensation from the upper limbs and upper half of the body travels laterally in the dorsal columns and form the cuneate fasciculus. The neurons in the dorsal root ganglia that send axons in the gracile and cuneate fasciculi (also named first order neurons) synapse onto second order neurons in the nucleus gracilis and nucleus cuneatus, respectively. Both these nuclei are located in the medulla. The axons of the second order neurons decussate (cross-over from one side of the medulla to the other side) and form the medial lemniscus that carries the information to the third order neurons located in the thalamus. The thalamic neurons then project to neurons of the primary somatosensory cortex for the conscious perception of the proprioception, vibration and touch sensations (Blumenfeld 2002).

Rather than continuing their ascend, some fibers of the posterior columns enter the gray matter of the spinal cord and synapse onto neurons located in the dorsal nucleus of Clarke. Fibers arising from this nucleus ascend in the lateral columns of the spinal cord white matter where they form the spinocerebellar tracts. These pathways travel through the brainstem and end in the cerebellar cortex. Thus, the spinocerebellar tracts carry the proprioception, vibration and touch sensations to the cerebellum for their unconscious perception important in coordination of muscular activity, facilitation of movement, motor planning and motor learning (Blumenfeld 2002).

Outputs from the cerebellum are carried by the Purkinje cells of the cerebellar cortex to the deep cerebellar nuclei (including the dentate nucleus) and vestibular nuclei (located in the brainstem). Through its wide spread projections not only to the deep cerebellar nuclei and vestibular nuclei, but also to the red nucleus, thalamus and primary motor cortex, the cerebellum is involved in motor coordination, planning and learning, balance and eye movements (Blumenfeld 2002).

The somatic motor pathways carry motor commands issued by the brain to muscles. This results in the execution of voluntary movements. The primary motor cortex of the cerebrum issues these motor commands. Thus, it is responsible for the execution of

movements, direction of movements and force of muscle contraction. Axons of cortical neurons that carry the motor information descend through the subcortical white matter and internal capsule, midbrain, pons and arrive in the medullary pyramids. The majority of the fibers decussates and continues the descent in the contralateral lateral columns of the white matter forming the lateral corticospinal tract. The rest of the fibers descend in the ipsilateral anterior columns of the spinal cord without decussating and form the anterior corticospinal tract. Both the lateral and the anterior corticospinal tracts synapse onto motor neurons located in the anterior horns of the gray matter of the spinal cord. Axons of these neurons exit the spinal cord through the ventral roots, form the motor nerves and deliver the somatic motor commands to muscles. The lateral corticospinal tract controls the muscles of the contralateral limb, while the anterior corticospinal tract controls the bilateral axial and girdle muscles (Blumenfeld 2002).

Thus, the primary motor cortex is responsible for the voluntary execution of movements, the cerebellum coordinates complex motor patterns and stores memory of learned movement patterns and the basal ganglia (caudate, putamen, globus pallidus, substantia nigra) modulate and adjust motor patterns at the subconscious level.

1.2.2 Clinical and Pathological Features of FRDA

FRDA typically presents before 25 years of age with progressive ataxia of gait and limbs, dysarthria, loss of deep tendon reflexes, extensor plantar responses, muscle wasting and loss of sensation, especially of vibration and joint position sense (Greenfield 1954; Geoffroy et al. 1976; Harding 1981; Durr et al. 1996). As the disease progresses, there may be horizontal nystagmus (involunatry rhythmic oscillations of the eyeballs, characterized by a smooth pursuit in one direction and a fast movement in the opposite direction), saccadic-pursuit eye movements (rapid correction eye movements to redirect the line of site during smooth pursuit of an object), difficulty with swallowing and breathing as well as cardiomyopathy, diabetes mellitus and skeletal deformities (Greenfield 1954; Geoffroy et al. 1976; Harding 1981; Durr et al. 1996). Some patients can develop optic nerve atrophy and hearing loss (Greenfield 1954; Geoffroy et al. 1976; Harding 1981; Durr et al. 1996). In contrast to the typical early onset form, late onset FRDA progresses more slowly and tendon reflexes are often retained (De Michele et al.

1994; Durr et al. 1996; Coppola et al. 1999). Magnetic resonance imaging in patients with typical and late onset FRDA reveals spinal cord atrophy that is sometimes associated with atrophy of the brainstem and cerebellum (Wessel et al. 1989; Klockgether et al. 1991; Wullner et al. 1993; Mascalchi et al. 1994; De Michele et al. 1995; Bhidayasiri et al. 2005).

The neurological features of FRDA are explained by the neuropathological findings characteristic to this disease. The peripheral sensory nerves are severely affected with loss of large myelinated axons and loss of neurons in the dorsal root ganglia (Greenfield 1954; Hughes et al. 1968; Oppenheimer 1979; Lamarche et al. 1984). The spinal cord shows neuronal loss in the nucleus dorsalis of Clark and loss of myelinated fibers in the posterior columns with the gracile fasciculus almost always more affected than the cuneate fasciculus (Greenfield 1954; Oppenheimer 1979; Lamarche et al. 1984). There is also degeneration of the corticospinal lateral and spinocerebellar tracts and, less frequently, of the corticospinal anterior tracts (Greenfield 1954; Oppenheimer 1979; Lamarche et al. 1984). Neurodegenerative changes seen in the dorsal columns and pyramidal tracts of the spinal cord can be traced through the medulla: neuronal loss in the gracile and cuneate nuclei and axonal degeneration in the pyramids (Greenfield 1954; Oppenheimer 1979; Lamarche et al. 1984). The loss of large, myelinated axons in the spinocerebellar pathways can also be traced through the inferior and superior cerebellar peduncles to the cerebellar Purkinje cells. In FRDA, these neurons degenerate, especially in the vermis of the cerebellum (Greenfield 1954; Oppenheimer 1979; Lamarche et al. 1984). Severe neuronal loss is also seen in the dentate nucleus (Oppenheimer 1979; Lamarche et al. 1984; Koeppen et al. 2007). Some cases also present with neuronal loss in the optic nerves and tracts, subthalamic nuclei, thalamus and globus pallidus (Oppenheimer 1979; Lamarche et al. 1984).

Hypertrophic cardiomyopathy (thickening of the ventricular septum and walls of the left ventricle) leads to arrhythmias and heart failure, which are the most common cause of death for these patients (Greenfield 1954; Hewer 1968; Sanchez-Casis et al. 1976; Lamarche et al. 1980; Harding 1981; Durr et al. 1996). The pathology of the cardiac degeneration consists of interstitial fibrosis, hypertrophy and degeneration of cardiac cells, muscle necrosis and intracellular accumulation of lipofuscin, iron and

calcium deposits (Greenfield 1954; Hewer 1968; Sanchez-Casis et al. 1976; Lamarche et al. 1980). Diabetes mellitus is seen in 10% of the patients and is associated with a decrease in the number of pancreatic β cells (Hewer 1968; Hewer and Robinson 1968; Harding 1981; Durr et al. 1996). Skeletal deformities include pes cavus (hammer toes) and kyphoscoliosis (abnormal lateral and posterior curvature of the vertebral column) (Harding 1981; Durr et al. 1996).

1.3 Human Frataxin

The frataxin gene (FRDA gene) has been localized on chromosome 9q13 (Chamberlain et al. 1988; Fujita et al. 1989; Campuzano et al. 1996). It is composed of 7 exons (1, 2, 3, 4, 5a, 5b, and 6). The major transcript (exons 1 to 5a) is a 1.3 kb mRNA that encodes a 210 amino acid protein called frataxin (Campuzano et al. 1996).

Frataxin mRNA expression is very high in heart, intermediate in liver, skeletal muscle and pancreas, and low in other tissues, including whole brain. In different parts of the Central Nervous System (CNS), frataxin mRNA expression is the highest in the spinal cord, with less expression in cerebellum and very little in cerebral cortex (Campuzano et al. 1996).

The amino acid sequence of frataxin predicts a small protein, without any transmembrane domain and with a cleavable signal peptide formed by the 22 N-terminal amino acids (Campuzano et al. 1996). Segmentation analysis has shown that the N-terminal amino acids form a non-globular domain with the typical features of a mitochondrial targeting peptide: α-helicity, abundant Arg, Ser and Leu residues, rare Glu and Asp residues (Gibson et al. 1996). Co-localization of frataxin with cytochrome-c oxidase (Campuzano et al. 1997; Koutnikova et al. 1997), the intracellular localization of frataxin-GFP fusion protein (Babcock et al. 1997; Priller et al. 1997), immunocytofluorescence and immunoelectron microscopy (Campuzano et al. 1997) have shown that frataxin is, indeed, a mitochondrial protein. Furthermore, the first 20 amino acids are sufficient to target frataxin N-terminal portion-GFP fusion protein to the mitochondria and mutation of the two Arg residues in the consensus of the mitochondrial signal peptide results in a diffuse cytoplasmic and nuclear localization of frataxin (Campuzano et al. 1997).

The N-terminal mitochondrial targeting sequence is proteolytically removed in two sequential steps by a zinc metallopeptidase called Mitochondrial Processing Peptidase (MPP). In the first step, MPP cleaves the 21 kDa frataxin precursor (p-fxn) between residues 41-42 yielding an 18.8 kDa intermediate (i-fxn). The second cleavage occurs between residues 55-56 and produces the 17 kDa mature frataxin (m-fxn). M-fxn corresponds to the endogenous frataxin found in human tissues (Branda et al. 1999; Cavadini et al. 2000).

It has been suggested that m-fxn is not only confined to the mitochondria but that an extramitochondrial pool of frataxin exists (Acquaviva et al. 2005; Condo et al. 2006). This cytosolic m-fxn has been demonstrated in several cell lines: human embryonic kidney HEK-293, cervical carcinoma HeLa, T-cell leukemia Jurkat, bone marrow neuroblastoma SH-SY5Y (Condo et al. 2006) and human colon carcinoma Caco-2 (Acquaviva et al. 2005). It appears that the extramitochondrial frataxin is able to functionally substitute for the mitochondrial frataxin in promoting cell survival, protection against reactive oxygen species (ROS) and apoptosis (Condo et al. 2006) and is involved in extramitochondrial ISC biosynthesis (Acquaviva et al. 2005). However studies in normal adult mouse tissues have shown that frataxin is strictly localized to mitochondria and have excluded the presence of a cytosolic pool of frataxin (Martelli et al. 2007).

1.4 Human Frataxin and FRDA

FRDA is the consequence of frataxin deficiency. FRDA patients have extremely low, sometimes even undetectable frataxin mRNA levels (Campuzano et al. 1996; Cossee et al. 1997) and show a severe reduction in frataxin expression ranging from 4 to 29% of normal levels (Campuzano et al. 1997). Frataxin deficiency is the result of a GAA trinucleotide repeat in the first intron of the gene (Campuzano et al. 1996; Durr et al. 1996; Pandolfo 1998). Repeats in normal genes contain between 7 and 40 triplets, while FRDA genes have over 66 triplets and they can go as high as 1700 GAA repeats. Smaller expansions allow for a higher level of residual gene expression (Campuzano et al. 1997). Most patients (95-98%) are homozygous for the expanded alleles (Campuzano et al. 1996; Durr et al. 1996) and the GAA repeats adopt a triple helical structure

(GAA·GAA·TTC) under physiological conditions. When the triplet sequence is long enough, two purine·purine·pyrimidine (R·R·Y) triplexes associate and form a novel stable non-B DNA structure called "sticky DNA". This structure inhibits transcription of the FRDA gene by sequestration of the RNA polymerases (Bidichandani et al. 1998; Ohshima et al. 1998; Sakamoto et al. 1999; Sakamoto et al. 2001), formation of a persistent RNA·DNA hybrid (Grabczyk et al. 2007) and/or aberrant pre-mRNA processing (Baralle et al. 2008). These properties are specific to GAA repeats since GGA interruptions inserted into long GAA repeats abolish sticky DNA formation and alleviate transcription repression possibly by introducing base mismatches into the R·R·Y triplex (Sakamoto et al. 2001).

Another model suggests that GAA·TTC repeats induce formation of heterochromatin through hypermethylation of DNA and reduced histone acetylation that could disrupt the binding of transcription factors and reduce the frataxin message (El-Osta and Wolffe 2000; Elgin and Grewal 2003; Saveliev et al. 2003; Herman et al. 2006; Gottesfeld 2007; Greene et al. 2007; Al-Mahdawi et al. 2008; Castaldo et al. 2008). Histone deacetylase inhibitors (HDACI) increase both frataxin mRNA and protein expression (Herman et al. 2006). Erythropoietin increases frataxin expression in FRDA lymphoblasts (Sturm et al. 2005), fibroblasts (Acquaviva et al. 2008) and patients (Boesch et al. 2007) acting on the frataxin protein at the post-translational level, but the exact mechanism is not known (Acquaviva et al. 2008).

There is a direct correlation between the number of GAA repeats, more precisely the number of repeats on the small allele, and age of onset, rate of disease progression and other disease manifestations. Earlier onset FRDA is associated with large repeats on the small allele. The frequency of some clinical signs (cardiomyopathy, skeletal deformities and extensor plantar response) increases with the size of GAA expansion, while cerebellar ataxia is associated with both the number of GAA repeats and the duration of the disease (Durr et al. 1996; Filla et al. 1996; Montermini et al. 1997). The relationship between the number of GAA repeats and the level of frataxin expression, and ultimately the severity of the disease, is sustained by the finding that there are no biologically relevant sequence differences in the promoter or 3′UTR (responsible for increasing mRNA stability) between the milder and classic forms of FRDA (Greene et al.

2005). There is also a direct correlation between the methylation of particular CpG sites on the FRDA gene and GAA expansion size and an inverse correlation between the degree of methylation and age of onset (Castaldo et al. 2008).

The remaining 2-5% of FRDA patients are compound heterozygotes for a GAA expansion on one allele and a point mutation on the other (Durr et al. 1996; Pandolfo 1998). Patients with truncated or missense mutations in the C-terminal half of mature frataxin have a phenotype similar to that of patients homozygous for the GAA expansion, while missense mutations located in the N-terminal half of the protein cause an atypical and milder clinical presentation (mild or no cerebellar ataxia, slow disease progression, retained or brisk tendon reflexes, absence of dysarthria) (Campuzano et al. 1996; Cossee et al. 1999).

Molecular and biochemical analyses of tissues from patients with FRDA have shown a deficient activity of the iron-sulfur cluster (ISC) containing subunits of mitochondrial respiratory complexes I, II and III, deficient activity of mitochondrial and cytosolic aconitase (also ISC), reduced levels of mitochondrial DNA (mtDNA) and increased iron regulatory protein 1 (IRP1) activity (Rotig et al. 1997; Bradley et al. 2000; Lobmayr et al. 2005). The levels of ATP synthesized in mitochondria are below normal and inversely proportional to the number of GAA repeats (Lodi et al. 1999). Despite normal ferrochelatase activity, free erythrocyte protoporphyrin is elevated (Morgan et al. 1979; Schoenfeld et al. 2005) and levels of mitochondrial heme *a* and heme *c* are reduced (Schoenfeld et al. 2005) suggesting a defect between protoporphyrin IX and heme *a* (Schoenfeld et al. 2005). Activity of cytochrome oxidase and cytochrome *c* are decreased presumably because a defect in the insertion of heme *a* and heme *c* into cytochrome oxidase and cytochrome *c*, respectively (Schoenfeld et al. 2005). Iron deposits have been noted in myocardial cells (Sanchez-Casis et al. 1976; Lamarche et al. 1980; Bradley et al. 2000; Michael et al. 2006) and in the dentate nucleus (Waldvogel et al. 1999; Boddaert et al. 2007) in FRDA patients, FRDA fibroblast cultures (Delatycki et al. 1999), spleen and liver (Bradley et al. 2000), although some of these findings have been challenged lately (Koeppen et al. 2007). High levels of circulating transferrin receptor (TfR) (Wilson et al. 2000) result from a redistribution of iron from the cytosol to the mitochondrial compartment. Finally, several markers of oxidative stress have been observed including

increased plasma levels of malondialdehyde (a lipid peroxidation product) (Emond et al. 2000), reduced blood glutathione (Piemonte et al. 2001; Tozzi et al. 2002) and increased urinary levels of 8-hydroxy-2′-deoxyguanosine (a marker of oxidative DNA damage) (Schulz et al. 2000). These complete the panel of biochemical changes.

Increased expression of TfR (Wilson et al. 2000), increased levels of IRP1 (Lobmayr et al. 2005), iron regulatory protein 2 (IRP2) (Li et al. 2008) and increased iron responsive element (IRE)-binding activity of IRP1 and IRP2 (Li et al. 2008) found in FRDA fibroblasts and lymphoblasts are evidence of cytosolic iron depletion and show that the intramitochondrial iron accumulation occurs at the expense of cytosolic iron (Li et al. 2008). The following model of how cytosolic iron deficiency decreases expression of frataxin in FRDA has been proposed: frataxin deficiency impairs the mitochondrial ISC assembly leading to mitochondrial iron overload. Excess mitochondrial uptake and sequestration causes depletion of cytosolic iron which can further lower the expression of frataxin by decreasing its transcription (Li et al. 2008).

1.5 Roles of Frataxin

All these findings suggest that frataxin acts both as an iron chaperone for heme synthesis and biosynthesis of ISC containing proteins and protects against oxidative damage.

It is still a debate if intramitochondrial iron accumulation is a primary event leading to ROS production and cellular damage (Babcock et al. 1997; Wong et al. 1999), or if it is a secondary event due to a deficit of ISC synthesis (Lill and Muhlenhoff 2008). Increased expression of TfR (Wilson et al. 2000) and increased levels of IRP1 (Lobmayr et al. 2005), IRP2 (Li et al. 2008) and increased IRE-binding activity of IRP1 and IRP2 (Li et al. 2008) found in FRDA fibroblasts and lymphoblasts are evidence of cytosolic iron depletion and show that the intramitochondrial iron accumulation occurs at the expense of cytosolic iron (Li et al. 2008). It has been proposed that high levels of ferrous iron (Fe^{2+}) in mitochondria could promote ROS formation through the Fenton reaction and, subsequently, protein degradation, lipid peroxidation and mtDNA damage (Emond et al. 2000; Schulz et al. 2000; Piemonte et al. 2001) and reduce frataxin expression (Li et al. 2008). This could explain the oxidative damage markers found in FRDA patients and

deficiencies of aconitase and respiratory complexes I, II and III leading to decreased mitochondrial respiration and oxidative phosphorylation (Rotig et al. 1997; Bradley et al. 2000). My work has elucidated the chemical forms of iron found in mitochondria (Popescu et al. 2007a) and the implications of this work are dealt with in Chapter II.

1.5.1 ISC and Heme Synthesis

IscU scaffold protein provides a platform for assembly of [2Fe-2S] or [4Fe-4S] centers prior to delivery to an apo target protein (Yabe et al. 2004; Johnson et al. 2005; Chandramouli et al. 2007; Rouault and Tong 2008). The intermediate [2Fe-2S] or [4Fe-4S] IscU-bound cluster is formed by delivery of iron and sulfur to the apo IscU. The sulfur donor is IscS (cysteine desulfurase) that catalyses the desulfuration of cysteine producing sulfide (Rouault and Tong 2008). The identity of the iron donor has not yet been fully established, but there is good evidence that frataxin accomplishes this function (Bencze et al. 2006; Rouault and Tong 2008). *In vitro* experiments have shown that frataxin forms a complex with IscU and iron is required to cross-link the two proteins and/or stabilize the structure of frataxin that is recognized by IscU (Yoon and Cowan 2003). In human heart, the monomeric and oligomeric forms of frataxin bind in a stable manner to IscU and IscU/IscS with an IscU: frataxin stoichiometry of 1:3 (O'Neill et al. 2005).

1.5.1.1 <u>The Role of Iron Regulatory Proteins</u>

Cellular iron uptake and storage are exquisitely regulated through the action of the two iron regulatory proteins, IRP1 and IRP2. Although both IRP1 and IRP2 can bind to a canonical mRNA element called IRE found on the mRNAs of several iron-regulated proteins (i.e TfR, ferritin, mitochondrial aconitase, ferroportin), they act by slightly different mechanisms. IRP1 is a bifunctional protein. The incorporation of a new iron into and the formation of a [4Fe-4S] cluster transform the IRP1 from an mRNA binding protein into cytosolic aconitase and enable it to catalyze the conversion of citrate to isocitrate. Thus, cytosolic aconitase and IRP1 are actually the same protein that cycles between a [4Fe-4S] form that predominates under high iron conditions and a [3Fe-4S] form that predominates when iron is low. In FRDA increased expression of IRP1 and

IRP2 leads to increased iron uptake due to increased expression of TfR and to reduced synthesis of the iron storage protein, ferritin. Normally in iron replete states, IRP1 assembles an ISC and loses the ability to bind to the IRE while IRP2 degrades. Reduced binding of IRPs to IREs decreases the stability of the mRNA encoding TfR leading to reduced expression of TfR at the cell membrane and also increases translation of ferritin for iron storage (Klausner and Rouault 1993; O'Halloran 1993; Ponka 1999).

1.5.1.2 Cytosolic ISC Proteins

The findings (Rotig et al. 1997; Bradley et al. 2000; Lobmayr et al. 2005) that in FRDA, cytosolic aconitase activity is deficient, but its IRE binding activity is increased indicate that aconitase/IRP1 is not damaged due to oxidative stress but rather the deficiency of cytosolic aconitase activity could be due to an inability to incorporate iron into the ISC. There is strong evidence that frataxin is an iron chaperone to the Fe-S cluster pathway and that mitochondrial ISC assembly machinery is essential for cytosolic ISC biogenesis (Seznec et al. 2005).

1.5.1.3 Mitochondrial ISC Proteins

Mitochondrial ISC proteins fulfill a variety of functions from metabolic reactions and enzyme catalysis to electron transfer and regulatory processes. Several of these ISC proteins are important for FRDA: mitochondrial aconitase (citric acid cycle), ferredoxin (maturation of ISC proteins and biosynthesis of heme), ferrochelatase (biosynthesis of heme), NADH ubiquinone oxidoreductase of complex I, succinate dehydrogenase of complex II and ubiquinone cytochrome c oxidoreductase of complex III (the last three involved in electron transport chain) reviewed in (Lill and Muhlenhoff 2005). Among these, mitochondrial aconitase (Rotig et al. 1997; Bradley et al. 2000; Lobmayr et al. 2005) and ferrochelatase (Morgan et al. 1979; Schoenfeld et al. 2005) have been found consistently downregulated in FRDA.

Mitochondrial aconitase is a [4Fe-4S] cluster containing protein whose main function is to catalyze the conversion of citrate to isocitrate in the Krebs cycle. It has been recently shown that mitochondrial aconitase has a dual function. The oxidized form

of this ISC associates with mtDNA to provide stability during oxidative stress reviewed in (Shadel 2005).

Frataxin has also been shown to be a high affinity partner for ferrochelatase, capable of both iron delivery to ferrochelatase and mediating the final step in mitochondrial heme biosynthesis (Yoon and Cowan 2004). Human frataxin and ferrochelatase seem to interact only in the presence of iron (Bencze et al. 2007).

1.5.2 Assembly and Functions of Frataxin

1.5.2.1 Iron Storage Protein

When expressed in *Escherichia Coli* and *Saccharomyces cerevisiae*, m-fxn (residues 56-210) assembles into a stable homopolymer (600kDa-1MDa) that can bind approximately 5-10 Fe atoms/frataxin subunit (Cavadini et al. 2002). Human heart contains frataxin species of increasing molecular mass, ranging from monomers to polymers >1 MDa. Such large aggregates can sequester iron cations in a non-toxic, but bioavailable form and may function as iron storage proteins similar to ferritin (Cavadini et al. 2002). This data is supported by the fact that, while both the frataxin trimer and homopolymer can deliver iron to ISC and heme pathways, only the frataxin homopolymer has ferroxidase activity and is able to detoxify redox-active iron by sequestering it in a protein-protected compartment (O'Neill et al. 2005).

Expression of a truncated form of frataxin (d-fxn) (residues 78-210) does not yield any assembly. Since the two forms (m-fxn and d-fxn) are produced with the same efficiency and exhibit similar folds, it was concluded that assembly of human frataxin is done by stable subunit-subunit interactions involving the non-conserved N-terminal region (O'Neill et al. 2005). Unlike prokaryotic and yeast frataxin homologues, iron is not required for assembly of human frataxin subunits (O'Neill et al. 2005).

Frataxin homopolymers consist of ordered rod-shape polymers of globular particles that have small electron dense cores resembling the iron cores of ferritin (Cavadini et al. 2002). X-ray Absorption Spectroscopic (XAS) studies of human frataxin polymers assembled *in vitro* showed that the iron cores of frataxin contain ferrihydrite, a biomineral composed of ferric oxide/hydroxide octahedra. Ferrihydrite crystallites in the frataxin core are similar, but less ordered than iron cores of ferritin (Nichol et al. 2003).

1.5.2.2 Iron Chaperone

The crystal structure of human frataxin showed the existence of a conserved anionic surface patch that could be a part of an iron binding site. Frataxin monomer doesn't bind iron, but it could do so by assembling with itself or other proteins through its acidic patch. It was also shown that 15 conserved uncharged residues form a flat, neutral surface on the β sheet that could be able to mediate protein-protein interactions (Dhe-Paganon et al. 2000).

Since frataxin has been proven to form complexes with IscU, IscU/IscS, aconitase and ferrochelatase (Yoon and Cowan 2003; Yoon and Cowan 2004; O'Neill et al. 2005), it is postulated that frataxin is the iron donor for ISC assembly and heme synthesis. Both trimeric and assembled forms of frataxin can donate iron to IscU, aconitase and ferrochelatase *in vitro* (O'Neill et al. 2005) and iron is required for these interactions (Yoon and Cowan 2003; Yoon and Cowan 2004; Bencze et al. 2007).

Both frataxin trimers and polymers enhance Fe(II) availability to ferrochelatase, whereas only assembled frataxin has ferroxidase activity, sequesters redox-active iron and limits oxidative damage to DNA. Ferroxidase activity is predominant at Fe(II)/subunit ratio of <1. At higher ratios, autoxidation overrides the ferroxidation. The ferroxidase activity at <1Fe(II)/subunit is consistent with the presence of less than one ferroxidation site/subunit. This implies that assembly is required for the ferroxidase activity of human frataxin (O'Neill et al. 2005).

Frataxin deficiency causes a defect in heme synthesis between protoporphyrin IX and heme. Activity of coproporphyrinogen oxidase and cytochrome oxidase are decreased. Levels of mitochondrial heme and cytochrome *c* are also decreased. Deficiency of cytochrome oxidase activity and decreased levels of cytochrome *c* are due not only to deficiency of heme, but also to a decreased loading of heme onto these proteins (Schoenfeld et al. 2005). Ferrochelatase activity is similar in control and FRDA cells, but zinc-chelatase activity is increased in FRDA showing an altered metal-specificity of ferrochelatase (Schoenfeld et al. 2005). Increased levels of zinc protoporphyrin IX have been found in yeast totally lacking frataxin (Lesuisse et al. 2003) and the same may be true of human FRDA.

1.5.3 Protection from Oxidative Stress

Direct evidence exists that assembled frataxin has ferroxidase activity and is able to sequester redox-active iron limiting iron-induced oxidative damage to DNA (O'Neill et al. 2005). FRDA fibroblasts and lymphoblasts are more sensitive to oxidative stress than unaffected cells (Wong et al. 1999; Sturm et al. 2005) and the antioxidant glutathione is decreased in FRDA, possibly as a result of an excess consumption required to eliminate H_2O_2 (Piemonte et al. 2001; Tozzi et al. 2002).

No increase in chelatable (redox-active) mitochondrial iron has been found (Sturm et al. 2005) and I have shown that mitochondrial iron is largely mineralized (Popescu et al. 2007a). It has also been shown that the activity and expression of superoxide dismutases (SOD) is not induced in FRDA fibroblasts, supporting the idea that little redox-active iron is present in FRDA cells and an alternative source of free radicals contributes to the disease pathology (Chantrel-Groussard et al. 2001; Jiralerspong et al. 2001). The effects of oxidative stress in FRDA fibroblasts can be partially reversed by mitochondria-targeted antioxidants (Jauslin et al. 2003) and by transduction of affected fibroblasts with adeno-associated virus and lentivirus vector constructs that encode frataxin (Fleming et al. 2005). It is clear that oxidative stress has a role in FRDA pathology but it is still to be established whether this is generated by increased ferrous iron inside mitochondria, alternative sources of free radicals, impaired defense mechanisms due to frataxin deficiency or a combination of these.

1.5.4 Electron Donor to Respiratory Complex

Physical interaction between frataxin and components of mitochondrial respiratory complex II - FAD-binding domain of succinate dehydrogenase A flavoprotein and succinate dehydrogenase B ISC-containing protein - suggests that frataxin may play a role in the entrance of electrons into the electron transport chain. In this scenario, frataxin deficiency is associated with inappropriate incorporation of electrons to the respiratory chain and incomplete reduction of ubiquinone (Q) to ubiquinol (QH2). The formation of the pro-oxidant semiquinone ($Q^{\cdot -}$) leads to ROS formation and mitochondrial oxidative stress (Gonzalez-Cabo et al. 2005). In this case ROS are derived independently of excess ferrous iron and Fenton chemistry.

Frataxin increases triglyceride synthesis, maximizes Krebs cycle activity, increases mitochondrial calcium uptake, activates mitochondrial respiration and activates the oxidative phosphorylation (Ristow et al. 2000; Pomplun et al. 2007).

1.5.5 Conclusion

The mitochondrion is known as an essential and dynamic component of cellular biochemistry that is heavily involved in iron metabolism. Since the mitochondrion is the only site of heme synthesis and a major site of ISC synthesis, most of the iron sequestered by the cell is targeted to mitochondria where the excess iron can be stored in mitochondrial ferritin (MtFt) in a non-toxic, but bioavailable form (Napier et al. 2005). The mitochondrion uses some of the heme and ISC generated for its own metabolism (i.e. Krebs cycle, respiratory chain) and exports the rest to the cytosol (Napier et al. 2005).

Frataxin appears to play numerous roles in mitochondria. It regulates the flux of iron through the ISC and heme biosynthetic pathways. The distinct binding affinities of frataxin for ferrochelatase (heme synthesis) and IscU (ISC synthesis) control how much iron passes from frataxin to each of these two major iron dependent pathways. Frataxin has a protective role against oxidative stress, by mineralizing excess iron and/or influencing activity of the SODs. Frataxin is directly involved as an inducer of oxidative phosphorylation and mitochondrial respiration as well as indirectly through frataxin's role in ISC and heme synthesis and protection of the proteins against oxidative damage. Iron binding and assembly properties of frataxin strongly support the idea that this protein can store iron and, at the same time, act as an iron chaperone.

1.6 Mouse Models of FRDA

The mouse frataxin gene (Frda gene) is localized on chromosome 19 and encodes a 207 amino acid protein with 73% amino acid identity to human frataxin. The N-terminal region of mouse frataxin also contains a mitochondrial targeting signal (Koutnikova et al. 1997).

In the adult mouse, frataxin mRNA expression is detected in heart, liver, skeletal muscle, kidney, spleen, thymus, brown adipose tissue, axial skeleton, teeth and skin, and more weakly in whole brain and lungs. In the nervous system, maximum expression is detected in spinal cord and dorsal root ganglia (Jiralerspong et al. 1997; Koutnikova et al. 1997). These data show that mouse frataxin mRNA distribution is similar to that observed in humans, and these tissues are the ones most affected by frataxin deficiency. During embryonic development, mRNA expression is first detected in embryonic day (ED) 10.5, reaching maximum expression in ED 14.5 and persisting into postnatal period (Jiralerspong et al. 1997).

Concerning the assembly properties of mouse frataxin, a high molecular weight pool of frataxin is present in mouse heart indicating that frataxin can assemble under physiological conditions (Cavadini et al. 2002).

Disruption of mouse frataxin by deletion of exon 4 of the frataxin gene generates asymptomatic heterozygotes and embryonic lethal homozygotes, suggesting that the milder phenotype seen in humans is associated with residual frataxin expression and that frataxin has an important role during development. Embryonic death occurs between ED 6.75 and ED 7.5. Cell death is not the consequence of abnormal iron accumulation since there are no visible iron deposits in dead embryos (Cossee et al. 2000).

The human frataxin gene rescues Frda knockout mice. Rescued mice display normal phenotypes, behavioral and biochemical (activity of mitochondrial respiratory chain complexes I-IV, aconitase, citrate synthase) parameters showing that human frataxin can substitute for endogenous murine frataxin (Pook et al. 2001). Human frataxin is properly processed, targeted to mitochondria and expressed in the appropriate tissues. However, its expression is higher in brain, heart, skeletal muscle and liver, and lower in blood when compared to mouse frataxin. This indicates the existence of tissue specific

mechanisms that regulate the Frda locus, that may not affect human FRDA expression equally well (Pook et al. 2001; Sarsero et al. 2004).

Protein expression analyzed in transgenic mice, generated with a bacterial artificial chromosome (BAC) genomic reporter construct consisting of an inframe fusion between human FRDA gene and the gene coding for enhanced green fluorescent protein (EGFP), shows frataxin expression beginning with ED 3.5. All the major internal organs exhibit EGFP expression, and the FRDA-EGFP expression is two times higher in homozygous than hemizygous mice (Sarsero et al. 2005). This shows that frataxin expression is ubiquitous and proportional to the number of functional frataxin alleles.

The first viable FRDA mouse model has been created using a conditional gene-targeting approach. This technique yielded two mouse lines with complete frataxin deficiency in targeted tissues: MCK line (skeletal and cardiac muscles mutant) and NSE line (neuronal, heart and liver mutant). These mutants show progressive pathophysiological and biochemical features of the human disease: cardiac hypertrophy and accumulation of damaged mitochondria, large sensory neurons dysfunction, deficiency of complexes I-III of the respiratory chain and mitochondrial aconitase. The onset of the pathology and inactivation of ISC is followed by time-dependent intramitochondrial ferric iron accumulation in the heart of MCK mutants, demonstrating that iron deposits are rather the consequence, and not the causative mechanism (Puccio et al. 2001). Chelation therapy reduces iron in the heart of the MCK mutant and limits heart hypertrophy, but can not rescue the metabolic defects (Whitnall et al. 2008).

Neuron-specific deletion of frataxin has been generated in two mutants that develop progressive mixed cerebellar and sensory ataxia, the most prominent features of FRDA. The Cb (cerebellum) mutant has significant reduction in frataxin in the cerebellum, while the Br (brain) mutant shows frataxin reduction in cerebellum, brain, brain stem and spinal cord. Non-neuronal tissues are not affected. Despite the more restricted frataxin deficiency, the Cb mutant shows a more severe neurological deficit with loss of ambulation by 1 year of age. These mutants show some features that are very similar to the human disease: degeneration of the posterior columns of the spinal cord, of the neurons in Clarke's columns and of the large sensory neurons in dorsal root ganglia, and absence of motor neuropathy. ISC deficiency has also been observed.

Neurodegeneration in dorsal root ganglia implies autophagy and lipofuscin accumulation. Autophagy leads to removal and degradation of damaged cytosolic proteins and organelles. Lipofuscin is a peroxidation product composed of proteins, lipids, carbohydrates, iron and other metals. Their accumulation is due to incomplete autophagocytosis and lysosomal degradation of mitochondria and could explain the lack of detectable iron deposits in dorsal root ganglia (Simon et al. 2004).

While cardiomyocytes seem to compensate for frataxin deficiency by mitochondrial proliferation and cellular hypertrophy, dorsal root ganglia use the autophagic process as a protective mechanism for the elimination of defective mitochondria that enables them to survive longer without frataxin. The progressive autophagic process reflects therefore the slowly progressive nature of the neurological phenotype (Puccio et al. 2001; Simon et al. 2004). Removal of exon 4 of the Frda gene targeted to pancreatic β-cells causes slowly progressive diabetes in mice. Increased formation of ROS, increased apoptosis and decreased proliferation of pancreatic β-cells leading to reduced islet mass, impaired insulin secretion and eventually to type II diabetes (relative deficiency of insulin producing β-cells) (Ristow et al. 2003).

A frataxin knockin mouse has been created in an effort to generate a more appropriate model for the human disease. After introduction of a $(GAA)_{230}$ repeat in the first intron of the mouse Frda gene, frataxin expression is reduced to 75% of wild type (WT) expression. Since these levels are too high for the mouse to develop a FRDA-like phenotype, frataxin knockin mice ($frda^{(GAA)230/(GAA)230}$) have been crossed with $frda^{+/-}$ generating frataxin knockin/knockout mice ($frda^{-/(GAA)230}$) (Miranda et al. 2002). Although frataxin levels in these mice are 25-36% of normal levels (low enough to cause FRDA in humans), these mice are viable and do not develop any anomalies of motor coordination, iron metabolism or response to iron loading (Miranda et al. 2002). However, the frataxin knockin ($frda^{(GAA)230/(GAA)230}$) mice recapitulate the genetics and epigenetics of FRDA: they show significant reduction in the levels of frataxin mRNA in brain, cerebellum and heart (Rai et al. 2008) and changes in H3 and H4 post-translational modifications in chromatin near the GAA repeat (Rai et al. 2008) that correspond to those found in FRDA cells (Herman et al. 2006). Treatment with HDACI increases acetylation

of H3 and H4 in chromatin near the GAA repeat and restores both frataxin mRNA and protein expression (Rai et al. 2008).

The mouse models, especially the MCK mutant (frataxin deficient in skeletal and cardiac muscle) provides new insights into the link between FRDA and oxidative stress. Lack of induction of SOD activity suggests that continuous oxidative damage to ISC results from inadequate SOD activity (Chantrel-Groussard et al. 2001). The stable or small increase in oxidative stress markers may be due to concomitant decrease of the respiratory chain activity (the major source of ROS production in the cell). It has been suggested that the excess iron mineralization is the consequence of ISC deficiency, and not the causative mechanism of ROS production and little redox-active iron, if any, is present in FRDA cells (Puccio et al. 2001; Seznec et al. 2004; Seznec et al. 2005).

Frataxin overexpressing mice show an increased induction of oxidative phosphorylation (Pomplun et al. 2007) and an altered response during hematopoietic differentiation (Miranda et al. 2004), with no other abnormal biochemical or clinical phenotypes (Miranda et al. 2004). Thus, it has been concluded that overexpression of frataxin in mice is innocuous and is not a concern when designing gene therapy treatments for FRDA (Miranda et al. 2004). Frataxin expression is decreased during erythropoietic response triggered by phenylhydrazine (PHZ; causes hemolytic anemia and triggers active erythropoiesis in the spleen) in both WT and frataxin overexpressing mice. However the response is delayed in frataxin overexpressing mice compared to WT (Miranda et al. 2004). Similar results have been obtained in mouse Friend erythroleukemia cells (Becker et al. 2002). Dimethyl sulfoxide (DMSO) induction of erythroid differentiation and hemoglobinization and protoporphyrin IX down-regulates frataxin expression, while TfR and β-globin mRNA levels are increased. Since downregulation of frataxin leads to mitochondrial iron loading, these data suggests that reduced frataxin during erythroid differentiation results in iron sequestration for heme biosynthesis (Becker et al. 2002), or that less frataxin is required for heme synthesis than for ISC synthesis because of frataxin's high affinity for ferrochelatase. The binding affinity between frataxin and ferrochelatase is 28 times greater than the affinity between frataxin and ISU, and thus reduced frataxin levels have a bigger impact on the ISC pathway, keeping the iron available for heme incorporation (Yoon and Cowan 2004).

1.7 Yeast Model

The frataxin gene (*YFH1*) encodes the yeast homologue of human frataxin (Yfh1p), a 174 amino acid protein. It is targeted to mitochondria and processed in two steps by yeast mitochondrial processing peptidase (Babcock et al. 1997; Foury and Cazzalini 1997; Koutnikova et al. 1997; Wilson and Roof 1997; Branda et al. 1999).

1.7.1 FRDA Knockout Yeast

yfh1Δ cells exhibit respiratory deficiency due to loss of mtDNA, deficiency of aconitase and mitochondrial ISC containing proteins, unregulated and extensive mitochondrial iron accumulation and increased sensitivity to oxidative stress (hydrogen peroxide, ferrous iron) (Babcock et al. 1997; Foury and Cazzalini 1997; Koutnikova et al. 1997; Rotig et al. 1997; Wilson and Roof 1997; Foury and Talibi 2001). Frataxin deficiency leads to increased expression of the iron regulon (Foury and Talibi 2001) and transcription of the latter seems to respond directly to ISC biosynthesis, and not to free iron (Chen et al. 2004).

Normal human frataxin is able to complement the deficiency of *yfh1Δ* yeast, while human frataxins carrying mutations found in FRDA patients are unable to do so (Wilson and Roof 1997; Branda et al. 1999; Cavadini et al. 2000). Also, excess zinc in the growth medium prevents iron accumulation and increases the growth rate of *yfh1Δ* cells and their resistance to oxidative stress, but cannot restore the deficiency of ISC and heme proteins or the mitochondrial respiration, suggesting a possible use of zinc against oxidative stress in frataxin deficiency (Santos et al. 2003). There is a lack of information on zinc in FRDA but it is possible that zinc can fill some of the roles of iron and/or block iron uptake.

Yeast cells have no ferritin gene, but over-expression of either human MtF (Campanella et al. 2004) or cytosolic L type ferritin (Desmyter et al. 2004) rescues the respiratory defect and lengthens the lifespan of *yfh1Δ* yeast. This indicates that iron mineralization by whatever means, has a beneficial effect on iron overloaded mitochondria.

1.7.2 Yeast with Chronically Reduced Levels of Frataxin

Yeast with 15-20 fold reduction in frataxin show intramitochondrial iron accumulation and considerable oxidative damage in both mitochondrial and nuclear DNA (Karthikeyan et al. 2003). This yeast model was developed as a better model for human FRDA.

1.7.3 Role of Frataxin in Mitochondrial Iron Export

Mitochondrial iron accumulation in *yfh1Δ* appears at the expense of cytosolic iron (Babcock et al. 1997). Reintroduction of *YFH1* in *yfh1Δ* results in the export of accumulated mitochondrial iron into the cytosol, showing that excess iron deposits in *yfh1Δ* yeast are bioavailable (Radisky et al. 1999) and can be incorporated in ISC and exported (Chen et al. 2002). It has been suggested that part of the excess mitochondrial iron is ferric citrate acting either as an iron carrier, or as a promoter of oxidative stress (Chen et al. 2002) or insoluble ferric phosphate, explaining the unavailability of iron for yeast ferrochelatase and the synthesis of zinc protoporphyrin instead of iron protoporphyrin (Lesuisse et al. 2003). One of the questions still to address is whether pathological iron can be mobilized and exported in FRDA.

1.7.4 Role of Frataxin as Iron Chaperone

While ISC can be inactivated by oxidative stress, this does not seem to be the case in FRDA. Low activities of aconitase and ferredoxin are accompanied by abundant expression of their apo-forms (lacking the ISC) and the small amounts of active protein synthesized are stable. This shows that deficiency of ISC containing proteins appears to be the result of decreased incorporation of ISC in the apo-proteins, and not the result of oxidative damage to the protein itself (Chen et al. 2002). This also suggests that, at least in yeast, frataxin is not essential for ISC synthesis, but renders the process more efficient (Duby et al. 2002).

Yfh1p has been reported to interact with several proteins but some of these interactions need to be confirmed. Yfh1p physically interacts with aconitase, Isu1/Nfs1 (ISU scaffold protein/cysteine desulfurase), ferrochelatase, succinate dehydrogenase and subunits of the electron transfer flavoprotein complex (Gerber et al. 2003; Lesuisse et al.

2003; Park et al. 2003; Bulteau et al. 2004; He et al. 2004; Ramazzotti et al. 2004; Gonzalez-Cabo et al. 2005). Interactions with ISC containing proteins are stabilized by ferrous iron and result in iron loading onto the ISC (Gerber et al. 2003; Park et al. 2003). Thus, frataxin is able to bind iron and acts as an iron chaperone to ISC and heme pathways.

Protein crystallography of yeast frataxin has identified conserved acidic residues in the helix1 – strand 1 protein residue, that undergo amide chemical shift changes and could be iron-binding sites on frataxin. Even more, ferrochelatase appears to bind to frataxin's helical plane in a manner that includes its iron-binding interface (He et al. 2004).

1.7.5 Role of Frataxin as Iron Storage Protein

Like human frataxin, Yfh1p can assemble *in vitro* and *in vivo* forming large homopolymers (600kDa-1Mda) when exposed to excess iron (Adamec et al. 2000) and its assembly responds to increases in mitochondrial iron uptake (Gakh et al. 2008). *In vitro*, the polymers sequester 2400-3000 atoms of iron in a ferrihydrite core. Unlike human frataxin, assembly of Yfh1p requires the presence of iron for its subunit-subunit assembly. Yeast apofrataxin does not show any tendency to self-associate (Adamec et al. 2000; Gakh et al. 2002; Nichol et al. 2003).

Yfh1p assembly is driven by two sequential iron oxidation reactions. At a low Fe^{2+}/frataxin subunit stoichiometry, a ferroxidase reaction induces the first assembly step and the formation of frataxin trimer (α3). Initially the Fe^{2+} is loosely bound and can be easily made bioavailable. As the iron/frataxin subunit ratio increases, autoxidation overrides ferroxidation and higher order polymers are produced (α6, α12, α24, α48). Fe^{3+} becomes less and less accessible with formation of a stable iron-protein complex that can store 50-75 atoms of iron per subunit (Park et al. 2002; Park et al. 2003). These data support the hypothesis that Yfh1p is an iron storage protein that can also function as an iron chaperone.

Mutations that impair the ferroxidation or mineralization activity of Yfh1p increase the sensitivity of yeast cells to oxidative stress, shorten their life span and prevent survival in the absence of the anti-oxidant enzyme SOD (Gakh et al. 2006).

These mutations slow down frataxin assembly but do not alter its iron chaperone function (Gakh et al. 2006). Thus, iron detoxification is another function of frataxin relevant to anti-oxidant defense and cell longevity.

1.8 Mitochondrial Ferritin

Cells contain two kinds of ferritin: cytosolic and mitochondrial (Arosio et al. 2008).

1.8.1 Cytosolic Ferritin

Cytosolic ferritin is a heteropolymer composed of 24 subunits of 2 types (H or heavy chains and L or light chains) that can store up to 4500 atoms of iron. H chains are encoded on chromosome 11q13 and have ferroxidase activity. Each H chain has a binuclear center that binds 2 Fe(II) and catalyses their oxidation to Fe(III). L chains are encoded on chromosome 19q13 and assist in iron core formation. Besides molecular oxygen, ferritin is able to use hydrogen peroxide for the oxidation of Fe(II) and shows ROS detoxification abilities. Iron release from ferritin is realized through reduction, probably by a NAD(P)H-dependent ferrireductase. Cytosolic ferritin synthesis is regulated at the level of translation in response to iron. Its mRNA has an IRE in the 5' UTR. In low iron conditions, IRP1 binds to IRE and repress ferritin translation. When cellular iron increases, an iron atom is inserted in the [3Fe-4S] cluster of IRP1. The new formed [4Fe-4S] cluster destabilizes the binding of IRP1 to IRE and increases the synthesis of ferritin in order to increase iron storage capacity of the cell. In conclusion, ferritin is an iron storage protein that keeps iron in a non-toxic, and yet bioavailable form (reviewed in (Harrison and Arosio 1996; Arosio et al. 2008)).

1.8.2 Mitochondrial Ferritin

Discovery of MtFt has led to new insights into iron metabolism and mitochondrial associated diseases.

MtFt gene is localized on chromosome 5q23. It is an intronless gene that encodes a 242 amino acid protein (30 kDa). MtFt precursor is targeted to mitochondria and processed to a 22 kDa subunit that assembles into typical ferritin shells and has

ferroxidase activity. So, MtFt is an unusual H-type ferritin targeted to mitochondria (Levi et al. 2001).

Unlike cytosolic ferritins, MtFt mRNA lacks an IRE in its 5'UTR and the factors regulating its synthesis remain poorly understood (Drysdale et al. 2002). While the sequence of MtFt is very similar to cytosolic H ferritin (Levi et al. 2001), Ser144 found in MtFt but absent in H ferritin is thought to reduce ferroxidase activity of MtFt. As a result, MtFt is thought to behave like cytosolic L ferritins that tightly sequester excess iron (Bou-Abdallah et al. 2005). MtFt is expressed at high levels in erythroblasts from patients with sideroblastic anemia (impaired heme synthesis) and testis and at lower levels in pancreatic islets of Langerhans, brain, spinal cord and adipocytes (Drysdale et al. 2002; Levi and Arosio 2004), whereas frataxin is expressed in all tissues. Hydrogen peroxide catalyzed ferrihydrite mineralization is supported by frataxin and cytosolic ferritins, but not supported by MtFt (Bou-Abdallah et al. 2005). Therefore one of frataxin's unique roles in the mitochondria may be to protect DNA from hydrogen peroxide (Karthikeyan et al. 2003) and MtF may serve different but complementary roles in iron detoxification.

Overexpression of MtFt in normal mouse fibroblasts (Nie et al. 2005) and in HeLa cells (Corsi et al. 2002) results in a mitochondrial iron overload with preferential iron sequestration in MtFt as ferrihydrite, at the expense of cytosolic iron. Overexpression of MtFt in TA-H1299 cells (non-small cell lung carcinoma) increases the sensitivity of these cells to oxidative stress (Lu et al. 2009).

Yeast has no ferritin gene, but over-expression of either MtFt (Campanella et al. 2004) or cytosolic L type ferritin (Desmyter et al. 2004) rescues the respiratory defect and lengthens the lifespan of *yfh1Δ*. This indicates that iron mineralization by whatever means, has a beneficial effect on iron overloaded mitochondria. MtFt seems to provide a redundant mechanism to store iron and control ROS formation primarily through regulation of mitochondrial iron availability (Campanella et al. 2009).

1.9 General Hypothesis and Research Objectives

1.9.1 Hypothesis

The chemical form of mitochondrial iron and the metal distribution within the nervous system are altered in FRDA.

1.9.2 Research Objectives

a. Determine the chemical form of mitochondrial iron in FRDA fibroblasts and compare it to that of control fibroblasts.

b. Validate RS-XRF for brain metal mapping.

c. Map the distribution of iron, copper and zinc in the cerebellar cortex, cerebellar white matter and dentate nucleus.

d. Map the distribution of iron, copper and zinc in the brain and spinal cord from a patient diagnosed with spinocerebellar ataxia (SCA).

CHAPTER II

The Chemical Form of Mitochondrial Iron in Friedreich's Ataxia

2.1 Introduction

FRDA is a progressive neurodegenerative disease inherited as an autosomal recessive trait that affects 1:50,000 Caucasians (Campuzano et al. 1996; Durr et al. 1996). The molecular defect in FRDA results from a hyper-expansion of a GAA trinucleotide repeat in the first intron of the frataxin gene that interferes with transcription of frataxin (Campuzano et al. 1996). Patients with fewer GAA repeats on the smaller allele make more frataxin, and as a result their disease starts later in life and/or progresses more slowly (Durr et al. 1996). Most patients are homozygous for the expanded alleles (Campuzano et al. 1996; Durr et al. 1996) and their GAA repeats adopt a triple helical structure forming a novel stable DNA structure called "sticky DNA". This inhibits the transcription of the FRDA gene by sequestration of the RNA polymerases (Bidichandani et al. 1998; Ohshima et al. 1998; Sakamoto et al. 1999; Sakamoto et al. 2001). Genomic instability is a feature of human FRDA (Durr et al. 1996) and tissue specific expansions of GAA repeats have been described in cerebellum and dorsal root ganglia in a mouse model expressing human frataxin in the context of elevated GAA repeats known to cause human disease (Clark et al. 2007).

FRDA is the consequence of deficiency of frataxin, a nuclear encoded mitochondrial targeted protein (Gibson et al. 1996; Babcock et al. 1997; Campuzano et al. 1997; Koutnikova et al. 1997; Priller et al. 1997). FRDA patients have extremely low, sometimes undetectable frataxin mRNA levels (Campuzano et al. 1996; Cossee et al. 1997) and show a severe reduction in frataxin expression ranging from 4 to 29% of normal levels (Campuzano et al. 1997). In mouse (Al-Mahdawi et al. 2006) as well as invertebrate models of FRDA (Anderson et al. 2005; Gakh et al. 2006; Vazquez-Manrique et al. 2006; Llorens et al. 2007), reduced longevity and chronic oxidative stress is a common feature.

Characteristic features of FRDA are degeneration of neurons especially in dorsal root ganglia, spinal cord and cerebellum (Hughes et al. 1968; Oppenheimer 1979; Lamarche et al. 1984), cardiomyocytes (Hewer 1968; Sanchez-Casis et al. 1976; Lamarche et al. 1984) and pancreatic beta cells (Hewer 1968; Hewer and Robinson 1968). These cells are metabolically active, non-dividing and long-lived and express frataxin at high levels (Campuzano et al. 1996).

There is considerable evidence that frataxin is a bifunctional protein that acts as both a chaperone for ferrous iron and an iron storage protein that mineralizes iron as ferrihydrite, a biomineral composed of ferric oxide/hydroxide octahedra.

Frataxin chaperones ferrous iron to the ISC pathway by forming a complex with scaffold proteins and cysteine desulfurase (Gerber et al. 2003; Muhlenhoff et al. 2003; Yoon and Cowan 2003; Ramazzotti et al. 2004), and to the heme biosynthetic pathway by interacting with ferrochelatase (Lesuisse et al. 2003; Park et al. 2003; Yoon and Cowan 2004; Schoenfeld et al. 2005). It also stabilizes aconitase during oxidative stress (Bulteau et al. 2004; Bulteau et al. 2005). Frataxin is also expressed in the cytosol where it is involved in ISC synthesis (Acquaviva et al. 2005; Lu and Cortopassi 2007). When frataxin is knocked down in normal embryonic kidney cells, the earliest consequence is a defect in cytoplasmic iron sulfur proteins followed by increased oxidative damage. This leads to a decline in mitochondrial aconitase activity, deficiency of ISC and deficiency of heme, followed by an increase of mRNA levels of major enzymes involved in heme biosynthesis (i.e. mitochondrial monoamine oxidase A and mitochondrial δ-aminolevulinate synthase 1) (Lu and Cortopassi 2007).

The first step in human frataxin assembly is the formation of the trimer that binds a single atom of iron at its 3-fold channel (O'Neill et al. 2005; Karlberg et al. 2006). Changes in the channel conformation at the 3-fold axis of the trimer are proposed to regulate whether ferrous iron is oxidized for storage or made available for transfer to proteins that require iron (Karlberg et al. 2006). Frataxin binds iron in yeast (Adamec et al. 2000) and its assembly responds to increases in mitochondrial iron uptake (Gakh et al. 2008). Like yeast frataxin (Adamec et al. 2000; Gakh et al. 2002; Park et al. 2002; Park et al. 2003), human frataxin mineralizes iron *in vitro* as ferrihydrite within a 48 subunit polymer (Cavadini et al. 2002; Nichol et al. 2003; O'Neill et al. 2005; O'Neill et al. 2005) but unlike yeast, human frataxin polymerizes in the absence of excess iron through subunit interactions mediated through residues in the N-terminus that are not conserved in yeast (O'Neill et al. 2005). A pool of high molecular weight frataxin protein has been identified in mouse and human heart suggesting that frataxin assembles *in vivo* (Cavadini et al. 2002; O'Neill et al. 2005) but it remains to be established if frataxin polymers mineralize iron *in vivo* in human FRDA.

Frataxin homopolymers consist of ordered rod-shape polymers of globular particles that have small electron dense cores (Cavadini et al. 2002; Gakh et al. 2002) resembling the iron cores of ferritin (Cavadini et al. 2002). XAS studies of human frataxin polymers assembled *in vitro* showed that the ferrihydrite crystallites in the frataxin core are similar to, but less ordered than iron cores of ferritin (Nichol et al. 2003).

The importance of oxidative stress in FRDA pathology has been a subject of debate. Studies using mouse FRDA models indicate that oxidative stress varies between tissues. Conditional knockouts in heart and neural tissues show little evidence of oxidative stress (Puccio et al. 2001; Seznec et al. 2004; Seznec et al. 2005), while pancreas (Ristow et al. 2003) and liver (Thierbach et al. 2005) knockouts are sensitive to oxidants. Mouse models expressing only low levels of human frataxin show decreased aconitase activity and mild oxidative stress with iron accumulation as a late event leading to progressive neurodegeneration and cardiac pathology (Al-Mahdawi et al. 2006). Cultured fibroblasts and lymphoblasts from FRDA patients display increased sensitivity to oxidative stress (Wong et al. 1999; Wong et al. 2000) and FRDA patients display signs of increased oxidative stress, including elevated markers of free radical damage to DNA, lipid peroxidation, reduced plasma levels of glutathione, reduced aconitase activity and elevated IRP1 (Rotig et al. 1997; Piemonte et al. 2001; Karthikeyan et al. 2003; Lobmayr et al. 2005). Iron deposits are seen in patients' myocardial cells (Sanchez-Casis et al. 1976; Lamarche et al. 1980; Bradley et al. 2000), hepatocytes and spleen (Bradley et al. 2000) and FRDA fibroblast cultures (Delatycki et al. 1999). Magnetic Resonance *in vivo* studies show increased iron in the dentate nucleus of FRDA patients (Waldvogel et al. 1999; Boddaert et al. 2007) but these findings have been challenged by biochemical studies of post-mortem tissues that failed to reveal an increase in iron (Koeppen et al. 2007). Over-expression of frataxin in FRDA lymphoblasts changes the proportion of filterable and non-filterable iron, indicating that frataxin has a direct influence on the chemical form of iron (Tan et al. 2001).

The chaperone function of frataxin has been dissected from its function in mineralizing iron in yeast. Frataxin with mutations that reduce the ferroxidase activity of frataxin and impair iron mineralization, leave its iron chaperone function unimpaired.

Yeast expressing frataxin with these mutations exhibits mild chronic oxidative damage that reduces cellular lifespan (Gakh et al. 2006). However unlike yeast, human cells have ferritin that can also mineralize iron with great efficiency and in some cells provide a redundant mechanism of iron detoxification (Arosio et al. 2008; Campanella et al. 2009).

Cells have two kinds of ferritin. A heteropolymer formed from H and L subunits is found in the cytosol and other cellular compartments (Renaud et al. 1991; Arosio et al. 2008) while a homopolymer formed from an H-type subunit is targeted to mitochondria (Levi et al. 2001). MtFt is expressed at high levels in erythroblasts from patients with sideroblastic anemia, in normal testis and at lower levels in pancreatic islets of Langerhans, brain, spinal cord and adipocytes (Levi et al. 2001; Drysdale et al. 2002; Levi and Arosio 2004; Santambrogio et al. 2007). Unlike cytosolic ferritins, MtFt mRNA lacks an IRE in its 5′ UTR, and the factors regulating its synthesis remain poorly understood. MtFt synthesis is induced when heme synthesis is disrupted in erythroid cells (Cazzola et al. 2003) but the generality of this control mechanism to other cell types has not been established. While the sequence of MtFt is very similar to cytosolic H ferritin, Ser144 found in MtFt but absent in H ferritin is thought to reduce ferroxidase activity of MtFt. As a result, MtFt is thought to behave like cytosolic L ferritins that tightly sequester excess iron (Bou-Abdallah et al. 2005). MtFt may have a ferrihydrite iron core that is similar to that of cytosolic ferritins, but the unique microenvironment in mitochondria could favor the mineralization of other iron oxides. The mineral form of MtFt iron cores assembled *in vivo* remains to be determined.

MtFt and frataxin may serve complementary roles in iron detoxification. Since both human MtFt (Campanella et al. 2004) and L ferritin (Desmyter et al. 2004) have the ability to partially rescue frataxin knock-out yeast, MtFt seems to provide a redundant mechanism to store iron and control reactive oxygen species formation primarily through regulation of mitochondrial iron availability (Campanella et al. 2009). In yeast, frataxin assembly driven by increased mitochondrial iron uptake (Gakh et al. 2008) detoxifies redox-active iron by sequestering it in a non-toxic form in a protein-protected environment (O'Neill et al. 2005). Frataxin may also play a unique role in protecting the DNA from Fenton chemistry (Rotig et al. 1997; Isaya et al. 2004) since hydrogen peroxide catalyzed ferrihydrite mineralization is supported by frataxin but is not

supported by MtFt (Grant et al. 1998; Zhao et al. 2002; Bou-Abdallah et al. 2005; Ilari et al. 2005; Su et al. 2005).

2.2 Hypothesis and Research Objectives

2.2.1 Hypothesis

The chemical form of iron is altered in mitochondria of fibroblasts from FRDA patients and is different from that of mitochondrial iron from control fibroblasts.

2.2.2 Research Objectives

a. Determine the chemical form of mitochondrial iron in FRDA fibroblasts and compare it to that of control fibroblasts.

b. Characterize the iron storage proteins and changes in their expression in FRDA versus control fibroblasts.

2.3 Materials and Methods

2.3.1 Cell culture

2.3.1.1 Fibroblast Cell Lines

Primary fibroblasts were obtained from the NIGMS Human Genetic Cell Repository (Coriell Institute for Medical Research) and Canadian Repository for Mutant Human Cell Strains (McGill University) (Table 1). Donor cell lines GM04078 and GM03816 were derived from a brother and sister with a diagnosis of FRDA at both the molecular and clinical levels with the sister being less severely affected. The McGill cell line MCH070 and Coriell GM08400 were sex matched controls. Clinical summary and case histories provided by Coriell confirmed the absence of the disease in GM08400 and GAA triplet expansions of the frataxin gene were determined to be in the normal range for the McGill line MCH070 (M. Pandolfo, unpublished).

Table 1. Fibroblast primary cell lines.

Sex (family)	ID	GAA repeats	Diagnostic	Provenience
M (1)	GM04078	420/541	FRDA	Coriell
F (1)	GM03816	330/380	FRDA	Coriell
M (2)	MCH070	<66	Control	McGill
F (3)	GM08400	Not determined	Control	Coriell

Table 2. Iron enrichment of the growth medium.

	MEM + 10% CCS	Blood (Kratz et al. 2008)
Iron	70.46 µg/dl	41 – 141 µg/dL
TIBC[a]	97.41 µg/dl	251 – 406 µg/dL
% Saturation[b]	72%	16 – 35%

[a] Total Iron Binding Capacity

[b] (Iron / TIBC) x 100

2.3.1.2 Growth Medium

Fibroblasts were cultured in Eagle's Minimal Essential Medium (MEM) with Eagle's salts (GIBCO) supplemented with 10% Cosmic Calf Serum (CCS) (Hyclone) (growth medium) so that the iron content of the culture medium was very close to that of human serum (Table 2).

2.3.1.3 Fibroblast Cultures

Upon arrival, the 25 cm^2 culture flasks (T25, Falcon) were wiped with 70% ethanol and incubated at 37ºC overnight in a humidified atmosphere of 5% CO_2 in air as per Coriell's instructions. On observation, the fibroblasts were nearly confluent, arranged in parallel arrays, displayed the normal spindle-shaped morphology and showed no signs of contamination.

The next day fibroblasts were fed by withdrawing the shipping medium and replacing it with 5 ml growth medium. The cultures were then incubated at 37º in a humidified atmosphere of 5% CO_2 in air. Cells were fed twice a week and split 1:5 when they reached confluence.

2.3.1.4 Cell Harvesting

Confluent cell cultures were rinsed three times in Puck's balanced salt solution (PBSS) to remove all traces of serum. The fibroblasts were then incubated in 0.025% trypsin/0.01% ethylenediaminetetraacetic acid (EDTA)/PBSS for 5-10 minutes at 37ºC. Using a phase contrast microscope, the cells were closely monitored. When most of the cells lifted off the surface, the trypsin solution was flushed over the surface to assist in dislodging the remaining attached fibroblasts. To inactivate the trypsin, 0.1 ml CCS/1 ml cell suspension was added. The resulting cell suspension was centrifuged at 800 RPM for 10 minutes and then resuspended in growth medium.

To determine the number of viable cells, an aliquot of 0.4 ml cell suspension was stained with 0.1 ml of 0.3% Nigrosin dye. Viable cells remained unstained, whereas the Nigrosin dye stained the dead or dying cells in purple-black. Viable cells were counted in the four square compartments of each of the two sides of a hemacytometer (Improved

Neubauer Levy Hemacytometer, Hausser Scientific Partnership). The number of viable fibroblasts per ml was calculated using the following formulas:

$$\text{Average total count} = (\text{Total Count side1} + \text{Total Count side2})/2 \quad (2.1)$$

$$\text{Number of viable cells/ml} = (\text{Average total count}/4) \times 10 \times 1000 \times (5/4) \quad (2.2)$$

2.3.1.5 Fibroblast Subculture

Using the cell count described above, the cell suspension was diluted to the desired cell concentration in growth medium (5.0-6.0 x 10^4 cells/ml) and each T25 vented cap flask was seeded with 5 ml of final cell suspension (1.0-1.2 x 10^4 cells/cm^2). Flasks were placed in the 37ºC, 5% CO_2 incubator and checked the next morning for cell attachment.

2.3.1.6 Long-term Storage of Cells

Following cell harvesting and counting, the cell suspension was diluted to the desired cell concentration in growth medium (10^6 cells/ml) and 1 ml of the resulting cell suspension was placed into each of the several cryovials (Nalgene). To each vial, 53 µl DMSO was added. Cryovials were then sealed and placed into an isopropanol filled cryocontainer (Nalgene Cryo 1ºC Freezing Container, Nalgene Company) which was stored overnight in a -70ºC freezer. The following morning, the cryovials were transferred to a liquid nitrogen storage dewer.

2.3.1.7 Cell Recovery from Cryogenic Storage

The desired number of cryovials were removed from liquid nitrogen and immediately placed in a water bath at 37ºC. When completely thawed, the content of each cryovial was diluted in 5 ml growth medium. To remove all traces of cryoprotectant, the cell suspension was centrifuged and re-diluted in 5 ml fresh growth medium. An aliquot was removed for cell counting. Based on the results of the cell count, the cell suspension was diluted in growth medium and reseeded at 1.0-1.2 x 10^4 cells/cm^2.

2.3.2 Isolation of Mitochondria

Mitochondria were isolated from 20–40 million cells from pooled confluent cultures. The cell pellet was homogenized on ice using a 7 ml Dounce homogenizer with a Teflon pestle (Pyrex) by moving the pestle up and down 20 times. The amount of homogenization needed to rupture the cells was determined by microscopic examination during the homogenization process. The 'heavy' mitochondrial fraction (HMF) was obtained using a mitochondrial isolation kit (MITOISO1, Sigma) employing two differential centrifugation steps at 4ºC each using one low speed (1,000 x *g*) and one high speed (3,500 x *g*) centrifugation as per kit instructions. This yielded a mitochondrial fraction with low contamination from peroxisomes and lysosomes. The final mitochondrial pellet was suspended in 20 µl storage buffer (10 mM HEPES, pH 7.4, 0.25 M sucrose, 1 mM ATP, 0.08 mM ADP, 5 mM sodium succinate, 2 mM K_2HPO_4, 1 mM DTT) provided by the kit and aliquots were prepared for transmission electron microscopy, XAS analysis and Western blotting.

2.3.3 Transmission Electron Microscopy

Aliquots of HMF were prepared for transmission electron microscopy (TEM) following standard protocols (Locke and Huie 1980) to confirm mitochondrial purity and membrane integrity.

The mitochondria were fixed overnight in 2.5% Glutaraldehyde in 0.1 M Phosphate Buffer (PB), pH 7.4 at 4ºC. In order to keep the mitochondrial pellet together, the next morning the mitochondria were resuspended in a warm 2% Bactoagar in 0.1 M PB and immediately centrifuged in a Beckman microfuge so that the agar was not allowed to cool and solidify before the mitochondria were pelleted at the bottom of the microfuge tube. The tube was then placed in the refrigerator for 15 minutes to allow the agar to solidify. The mitochondrial pellet was removed by cutting the tube with a razor blade and removing the excess agar.

The small piece of agar containing the mitochondrial pellet was then washed in 0.1 M PB containing 0.22 M sucrose, postfixed with 0.8% osmium tetroxide in 0.1 M PB containing 0.22 M sucrose at 4ºC for 1 hour, washed in 0.1 M PB, dehydrated in increasing concentrations of ethanol and then acetone. This was followed by infiltration

with Epon 812 : acetone, pure Epon 812 overnight and polymerization of the samples in a 60ºC oven for 48-72 hours.

After polymerization, the blocks were rough trimmed with a double edge razor blade, smooth trimmed with a glass knife cut on a LKB Knife Maker Type 7801A and thin sections were cut using a diamond knife (Du Pont) on a Reichert-Jung Ultracut microtome. The gold and silver sections were flattened with toluene vapours and then lifted on the dull side of 300 mesh square copper grids (EM Sciences), stained on grid with 2% uranyl acetate and Reynold's lead citrate and examined with a Philips 410LS transmission electron microscope. For each sample approximately 4 grids and 4 micrographs were examined.

2.3.4 X-ray Absorption Spectroscopy

2.3.4.1. Sample Preparation for XAS

To reduce ice diffraction artefacts, mitochondria for XAS were suspended in a minimal amount of storage buffer in 20% glycerol prior to flash freezing. Samples (30 µl) were loaded into 1 mm path length Lucite sample cells and flash-frozen in isopentane chilled in liquid nitrogen. Samples were stored and transported to the synchrotron in liquid nitrogen. Human frataxin, iron loaded *in vitro* (a kind gift of Dr. G. Isaya) and iron loaded horse spleen holoferritin (Sigma) served as models of less ordered and highly ordered ferrihydrite respectively as previously described (Nichol et al. 2003). Dry human met-hemoglobin and bovine hemin (Sigma) were dissolved in 20% glycerol and used as saturated solutions. Metalloproteins were prepared in 20% glycerol. Other iron model compounds were prepared for transmittance measurements by intimately grinding each with a boron nitride diluent and pressing each into a 2 mm thick sample holder between layers of metal-free Mylar.

2.3.4.2 X-ray Absorption Near Edge Structure

Data from mitochondria was acquired on the SPEAR 3 storage ring (85-100 mA at 3.0 GeV) on beamlines 9-3 and 10-2 each equipped with a Silicon (220) double-crystal monochromator. Data from some model compounds were also collected on SPEAR 3 beamline 2-3 and SPEAR 2 beamline 7-3. The incident and transmitted X-ray intensities

were monitored using N_2-filled ionization chambers. The Fe K X-ray absorption near-edge spectra of mitochondria were recorded as K fluorescence excitation spectra using a solid state array of 30 germanium detectors (Canberra) (Cramer et al. 1988). The X-ray energy was calibrated with reference to the lowest K-edge energy inflection point of a standard metallic iron foil (EXAFS Co), run concurrently, the energy of which was assumed to be 7111.3 eV. Harmonic rejection was accomplished on beamline 9-3 using an upstream vertically collimating Rh-coated mirror and downstream refocusing Rh-coated mirror and on beamline 10-2, by detuning one monochromator crystal to approximately 50% off peak. Four sweeps were collected for each sample. Photoreduction was seen in two independent unaffected HMFs after warming to liquid nitrogen temperatures (Figure 1). Therefore each dataset was examined for photoreduction between sweeps and between datasets. In order to reduce X-ray damage, samples were maintained at between 5 and 10 K in a liquid helium flow cryostat (Oxford instruments) and each sample was exposed to X-rays for only 1 hour (4 sweeps).

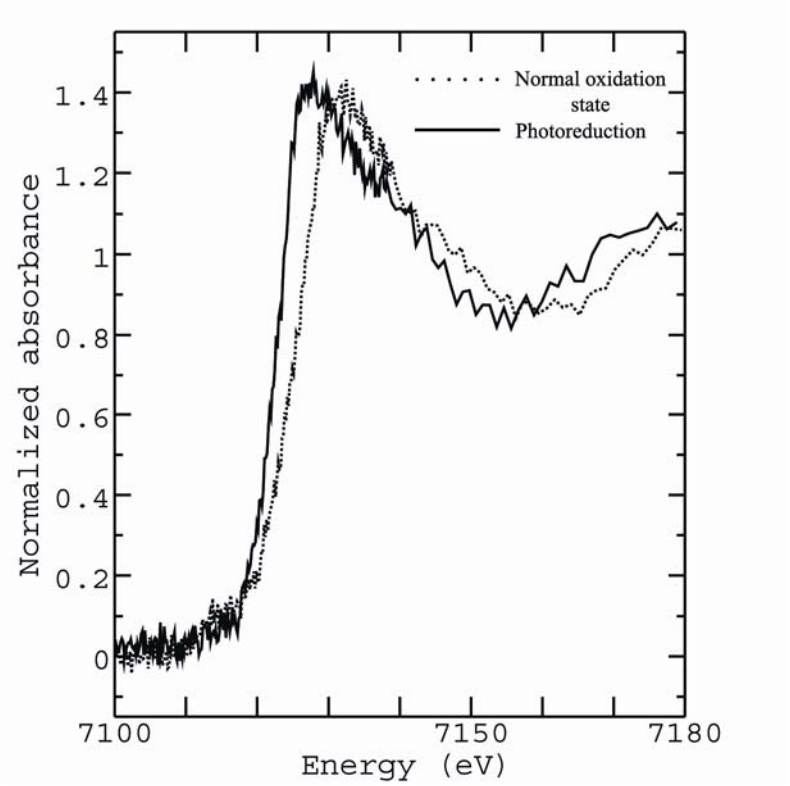

Figure 1. Photoreduction of unaffected HMF. Unaffected HMF shows photoreduction upon second run after warming to liquid nitrogen temperatures, seen as the translation of the spectrum (——) to a lower energy than the normal oxidation state (• • •).

2.3.4.3 XAS Data Analysis

Data analysis was performed using the EXAFSPAK suite of computer programs. Quantitative determination of the different chemical forms of iron present was carried out by least-squares fitting of the near-edge spectra to linear combinations of the spectra of standards, as previously described (Pickering et al. 1998).

From a library of more than 30 model iron compounds, 22 were retained during several rounds of refinement and these were used to fit all the near edges (Table 3). An important distinction with this type of analysis is that incorporation of the spectrum of a particular compound in a fit is an indication of the presence of a class or species, rather than of the particular compound from which the spectrum in question was obtained. No smoothing or related data manipulations were performed.

2.3.5 Polyacrylamide Gel Electrophoresis (PAGE) and Western Blotting

2.3.5.1 Sodium Dodecyl Sulfate Polyacrylamide Gel Electrophoresis (SDS-PAGE)

The HMF was diluted 1:2 with sample buffer (2% SDS, 5% β-mercaptoethanol, 25% glycerol, 0.001% bromophenol blue, 0.0625 M Tris-HCl, pH 6.8) and homogenized. Samples were sonicated (10 pulses, Sonifer® Cell Disruptor Model W140, Heat Systems – Ultrasonic, Inc.) then boiled for 10 minutes and centrifuged for 10 minutes at 12,000 x *g*. The supernatant was transferred to fresh tubes.

Small aliquots (5 µl) were used for protein quantification. Protein concentration was measured using the BioRad Protein Assay (BioRad) based on the Bradford dye-binding procedure (Bradford 1976) and the color change was quantified with a spectrophotometer (BioRad SmartSpecTM Plus) at an assay wavelength of 595 nm.

SDS-PAGE was performed using the method originally described by Laemmli (Laemmli 1970) with the following modifications. Samples containing equal amounts of proteins (70 µg/lane) were loaded on 15% gels or on 4-15% precast gradient gels (BioRad). The precast gradient gels do not have SDS included in the separating gel or stacking gel. SDS is included in the running buffer (25 mM Tris, 192 mM glycine, 0.1% SDS) in addition to the sample buffer (above). Polypeptides were separated for 2 hours at 100 V.

Table 3. Iron model compounds and metalloproteins used in fits.

Model compounds and metalloproteins[a]	Chemical formula	Coordination
Fe (III)		
1. Ferrihydrite (horse spleen ferritin)	FeOOH	6O
2. Human frataxin holopolymer	FeOOH	6O
3. Goethite	FeOOH	6O
4. Hematite	α-Fe_2O_3	6O
5. Magnetite	$Fe^{3+}{}_2Fe^{2+}O_4$	6O
6. Ferric sulfate	$Fe_2(SO_4)_3$	6O
7. Ferric oxide	Fe_2O_3	6O
8. Ferric pyrophosphate	$Fe_4(P_2O_7)_3$	4O
9. Ferric phosphate	$FePO_4$	4O
10. Ferric citrate	$FeC_6H_5O_7$	3O
11. Heme (human met- hemoglobin)		5N
12. Hemin (bovine)		4N, 1Cl
13. Cytochrome c		4N
Iron-sulfur cluster		
14. Ferredoxin - oxidized (Anabaena)	$[Fe_2\text{-}S_2(SR)_2]^{2-}$	4S
15. Rubredoxin - oxidized (P. furiosus)	$[Fe(SR)_4]^{1-}$	4S
16. Iron regulatory protein - oxidized	$[Fe_3\text{-}S_4]^{+}$	4S
17. Rubredoxin – reduced (P. furiosus)	$[Fe(SR)_4]^{2-}$	4S
18. Ferredoxin – reduced (Anabaena)	$[Fe_2(SR)_4]^{3-}$	4S
Fe (II)		
19. Ferrous sulfide	FeS	1S
20. Ferrous ammonium sulphate	$[Fe(H_2O)_6](NH_4)_2(SO_4)$	6O
21. Ferrous hexaimidazole dichloride	$[Fe(imidazole)_6]Cl_2$	6N
22. Ferrous sulfate	$FeSO_4$	6O

[a] Spectra from the listed compounds are used in the fit to represent a general class or category of compound, rather than of the particular species from which the spectrum was obtained.

2.3.5.2 Discontinuous Native PAGE

The HMF was diluted 1:2 with sample buffer (25% glycerol, 0.001% bromophenol blue, 0.0625 M Tris-HCl, pH 6.8). Protein quantification was performed using the Bio-Rad Protein Assay. Samples (13 μg/lane) were loaded on 4-15% precast gradient gels (Biorad) and polypeptides were separated for 7 hours at 120 V. To ensure polypeptide separation under non-denaturing conditions the sample buffer did not contain SDS and β-mercaptoethanol and the running buffer did not contain SDS (Ornstein 1964).

2.3.5.3 Western Blotting

Immunoblotting was performed using the method of Towbin et al (1979) (Towbin et al. 1979) with the following modifications. Gels were equilibrated for 15 minutes in transfer buffer (25 mM Tris, 192 mM glycine, 20% methanol) and transferred to nitrocellulose (Pall Life Sciences) membrane using the BioRad wet transfer apparatus. The SDS-PAGE transfer was performed for 90 minutes at 75 V on ice. The non-denaturing PAGE transfer was done for 2 hours at 75V on ice using transfer buffer that contained 1% SDS. Complete transfer was monitored with Ponceau S stain (0.1% Ponceau S (Sigma) in 1% acetic acid) for detection of proteins on nitrocellulose membranes. Membranes were then washed with Tris-buffered saline (TBS) (20 mM Tris-HCl, pH 7.5, 0.5 M NaCl), and blocked in blocking solution (5% skim milk (Carnation), 0.1% Tween-20 (EM Science) in TBS) for 1 hour. Membranes were incubated with primary antibodies overnight at 4°C. Membranes were washed 3 times in blocking solution for 5, 15, and 5 minutes. Secondary antibodies incubation was done at room temperature for 2 hours with rocking. Membranes were washed 3 times in blocking solution for 5, 15, and 5 minutes, then washed in TBS containing 0.1% Tween for 15 minutes followed by a 5 minute wash in TBS. Horseradish peroxidase (HRP)-bound proteins were detected using a chemiluminescence kit (PerkinElmer Life Sciences, Inc.) and X-ray film (Kodak Biomax XAR).

2.3.5.4 Immunodetection of Proteins and Purity of Mitochondrial Fractions

Detection of frataxin homopolymers, monomers and enrichment of progressive cellular fractions with mitochondria was estimated by Western blotting using a

polyclonal antibody against human frataxin raised in rabbit (1:3000) (gift from Dr. Grazia Isaya) and a secondary goat anti-rabbit antibody tagged with HRP (1:4000) (BioRad).

Ferritin was detected on Western blots of both denaturing and non-denaturing gels with polyclonal antibodies against human heart ferritin, raised in sheep (1:1000) (Novus Biological) and a secondary HRP-tagged rabbit IgG anti-sheep antibody (1:4000) (Inter Medico). This human ferritin antibody cross-reacted with recombinant human MtFt (a kind gift of Dr. Paolo Arosio, University of Milan, Italy) as well as ferritin H and L subunits.

The purity of mitochondrial fractions was measured in two ways. Contamination of the HMF by cytosol was determined using the monoclonal antibody (JLA20) against chicken actin raised in mouse (1:5000) (Lin 1981) and HRP-tagged goat anti-mouse antibodies (1:3000) (BioRad). Lysosomal content of progressive cellular fractions was determined using a polyclonal antibody against human lysosomal-associated membrane protein 1 (LAMP1) synthetic peptide raised in rabbit (1:220) (Sigma) and HRP-tagged goat anti-rabbit (1:4000) (BioRad).

2.3.5.5 Iron Detection

Native blots were stained for iron with Ferene S (Chung 1985) (Sigma) overnight at 4ºC. The sensitivity of Ferene S stain on gels and blots was compared with the sensitivity of protein detection with HRP tagged antibodies. Serial dilution of ferritin and frataxin were separated under non-denaturing conditions. A gel was stained for iron with Ferene S. The duplicate gel was electroblotted on nitrocellulose and stained for iron with Ferene S. Then, ferritin and frataxin were detected with their respective antibodies on the same blot.

2.4 Results

2.4.1 HMF are Highly Enriched in Mitochondria

Mitochondria were isolated from fibroblasts from affected male and female siblings. Equal amounts of protein from successive pellets obtained during cell fractionation were examined using antibodies directed against marker proteins for the cytosol (actin), lysosomes (LAMP1) and frataxin to monitor enrichment and purity of the final HMF. Actin was not present in the HMF (Figure 2, lane 3) but was seen in whole cell lysates (Figure 2, lane 4), indicating little contamination of the HMF with cytosolic cytoskeletal elements. While some lysosomes were present in HMF (Figure 3C) they were not enriched during fractionation (Figure 3C, lane 4). The amount of the frataxin was highest in the HMF (Figure 3B, lane 4) indicating that the HMF was enriched in mitochondria. TEM confirmed that the HMF contained intact mitochondria with very few lysosomes and membrane fragments (Figure 4).

2.4.2 Mitochondria from Affected and Unaffected Cells are Rich in Ferrihydrite

Quantitative analysis using the near-edge region of the X-ray absorption spectrum was performed using a library of iron models (Table 3). Iron K near edge spectra of HMF are compared in Figure 5 and their respective fits are shown in Table 4. The spectra shown in Figure 5 are representative of 6 independent affected and 4 independent unaffected HMF samples (Table 4). All show that ferrihydrite is the predominant species and when all ferric oxides are summed they constitute most of total iron. Minor species such as hemin, some ferrous species and iron–sulfur clusters were fitted to both affected and unaffected HMF but not in any consistent way. The fit error or residual was low for all spectra (Table 4).

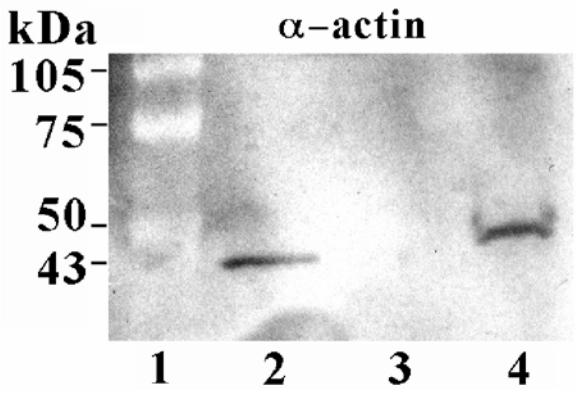

Figure 2. Estimation of cytosolic contamination of the HMF. The cytosolic protein actin was detected on Western blots with a monoclonal anti-actin antibody. Lane 1: molecular weight marker; lane 2: actin; lane 3: HMF lysate; and lane 4: whole fibroblast lysate.

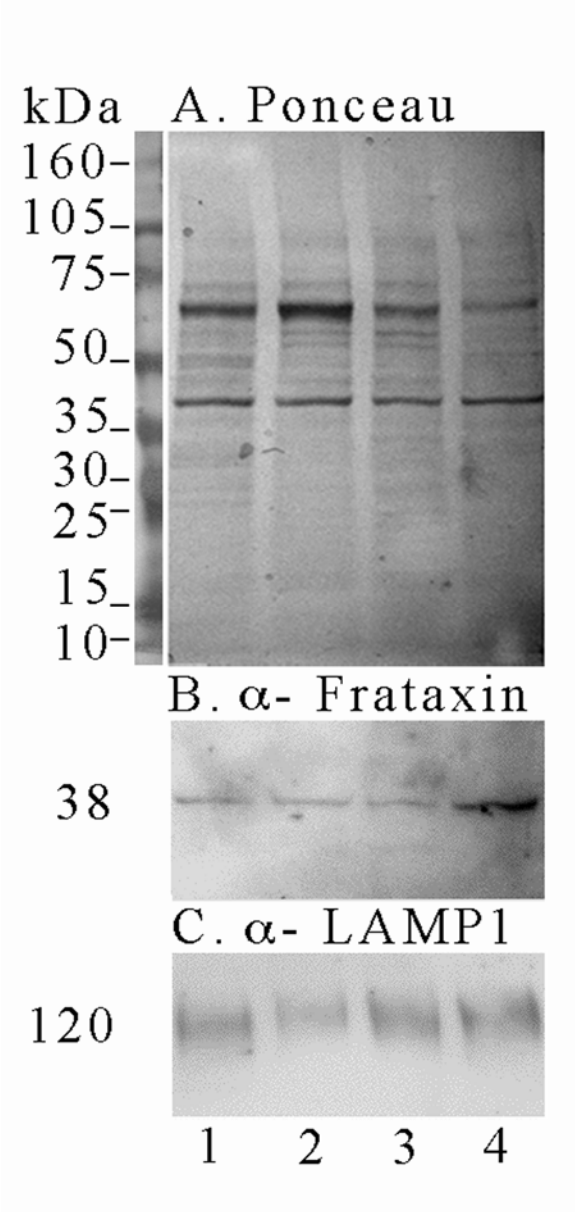

Figure 3. Estimation of mitochondrial enrichment and lysosomal contamination. Proteins in successive pellets from the mitochondrial isolation procedure were separated under denaturing conditions. Lane 1: whole cell lysate; lane 2: pellet from 1st 1,000 x *g* centrifugation; lane 3: pellet from 2nd 1,000 x *g* centrifugation; lane 4: HMF. (A) Ponceau stain shows equal protein loading, molecular weight markers on left; (B) anti-frataxin. Frataxin was present as a 38 kDa dimer; and (C) anti-LAMP1. A band was visible at 120 kDa, the predicted size for LAMP1.

Table 4. Percentage contributions of spectra of iron compounds and metalloproteins[a].

Sample	Ferrihydrite		Other iron oxides	Hemin	Other ferrous sp.	Fe–S clusters[b]	Fit-error[c]
	Ferritin	Frataxin					
Affected							
1. GM04078[A]							
Best fit	55 (6)		27 (6)[d]	13 (3)		5 (1)[b1]	0.040
Forced fit		40 (6)	40 (7)[d]	15 (4)		5 (1)[b1]	0.060
2. GM04078							
Best fit	73 (8)		13 (8)[d]		5 (1)[f]	9 (2)[b1]	0.120
Forced fit		70 (7)	16 (7)[d]		4 (1)[f]	10 (2)[b1]	0.149
3. GM04078							
Best fit	70 (5)			13 (7)	10 (1)[f]	7 (1)[b2]	0.071
Forced fit		50 (6)		40 (8)	6 (1)[f]	4 (2)[b2]	0.138
4. GM04078							
Best fit	39 (5)		25 (5)[d]		11(1)[g]	25(1)[b1]	0.069
Forced fit		26 (6)	38 (6)[d]		10 (1)[g]	26 (2)[b1]	0.108
5. GM03816[B]							
Best fit	72 (5)		16 (2)[e]	8 (5)	4 (1)[f]		0.693
Forced fit		57 (4)	22 (2)[e]	19 (7)	2 (1)[f]		1.027
6. GM03816							
Best fit	64 (1)				19 (1)[f]	17 (2)[b1]	0.362
Forced fit		64 (1)			18 (2)[f]	18 (2)[b1]	0.438
Unaffected							
7. MCH070[C]							
Best fit		86 (2)	8 (2)[e]		6 (1)[g]		0.179
Forced fit	90 (3)		4 (3)[e]		6 (1)[g]		0.243
8. MCH070							
Best fit		26 (9)	29 (8)[e]	20 (12)		25 (5)[b1]	0.753
Forced fit	34 (12)		25 (8)[e]	16 (12)		25 (5)[b1]	0.807
9. GM08400[D]							
Best fit		63 (6)	16 (4)[e]			21 (2)[b1]	0.638
Forced fit	67 (7)		12 (5)[e]			21 (2)[b1]	0.698
10. GM08400							
Best fit		84 (2)				16 (3)[b2]	0.825
Forced fit	84 (3)					16 (3)[b2]	1.115

[a] Percentage contribution of iron species to total iron in whole mitochondria. Samples number 1, 5, 7 and 9 are plotted in Figure 5A, B, C and D, respectively. Precisions, shown in parenthesis, are calculated as three times the estimated standard deviation, as derived from the diagonal elements of the covariance matrix; best fit using all model spectra in Table 3; the form of ferritin or frataxin that remained in the best fit was removed from the fit and alternate ferrihydrite was forced to fit; [b] Rubredoxin from P. furiosus; [b1] reduced rubredoxin; [b2] oxidized rubredoxin; [c] Fit error ($x10^{-3}$) or residual is the average of the sum of the squares of the differences between the observed and calculated signals for all data points in the spectrum; [d] Goethite; [e] Hematite; [f] $[Fe(H_2O)_6](NH_4)_2(SO_4)_2$; [g] $[Fe(imidazole)_6]Cl_2$.

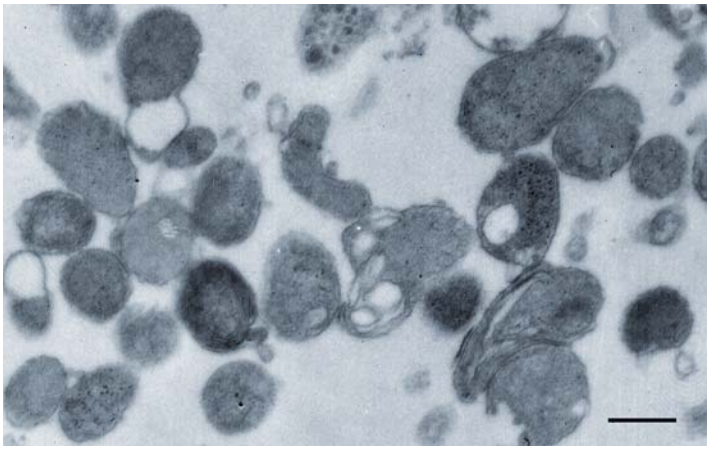

Figure 4. Mitochondrial fraction obtained from FRDA fibroblasts. Isolation of mitochondria using the mitochondrial isolation kit yielded a fraction highly enriched in mitochondria. Some membrane fragments and few lysosomes were found but no other organelles were identified; scale bar = 0.2 μm.

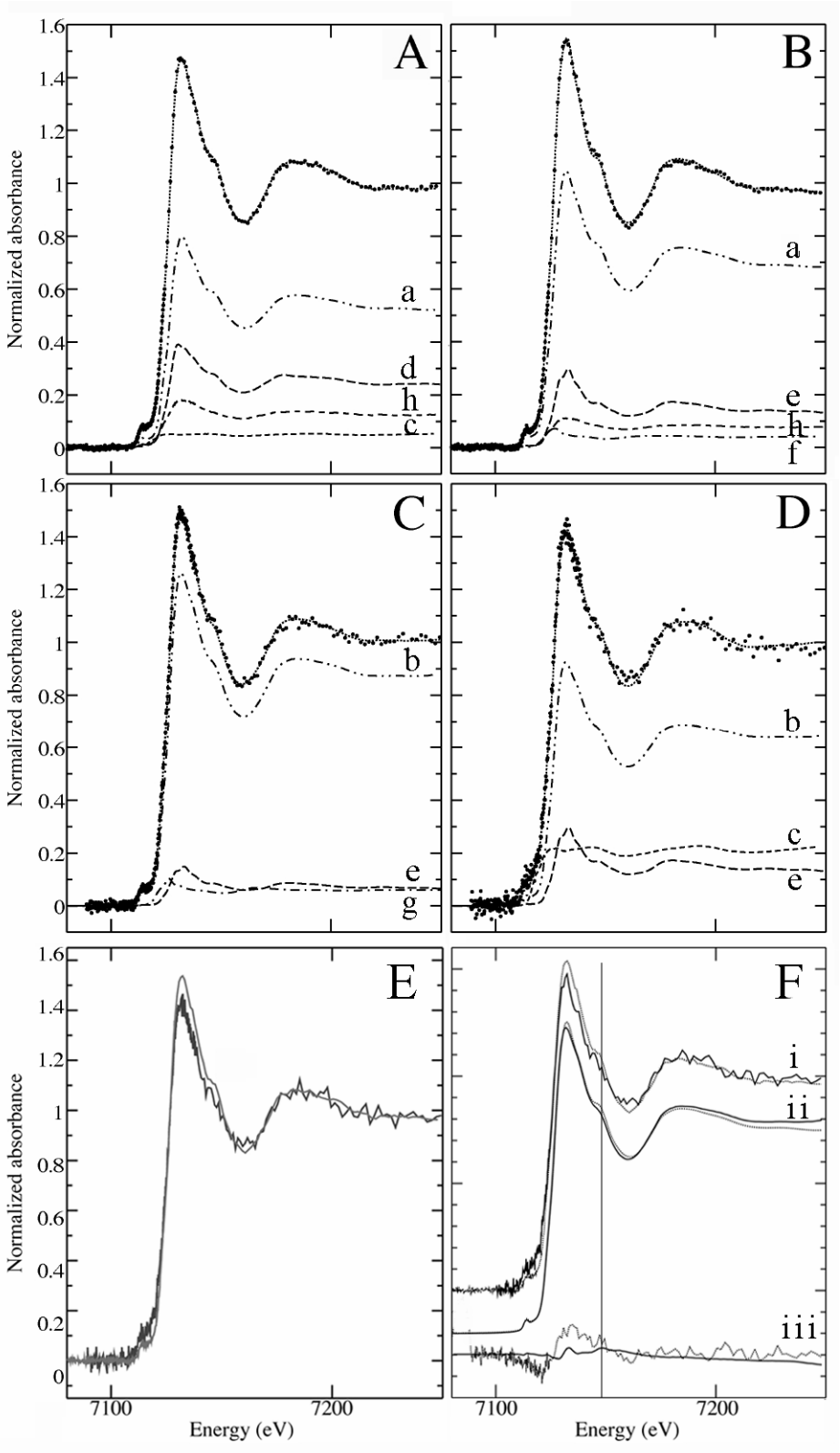
A
B
C
D
E
F
Normalized absorbance
Energy (eV)
7100
7200
a
b
c
d
e
f
g
h
i
ii
iii

Figure 5. Quantitative analysis of Fe K-edge spectra. Each panel shows the normalized spectrum of isolated mitochondria (• • •) together with the best fit (——). The components of the fit are scaled by their relative contributions: components are category as in Table 3. Each category has a unique line type shown in brackets and each species has a unique letter. Category 1, ferrihydrite (– • • –) (a) horse spleen ferritin, (b) human frataxin; Category 2, Fe–S cluster (- - -) (c) reduced rubredoxin; Category 3, other iron oxides (– – –) (d) goethite, (e) hematite; Category 4, other ferrous species (– • –) (f) ferrous ammonium sulfate hexahydrate, (g) ferrous hexaimidazole dichloride; Category 5, hemin (– - –) (h) see Table 3 (samples number 1, 5, 7 and 9) for numerical results of the fits. (A) affected male (GM04078); (B) affected female (GM03816); (C) unaffected male (MCH070); (D) unaffected female (GM08400). (E) spectra of affected and unaffected females overlaid showing differences between them; (F) (i) affected female fitted with unaffected female; (ii) horse spleen ferritin fitted with frataxin; (iii) difference between affected and unaffected HMF overlaid with difference between ferritin and frataxin (vertical line, shoulder feature near 7150 eV).

The highly ordered ferrihydrite of ferritin best fitted the HMF from affected fibroblasts (Figure 5A, B, Table 4) while the less ordered ferrihydrite of frataxin best fitted the unaffected HMF (Figure 5C, D, Table 4). When ferrihydrite from ferritin was removed from the fit for affected HMF (Table 4, forced fit), fit errors increased, the proportion of ferrihydrite, as found in frataxin, was less and the proportion of other highly ordered ferric oxides (goethite/hematite) increased. When ferrihydrite from frataxin was removed from the fit for unaffected HMF, fit errors increased and the proportion of other highly ordered ferric oxides was reduced and precisions were poorer. When overlaid the iron K-edges of affected and unaffected HMF were slightly different (Figure 5E). When the K-edge from affected HMF was fitted with unaffected HMF the difference between the two had features that matched differences between horse spleen ferritin and frataxin (Figure 5F). The difference between affected and unaffected spectra was greater than that between ferritin and frataxin (Figure 5F) indicating differences in other iron species other than ferrihydrite. Given that the near edge of ferritin and frataxin iron cores are similar and ferrihydrite is the predominant form of iron (Figure 5E) (Nichol et al. 2003), I sought to confirm the presence of holoferritin using conventional immunoblots of native and denatured proteins from HMF lysates.

2.4.3 Identification of Ferritin Subunits in HMF

Ferritin subunits were identified by their respective mobility on gels and cross-reaction with anti-ferritin antibody (Figure 6). Whole fibroblasts (Figure 6, lane 2) contained H and L subunits of cytosolic ferritin. In contrast, the predominant ferritin subunit in HMF (Figure 6, lanes 3 and 4) was larger than the L and H subunits (20.0 and 20.9 kDa respectively) and slightly larger than the recombinant MtFt peptide (21.1 kDa) (Figure 6, lane 1). The processed MtFt subunit is the largest ferritin subunit at 21.6 kDa and therefore I conclude that MtFt is the predominant form of ferritin in the HMF.

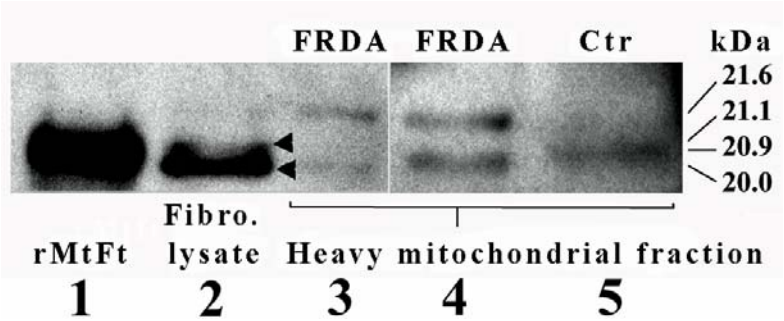

Figure 6. Identification of ferritin subunits in HMF. HMF were denatured and separated by SDS-PAGE on 4–15% gradient gels. Ferritin was identified using a polyclonal antibody raised against human heart ferritin. Lane 1: recombinant MtFt with reported MW of 21.1 kDa; lane 2: whole fibroblast lysate, arrowheads show H and L subunits; lane 3: HMF FRDA affected; lane 4: HMF FRDA affected; lane 5: Ctr, unaffected. Molecular weights predicted from the primary structure of each ferritin subunit are listed on the right; L subunit (20 kDa), H subunit (20.9 kDa), rMtFt (21.1 kDa), MtFt (21.6 kDa).

2.4.4 Mitochondrial Frataxin Polymers are Present in Unaffected Fibroblasts

Once I established that the predominant ferritin in HMF was MtFt, I sought to determine if it contained iron. The sensitivity of iron staining versus Western blotting was determined using dilutions of horse spleen ferritin and human frataxin. Immunoblotting easily detected 0.76 µg of ferritin protein but iron was removed by blotting (compare Figure 7A, a and b), reducing sensitivity of the Ferene S assay. A similar loss of iron after blotting was seen for frataxin (Figure 7B). Ferritin and frataxin were detected in unaffected fibroblasts by immunoblotting but no iron was detected indicating that iron had been lost or that apoferritin and apofrataxin predominated. Antibody detection of protein was more sensitive than iron staining of the same amount of ferritin and electroblotting reduced the sensitivity of iron staining (Figure 7).

2.4.5 MtFt is Elevated in FRDA Mitochondria

After spectra were collected, HMF proteins were separated under non-denaturing conditions. A high molecular weight band that cross-reacted with human heart ferritin antibodies but that migrated more slowly than the L-rich horse spleen holoferritin (440 kDa) standard was detected in affected HMF with a smaller amount in unaffected HMF (Figure 8A and B, upper panel). Since the predominant ferritin subunit in the HMF is the size predicted for MtFt, the high molecular weight holoferritin in the HMF is most likely MtFt. This MtFt stained for iron with Ferene S in affected but not unaffected HMF (Figure 8A and B lower panel). It was three times more abundant in affected than in unaffected HMF indicating that affected cells have elevated levels of MtFt protein. Note the absence of stainable iron in 0.76 µg of horse spleen ferritin (Figure 7A). Taken together, these data show that MtFt is increased and stores significant iron in FRDA cells. High molecular weight frataxin polymers were also detected in the control fibroblast HMF (Figure 8C).

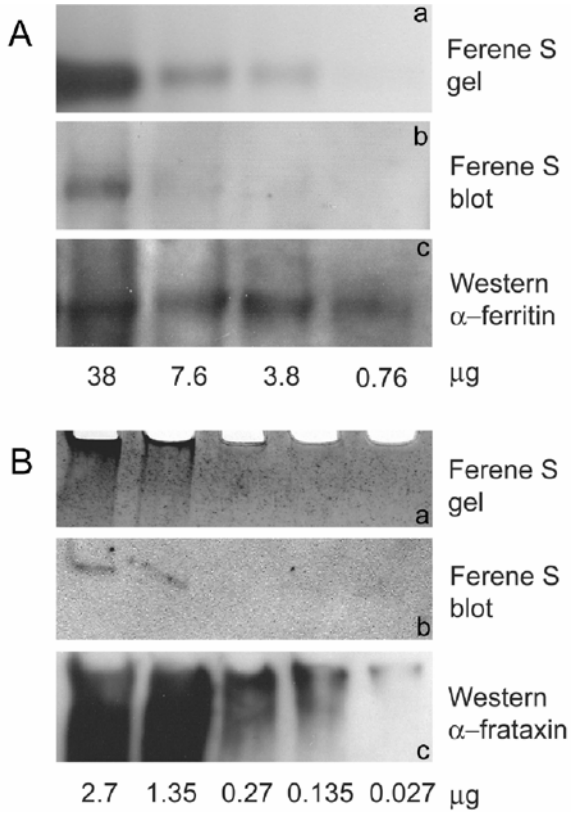

Figure 7. Sensitivity of Ferene S stain for iron and Western blotting for ferritin. Duplicate dilution series of (A) horse spleen holoferritin (38– 0.76 µg) and (B) human holofrataxin (2.7–0.027 µg) were separated under non-denaturing conditions. A gel was stained with Ferene S (A, panel a; B, panel a). The duplicate gel was electro-blotted to nitrocellulose and stained for iron with Ferene S (A, panel b; B, panel b). After iron staining, ferritin (A, panel c) and frataxin (B, panel c) were detected with their respective specific antibodies as described in experimental procedures. Exposure times were 1 minute for ferritin and 15 s for frataxin.

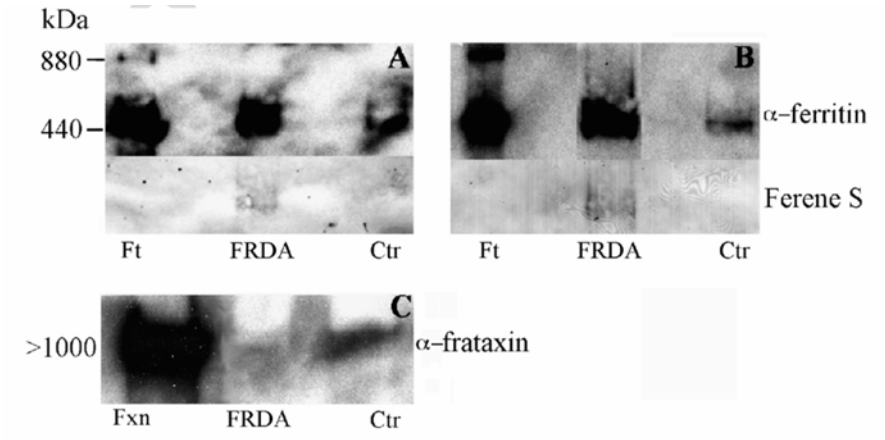

Figure 8. Mitochondrial ferritin is upregulated in HMF from affected cells. HMF proteins were separated under non-denaturing conditions on 4–15% gradient gels. (A) upper panel anti-heart ferritin, lower panel Ferene S iron stain (equal protein per lane). (B) upper panel anti-heart ferritin, lower panel Ferene S iron stain (equal volume per lane). (C) same as (A) but reacted with polyclonal anti-human frataxin antibodies. Lanes: Ft – horse spleen ferritin; FRDA – affected mitochondria (GM04078 in A, GM03816 in B); Ctr – unaffected mitochondria (MCH070 in A, GM08400 in B); Fxn –human holofrataxin.

2.5 Discussion

XAS is a powerful tool to speciate metals in intact systems without damaging the sample. X-rays probe all of the iron and therefore in a non-homogenous sample, like whole mitochondria, it provides an average composition. Near edge analysis indicates that on average, ferrihydrite is the predominant chemical form of iron in both FRDA and control mitochondria and ferric oxides constitute most of the total iron. Since XAS provides an average composition, individual mitochondria may have more or less.

The cell has multiple mechanisms to control the uptake and metabolism of iron in different forms. The relative importance of ferritin and frataxin in cytosolic and mitochondrial iron storage is poorly understood. I found that although ferrihydrite is present in both frataxin replete and frataxin deficient mitochondria, ferrihydrite seems to be associated with MtFt only in frataxin deficient mitochondria. In addition, only FRDA mitochondria have MtFt upregulated 3-fold and only MtFt from FRDA mitochondria stains for iron. An unanswered issue is what induces the apparent 3-fold increase in MtFt. Since MtFt mRNA lacks an IRE, "free" iron does not seem to be the trigger acting at the translational level (Levi et al. 2001; Drysdale et al. 2002). The only known stimulus for MtFt synthesis is the disruption of heme synthesis (Cazzola et al. 2003). In erythroid cells, heme synthesis is associated with a down regulation in frataxin expression and blockage of heme synthesis induces MtFt synthesis and iron uptake (Becker et al. 2002). When frataxin is limiting, iron is preferentially directed away from Fe–S cluster synthesis towards heme synthesis (Yoon and Cowan 2003) but since Fe–S cluster proteins are required in the final steps of heme synthesis (Yoon and Cowan 2004; Schoenfeld et al. 2005; Wingert et al. 2005), heme synthesis is blocked. In sideroblastic anemia, iron not incorporated into heme is shunted to MtFt (Levi et al. 2001; Drysdale et al. 2002; Cazzola et al. 2003) and the same may happen in FRDA at least in those cells that have the capacity to synthesize mitochondrial ferritin. Expression of MtFt in HeLa cells results in decreased levels of cytosolic ferritins, up-regulation of TfR and iron retention in mitochondria as MtFt (Corsi et al. 2002). Under stressful conditions (i.e. treatment with H_2O_2 and Antimycin A), MtFt expression also reduces the formation of ROS and increases the activity of mitochondrial ISC (Campanella et al. 2009). Overexpression of MtFt in frataxin deficient yeast (Campanella et al. 2004) and FRDA fibroblasts

(Campanella et al. 2009) rescues the respiratory function, prevents the mitochondrial iron accumulation and mitochondrial DNA damage and prevents the formation of ROS. Thus, cells with little or no apo-MtFt or those that cannot upregulate MtFt synthesis may be more vulnerable to frataxin deficiency than are fibroblasts.

The strong iron staining of the MtFt after electroblotting is intriguing (Figure 8A, B). It may indicate that MtFt binds iron tightly or its iron core differs from that of horse spleen ferritin. Contributions of other iron oxides to the XAS spectra may also represent ferritin-bound iron that is mineralized in a different form in the unique environment of the mitochondrial matrix. Other iron oxides naturally constitute a small fraction of horse spleen ferritin iron cores (Cowley et al. 2000) and are elevated in hemochromatosis, Alzheimer's disease (magnetite, wustite) and thalassemia (goethite) (Ward et al. 1994; Ward et al. 2000; Collingwood et al. 2005; Quintana et al. 2006). These studies propose that the presence of 'abnormal' iron oxides contributes to cellular pathology.

I also observed differences in frataxin levels between FRDA and control mitochondria. I expected and saw reduced levels of frataxin in affected fibroblasts. Assembled frataxin has been reported *in vivo* (Cavadini et al. 2002; O'Neill et al. 2005) in heart cells that are a prime target of FRDA pathology. I show that frataxin also assembles in mitochondria of control fibroblasts, a cell type spared in FRDA. Stainable iron could not be detected in the small amount of frataxin present in HMF. This was expected since human frataxin *in vitro*, binds much less iron than does ferritin and this is likely lost during electroblotting (Figure 7).

I focused on speciating mitochondrial iron because it may be possible to slow the progression of both the neurodegeneration and cardiomyopathy that characterize FRDA by devising treatment strategies that normalize mitochondrial iron chemistry. XAS provides a clinically relevant fingerprint of the iron chemistry of normal and abnormal mitochondria. Treatment strategies focus on removing iron from mitochondria by chelation or reducing the effects of iron-catalyzed Fenton chemistry with antioxidants (Wong et al. 1999; Wong et al. 2000). I found that much of the iron in FRDA mitochondria is already stored as relatively non-toxic, but also poorly bioavailable ferrihydrite of MtFt (Bou-Abdallah et al. 2005) and ferrous iron species constitute a small proportion of the total iron. The XAS analysis lacked the sensitivity to detect consistent

differences in non-ferrihydrite iron but ferrous species were detected and these may be sufficient to support the kind of mild chronic oxidative stress that is reported in mouse models (Al-Mahdawi et al. 2006). This data also supports recent work indicating that little redox-active iron is present in FRDA cells (Seznec et al. 2005; Sturm et al. 2005) and suggests that the lack of iron bioavailability is also a factor involved in FRDA pathogenesis. Therefore chelation strategies should take into account that at least in cells that can synthesize MtFt, non-ferrihydrite iron may represent a small fraction of total mitochondrial iron and chelating the small ferrous iron pool could prevent mitochondria from carrying out even minimal functions.

Fibroblasts, like cardiomyocytes and neurons, synthesize both frataxin and ferritin but the relative importance of each protein in iron homeostasis is poorly understood. In FRDA fibroblasts, the apparent upregulation and iron content of MtFt indicate that it plays an active role in iron detoxification through regulation of mitochondrial iron availability (Campanella et al. 2009). MtFt is upregulated in erythroid cells when heme synthesis is blocked and dysregulation of this pathway may also trigger MtFt synthesis in FRDA fibroblasts. By understanding how fibroblasts regulate MtFt synthesis we may better understand how to upregulate this protective protein in cardiac and neuronal cells of FRDA patients.

CHAPTER III

Mapping Brain Metals Using Rapid-Scanning X-ray Fluorescence

3.1 Introduction

FRDA is the most common inherited ataxia (Campuzano et al. 1996) and typically presents before 25 years of age with progressive ataxia of gait and limbs, dysarthria, loss of deep tendon reflexes, extensor plantar responses, muscle wasting and loss of sensation, especially of vibration and joint position sense (Greenfield 1954; Geoffroy et al. 1976; Harding 1981; Durr et al. 1996). As the disease progresses, there may be horizontal nystagmus, saccadic-pursuit eye movements, difficulty with swallowing and breathing as well as cardiomyopathy, diabetes mellitus and skeletal deformities (Greenfield 1954; Geoffroy et al. 1976; Harding 1981; Durr et al. 1996). Some patients can develop optic nerve atrophy and hearing loss (Greenfield 1954; Geoffroy et al. 1976; Harding 1981; Durr et al. 1996). In contrast to the typical early onset form, late onset FRDA progresses more slowly and tendon reflexes are often retained (De Michele et al. 1994; Durr et al. 1996; Coppola et al. 1999). Magnetic resonance imaging in patients with typical and late onset FRDA reveals spinal cord atrophy that is sometimes associated with atrophy of the brainstem and cerebellum (Wessel et al. 1989; Klockgether et al. 1991; Wullner et al. 1993; Mascalchi et al. 1994; De Michele et al. 1995; Bhidayasiri et al. 2005).

The neurological features of FRDA are explained by the neuropathological findings characteristic to this disease. The peripheral sensory nerves are severely affected with loss of large myelinated axons and loss of neurons in the dorsal root ganglia (Greenfield 1954; Hughes et al. 1968; Oppenheimer 1979; Lamarche et al. 1984). The spinal cord shows neuronal loss in the nucleus dorsalis of Clarke and loss of myelinated fibers in the posterior columns with the gracile fasciculus almost always more affected than the cuneate fasciculus (Greenfield 1954; Oppenheimer 1979; Lamarche et al. 1984). There is also degeneration of the corticospinal lateral and spinocerebellar tracts and, less frequently, of the corticospinal anterior tracts (Greenfield 1954; Oppenheimer 1979; Lamarche et al. 1984). Neurodegenerative changes seen in the dorsal columns and pyramidal tracts of the spinal cord can be traced through the medulla: neuronal loss in the gracile and cuneate nuclei and axonal degeneration in the pyramids (Greenfield 1954; Oppenheimer 1979; Lamarche et al. 1984). The loss of large, myelinated axons in the spinocerebellar pathways can also be traced through the inferior and superior cerebellar

peduncles to the cerebellar Purkinje cells. In FRDA, these neurons degenerate, especially in the vermis of the cerebellum (Greenfield 1954; Oppenheimer 1979; Lamarche et al. 1984). Neurons are also lost in the dentate nucleus (Oppenheimer 1979; Lamarche et al. 1984; Koeppen et al. 2007). Some cases also present with neuronal loss in the optic nerves and tracts, subthalamic nuclei, thalamus and globus pallidus (Oppenheimer 1979; Lamarche et al. 1984).

FRDA is caused by deficiency of the nuclear encoded mitochondrial protein, frataxin (Campuzano et al. 1996; Campuzano et al. 1997; Priller et al. 1997). Frataxin deficiency reduces heme and iron-sulfur cluster synthesis which can lead to iron accumulation in some cells and oxidative stress (Babcock et al. 1997; Foury and Cazzalini 1997; Koutnikova et al. 1997; Rotig et al. 1997; Wilson and Roof 1997; Bradley et al. 2000; Emond et al. 2000; Schulz et al. 2000).

In humans, iron deposits have been demonstrated in patient cardiomyocytes (Sanchez-Casis et al. 1976; Lamarche et al. 1980; Bradley et al. 2000), hepatocytes and spleen cells (Bradley et al. 2000) and FRDA fibroblast cultures (Delatycki et al. 1999) using Perls' stain and electron microscopy. Magnetic Resonance *in vivo* studies show increased iron in the dentate nucleus of FRDA patients (Waldvogel et al. 1999; Boddaert et al. 2007) but these findings have been challenged by biochemical studies of post-mortem tissues that failed to reveal an increase in iron (Koeppen et al. 2007). However, there are no human studies linking the nervous system neurodegeneration in FRDA to iron accumulation. Moreover, even though early work suggested a possible dysregulation of copper and zinc metabolism in FRDA patients (Barbeau et al. 1984; Huxtable et al. 1984; Shapcott et al. 1984), the possible involvement of copper and zinc in FRDA neurodegeneration has not been investigated.

Metals accumulate in the brain as a function of age (Morris et al. 1992; Bartzokis et al. 1997; Martin et al. 1998; Ogg et al. 1999; Zecca et al. 2004; Bartzokis et al. 2007) and there is increasing evidence that brain metal accumulation is found in a variety of neurodegenerative and ageing-related disorders (Rossi et al. 2004; Zecca et al. 2004; Frazzini et al. 2006; Molina-Holgado et al. 2007). For many years there has been tremendous interest in human brain metal metabolism but complete metal maps have not been available (Zecca et al. 2004). Such baseline data are required to fully understand the

relationship between metals, aging and neurodegenerative disease. While destructive analytic techniques such as atomic absorption and inductively coupled mass spectrometry have been used to quantify metals in selected brain regions (Hock et al. 1975; Dexter et al. 1987; Dexter et al. 1989; Duflou et al. 1989; Dexter et al. 1991; Dexter et al. 1992; Dexter et al. 1993; Rajan et al. 1997; Becker et al. 2005) and some magnetic resonance imaging sequences are used to image iron *in vivo* (Haacke et al. 2005), histochemistry has long been the gold standard to localize metals in brain slices. However Perls' and Turnbull's methods detect only nonheme iron (Perls 1867; Zaleski 1887; Gomori 1936; Meguro et al. 2007), copper histochemistry lacks sensitivity and specificity (Pilloni et al. 1998; Henwood 2003; Ferenci et al. 2005) and complex techniques are required to distinguish protein-bound from ionic zinc (Danscher et al. 1985; Lopez-Garcia et al. 2002). Because each of these methods employs a different chemistry, they cannot be combined or used sequentially on the same tissue section. Therefore, easy and quantitative assessment of interrelationships between metals has been lacking.

In contrast to histology, X-ray fluorescence (XRF) is element specific; hence each metal is detected irrespective of its chemical state. Traditional point-to-point XRF imaging has been successfully employed to map multiple metals in small areas of brain tissue sections at high resolution (Yoshida et al. 2001; Ishihara et al. 2002; Collingwood and Dobson 2006; Miller et al. 2006; Linkous et al. 2007), but the time required to map large areas of the brain in this way is prohibitive. This chapter shows the first results of rapid-scanning X-ray fluorescence mapping (RS-XRF) of brain. RS-XRF employs unique hardware and software to substantially increase scanning speed so as to be useful in mapping entire brain slices. Since FRDA human tissues are not readily available, the new method was initially validated by comparing the metal distribution in normal (N) and Parkinson's disease (PD) brain. PD was chosen because there is an extensive literature showing abnormalities in brain metals and iron in particular.

PD is the second most common neurodegenerative disease, affecting between 0.1 and 0.3% of the population (MacDonald et al. 2000). The diagnostic characteristic of idiopathic PD is the loss of dopaminergic neurons from the substantia nigra pars compacta leading to a reduction of dopaminergic transmission within the basal ganglia (Javoy-Agid et al. 1984; Agid et al. 1989). PD has been linked to genetic propensity,

other neurodegenerative diseases, cerebrovascular diseases, head trauma, pesticide exposure and use of psychoactive medications (Dick et al. 2007). While no link has been found between iron, copper or manganese exposure and PD (Dick et al. 2007), endogenous zinc and copper can be altered and iron is known to accumulate in the substantia nigra (Dexter et al. 1987; Dexter et al. 1989; Dexter et al. 1991; Dexter et al. 1992; Dexter et al. 1993). Iron also accumulates in the brain with age (Hallgren and Sourander 1958; Morris et al. 1992; Morris and Edwardson 1994; Zecca et al. 2004; Zecca et al. 2004; Bartzokis et al. 2007) and dysregulation of iron (Thomas and Jankovic 2004), zinc (Frederickson and Cuajungco 2005) and copper (Madsen and Gitlin 2007) has been linked to a variety of neurodegenerative (Dexter et al. 1987; Dexter et al. 1989; Jellinger et al. 1990; Sofic et al. 1991; Kawas and Brookmeyer 2001; Dick et al. 2007) and ageing-related disorders (Zecca et al. 2004; Zecca et al. 2004; Molina-Holgado et al. 2007). The motivation for this work was the prospect of doing systematic studies on metal pathology in neurodegenerative diseases in general with future direct application to FRDA.

3.2 Hypothesis and Research Objectives

3.2.1 Hypothesis

RS-XRF is a synchrotron technique capable of simultaneously colocalizing multiple metals in human brain slices on a practical time scale and identifying variations in metal distribution that may be linked to pathology of neurodegenerative disease.

3.2.2 Research Objectives

Compare the distribution of iron, copper and zinc in single slices from Parkinson's disease and control brains.

3.3 Materials and Methods

3.3.1 Rapid-Scanning X-ray Fluorescence Mapping

XRF imaging was performed at wiggler beam lines 6-2 and 10-2 at the Stanford Synchrotron Radiation Laboratories (SSRL). The beam lines were operated in standard configuration with a collimating mirror upstream of a Si (1 1 1) monochromator and a pair of total reflection focusing mirrors downstream. The beam was focused onto a 50 μm

diameter tantalum pinhole placed close to the sample (Figure 9). Since the sample was mounted at a 45º angle to the incident beam, the 100 μm thick pinhole was tilted such that the horizontal beam size was reduced to $50/\sqrt{2} = 35$ μm, which in turn results in a 50 μm footprint on the sample. The beam intensity I_0 was monitored with a N_2-filled ion chamber upstream of the pinhole. During scanning, small drifts of the beam with respect to the pinhole were corrected periodically. A photon counting 13-element germanium detector system (Canberra) with Gaussian shaping amplifiers employing 0.125 μs shaping times plus single channel analyzers was used to detect the XRF signal. For each element, the electronic (single channel analyzer) windows were set to capture the fluorescent photons from the Kα1 and Kα2 emission lines averaged at a mean Kα energy of $(2 \quad E_{K\alpha 1} + E_{K\alpha 2})/3$. The signals of all 13 detector elements within the window of each chemical element were added with a fan-in unit and the sum signals were fed into the readout system. The detector was placed at a 90º angle to the beam in order to minimize the unwanted scattering signal.

Conventional thick autopsy specimens are well suited to RS-XRF because the effective penetration/escape depth, defined as the thickness of sample needed to decrease the signal to 1/e, is 0.33, 0.56 and 0.65 mm for the iron, copper and zinc Kα fluorescence lines, respectively. Since the escape depth is constant, relative concentrations of a given metal in different brain samples can be compared. Comparing amounts of different metals is challanging because the escape depth and fluorescence yield of each metal is different.

The samples were mounted on a computerized xy translational stage and rapid scans were performed by continuously translating the sample horizontally across the beam. At the end of each line, a vertical step (40 μm/step) was performed, and the horizontal scan direction was reversed.

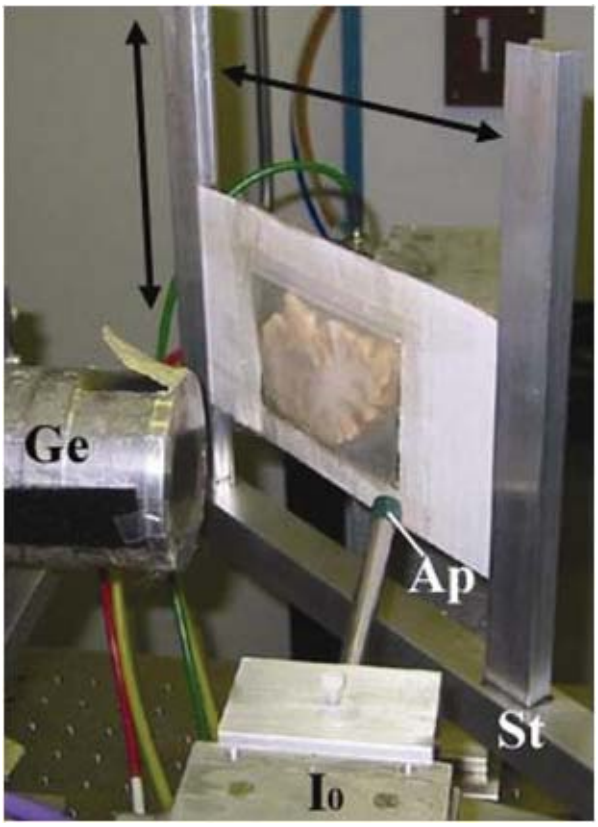

Figure 9. Rapid-scanning X-ray fluorescence mapping experimental setup. Synchrotron X-rays at 11 keV passed through a 50 μm aperture (Ap). The beam intensity was monitored with a N_2-filled ion chamber (I_0). The brain slice was mounted vertically on a motorized stage (St) at 45º to the incident X-ray beam and raster scanned in the beam. A 13-element Ge detector (Ge) was positioned at a 90º angle to the beam.

Data were recorded at two different scanning speeds (see Figures 10 and 14). Using standard hardware, data were collected at a rate corresponding to a travel distance of 40 μm per readout. The readout system used custom-built real-time software coupled with standard beam line hardware to provide deterministic data acquisition. The system had adjustable count times in units of 10 ms plus ~2.8 ms overhead per readout. At an incident beam energy of 11 keV and a flux of ~3×10^{10} photons s^{-1}, the scanning speed of ~1.75 mm s^{-1} was chosen. This corresponded to a total time of ~22.8 ms (20 ms readout time + 2.8 ms overhead) per 40 μm pixel. The X-ray dose under these conditions is 233 grays (every 22.8 ms). This is almost five orders of magnitude less than the common dose limit for crystallography studies which is 2×10^7 grays (Henderson and Schertler 1990) and about 13 times higher than the dose required to produce mild brain damage in duck embryos (Dilmanian et al. 2001). Synchronization of motor speed and readout time was critical in bidirectional scans in order to avoid misalignment of subsequent lines in the image. To avoid scanning times of more than 7 h, each half brain slice was mapped in segments that were later digitally reassembled.

To further increase scanning speed, new hardware was developed by collaborators at the SSRL, to scan with essentially no dead time between readouts. Conceptually, an entire line of data was collected into a local memory area and transferred to the control computer at the end of each line. The hardware used a programmable timer to precisely set the data measurement time and internal data buffers to decouple the measurement timing from the data transfer process. Electronics were implemented in a Xilinx Virtex-4 field programmable gate array featuring an embedded PowerPC microprocessor. The embedded system was built using Xilinx Embedded Development Kit software. The peripheral device contained a 32 bit timer with 10 ns resolution, sixteen 32 bit counters with a maximum count rate of 10 MHz, data point counter and trigger and interrupt logic. The peripheral device was implemented in very high speed integrated circuit hardware description language. At the end of each measurement, additional counter logic stored the measurement results in the buffer register and started the next measurement with no delay. An interrupt was generated after each measurement, and the microcontroller moved data from registers to large (8 MB) secondary buffers. A lower priority software process transferred the buffered data to the computer, so any delays at the communication

link or host computer did not affect the data acquisition timing. In addition to programmable measurement timing and input/output polarity, the electronics could convert data to 16 bit values and send measurement results only from specified counters to reduce the amount of transferred data.

Using this system, scanning speed was increased from 1.75 mm s^{-1} to 7 mm s^{-1} corresponding to a count time of 5.7 ms per 40 μm pixel. This enabled us to map the basal ganglia in 0.8 hours (Figure 14) as compared to the same sized area in 3.7 hours (Figure 11). At 3×10^{10} photons s^{-1}, this was sufficient to detect the Kα signal of iron, copper and zinc and to produce a high-quality image.

3.3.2 Image Analysis

For each element, a two-dimensional matrix (width × height) of signal counts was obtained. Data were plotted as elemental maps using Interactive Data LanguageTM (ITT Visual Information Systems). Fluorescence was normalized to take into account fluctuations in the intensity of the incoming X-ray beam. The fluorescence signal from metal-rich contaminant particles was reduced to the mean value of all pixels plus three standard deviations. While the plastic sheet protector (400 μm total thickness) contributed significantly to scatter (~46%), it kept the heavy brain slices from sagging during imaging. Counts contributed by a single thickness (200 μm) of plastic overlayer were removed using IDL.

3.3.3 Metal Quantification

Normalized fluorescence for each metal in N and PD brains was calculated within a standard 30 × 30 pixels box using IDL software. Normalized fluorescence is the fluorescence detected from the illuminated tissue volume normalized by the combined elastic and Compton scatter from the same region. This would be proportional to the amount of the fluorescing element per mass of tissue. The Mann–Whitney test was employed to determine if differences in pixel intensity between N and PD metal measurements were statistically significant. The median pixel intensity and the standard deviations for each box were plotted (Figure 12).

3.3.4 Clinical Information

Two brains were obtained from the Stanford University Medical Center, Stanford, CA, USA. The first was from an 80 year old Caucasian female who died of pneumonia. Examination by Dr. Hannes Vogel, a certified neuropathologist at Stanford University Medical Center, revealed no overt changes and the brain was assessed as normal. The second was obtained from a 70 year old Caucasian male, who died of respiratory failure secondary to neurological decline. The patient had been diagnosed with PD prior to death and pathologic examination was consistent with this diagnosis. Institutional review board approval was obtained and provided to SSRL prior to the commencement of the study. The experiment was compliant with the Health Insurance Portability and Accountability Act Privacy Rule and the patients' identities were not known to any of the authors.

Additional human tissue was obtained from the NICHD Brain and Tissue Bank for Developmental Disorders at the University of Maryland, Baltimore, Maryland, under contracts N01-HD-3-3368 and N01-HD-4-3383. Ethics approval (# Bio 07-75) was obtained from the University of Saskatchewan. A small coronal section of a control forebrain (N2) was from a 15 year old Caucasian female who died in a motor vehicle accident.

3.3.5 Preparation of Brain Slices

Brains were fixed and stored in buffered formalin. Brains were manually sliced with a knife and each slice was sealed in a metal-free plastic sheet protector (A-10CR, Itoya Ltd). The N brain slice was half of a coronal section of the forebrain through the genu of the internal capsule, rostral tip of dorsal thalamus and rostral third of the hypothalamus. The matching PD slice was slightly caudal to the N brain. The midbrain was sliced through the inferior colliculus, trochlear nucleus and superior cerebellar peduncle with the matching PD being slightly cranial. N2 was a coronal section of the forebrain through the basal ganglia at the level of the anterior commissure and rostral aspect of the hypothalamus.

3.4 Results

This method takes advantage of bright synchrotron X-rays and the rapid-scan technology described above. Brain slices were raster scanned across a small, collimated X-ray beam. The fluorescence signal of several metals was recorded simultaneously resulting in elemental maps of the brain slices. Maps showing the abundance and location of iron, zinc and copper were obtained in comparable brain slices from two subjects of advanced age, one normal (N) and one with PD (PD), and in a small section from a normal young brain (N2).

In many parts of the brain, high iron generally corresponded to low zinc and vice versa (Figure 10), seen most clearly in the basal ganglia (Figures 10B, C and 11A–C). The relative amount of each metal in N and PD was quantified by region (Figure 12A, B). Levels of zinc were slightly lower in PD across all regions ranging from 8% lower than N in the caudate to 30% in the internal capsule and putamen (Figure 12B). In contrast, iron levels varied widely by region (Figure 12A). The greatest differences between N and PD were seen in the basal ganglia (Figure 11A, D) and midbrain (Figure 13A, E), the areas that are most affected in PD. For example, the caudate had 60% less iron whereas the substantia nigra had 40% more (Figure 12A). Overall, the iron maps were in agreement with high-resolution MR imaging (Fatterpekar et al. 2002). A copper map was collected along with iron and zinc for N2 basal ganglia, N and PD midbrain (Figures 14B, F and 13). Consistent with previous studies, brain copper was less abundant than iron and zinc (Dexter et al. 1989). The comparative metal distribution and content by region is detailed below.

3.4.1 Cortex

Cortical iron and zinc localization was similar in PD and N with a prominent broad band, rich in both iron and zinc (Figure 10D arrows), corresponding to the heavily myelinated subcortical white matter (U fibers).

3.4.2 Basal Ganglia

In N, N2 and PD, the basal ganglia were very rich in iron (Figures 11A, D and 14B), in keeping with the known iron content of this brain region (Drayer 1988; Morris et

al. 1992; Morris et al. 1992). Iron-rich structures resembling neurites and neuronal cell bodies were seen in the putamen, head of the caudate nucleus and the lateral and medial globus pallidus in all brains. The laminae that define the limits of the putamen and globi pallidi were particularly metal-rich in PD (Figure 11D–F). PD iron (Figure 11F, arrows and inset) showed a gradient surrounding large vessels adjacent to the putamen that was not seen around similar-sized vessels in the N brain (Figure 11A) or in the PD midbrain (Figure 13E). No gradient of perivascular zinc was observed in N or PD.

3.4.3 Midbrain

Iron levels in both N and PD were highest in the substantia nigra when compared to other parts of the midbrain (Figure 13A, E). Measured in the medial substantia nigra, the PD midbrain had 40% more iron than the similar region in the N midbrain (Figures 13A, E and 12A). Zinc distribution was similar in N and PD (Figure 13C, G), but overall zinc was lower (Figure 12B). Since N and PD sections were at slightly different levels, this could affect the interpretation.

In general, copper and iron co-localized in midbrain (Figure 13A, B, E, F, arrowhead shows debris). While not abundant in midbrain, copper was seen in the substantia nigra and inferior colliculus (Figure 13B, H). While copper levels across these areas were similar in N and PD, the midline of the substantia nigra showed irregular low copper regions in PD co-localized with regions of very high iron.

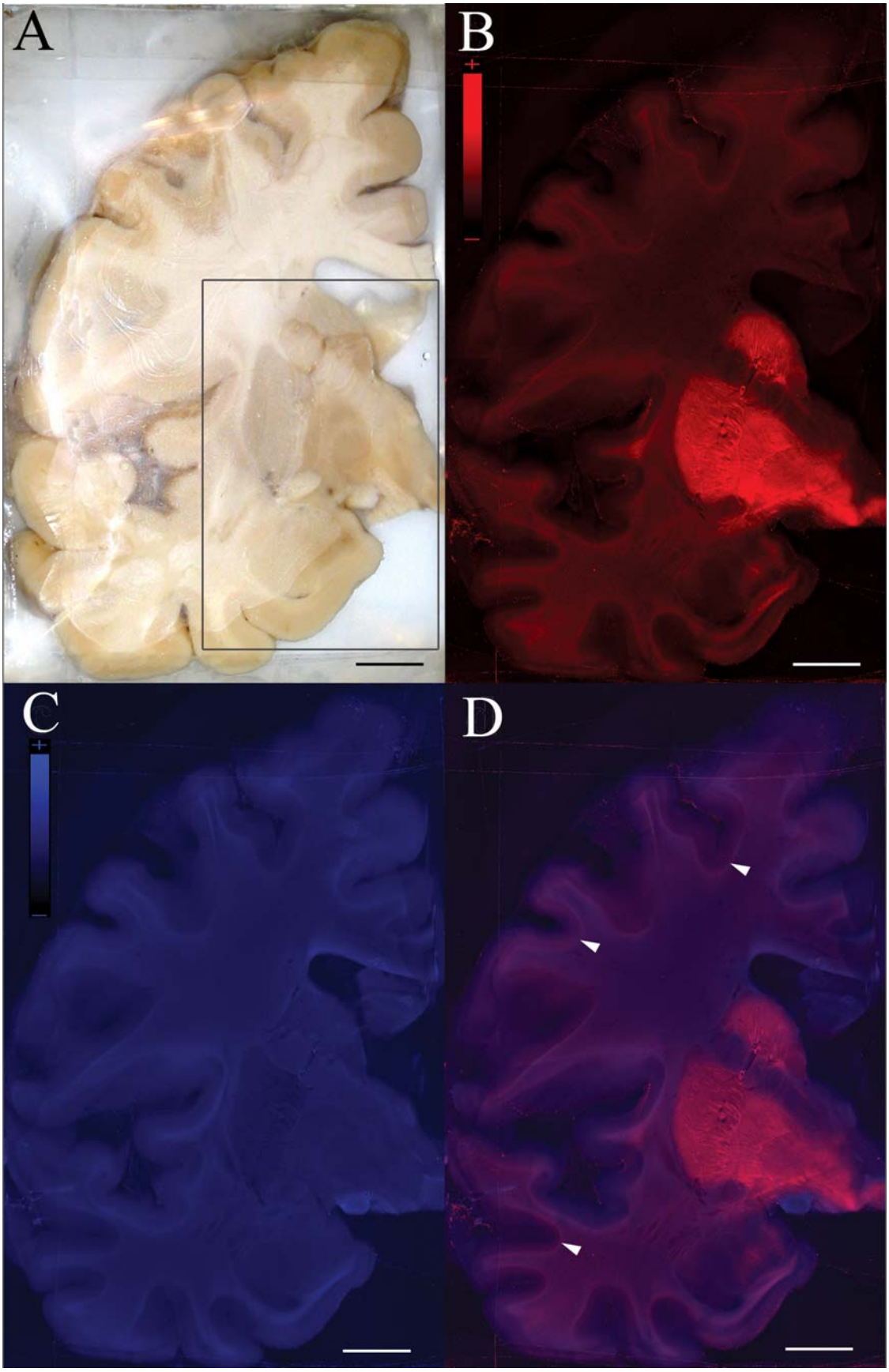
A
B
+
–
C
+
–
D

Figure 10. Metal levels in the brain vary widely by region. Normal (N) human forebrain, coronal section: A. optical image; B. iron map; C. zinc map; D. overlay of iron (red) and zinc (blue); square, area magnified in figure 11(A–C); arrow heads, subcortical white matter; scan speed 22.8 ms per pixel; scale bar = 7.5 mm; color scales (B, C) represent the normalized total Kα fluorescence counts, proportional to total metal present, from black (lowest) to color (highest).

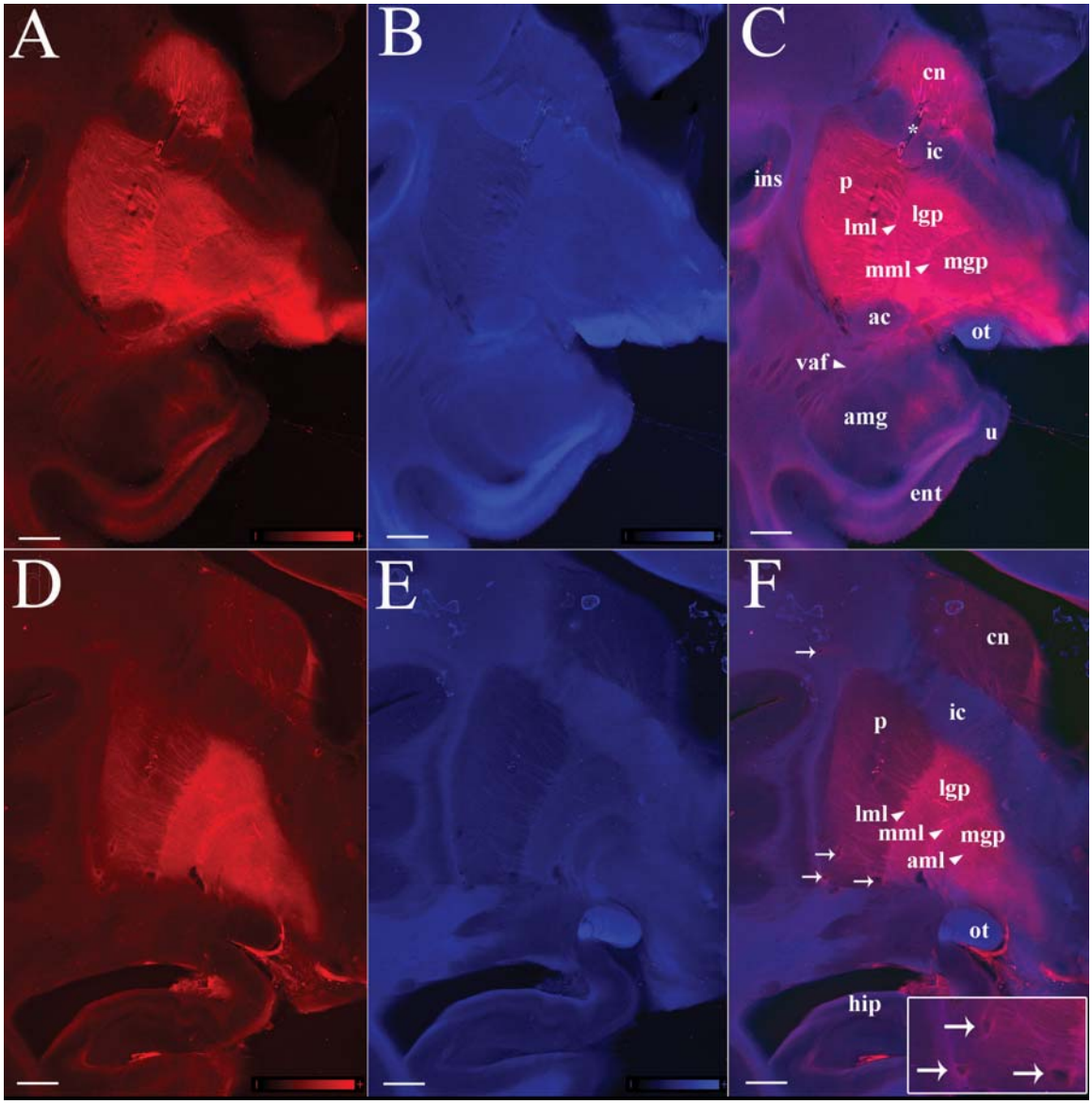
A
B
C
cn
*
ic
ins
p
lml
lgp
mml
mgp
ac
ot
vaf
amg
u
ent
D
E
F
cn
p
ic
lgp
lml
mml
mgp
aml
ot
hip

Figure 11. Metal content is abnormal in PD basal ganglia. Basal ganglia, coronal section normal (N) brain A–C (expanded view of Figure 10); PD brain D–F; A, D. Iron maps; B, E. Zinc map; C, F. Overlay of iron and zinc; cn – caudate nucleus; p – putamen; lgp – lateral globus pallidus; mgp – medial globus pallidus; lml – lateral medullary lamina; mml – medial medullary lamina; aml – accessory medullary lamina; ic – internal capsule; ins – insula; ot – optic tract; ac – anterior commissure; vaf – ventral amygdalofugal fibers; amg – amygdaloid nucleus; u – uncus; ent – enthorinal cortex; hip –hippocampus; * –blood vessel; arrows – perivascular iron (a magnified view of the three blood vessels in the putamen indicated by arrows is shown in inset); scale bar = 5 mm; color scales (A, B, D, E) represent the normalized total Kα fluorescence counts, proportional to total metal present, from black (lowest) to color (highest).

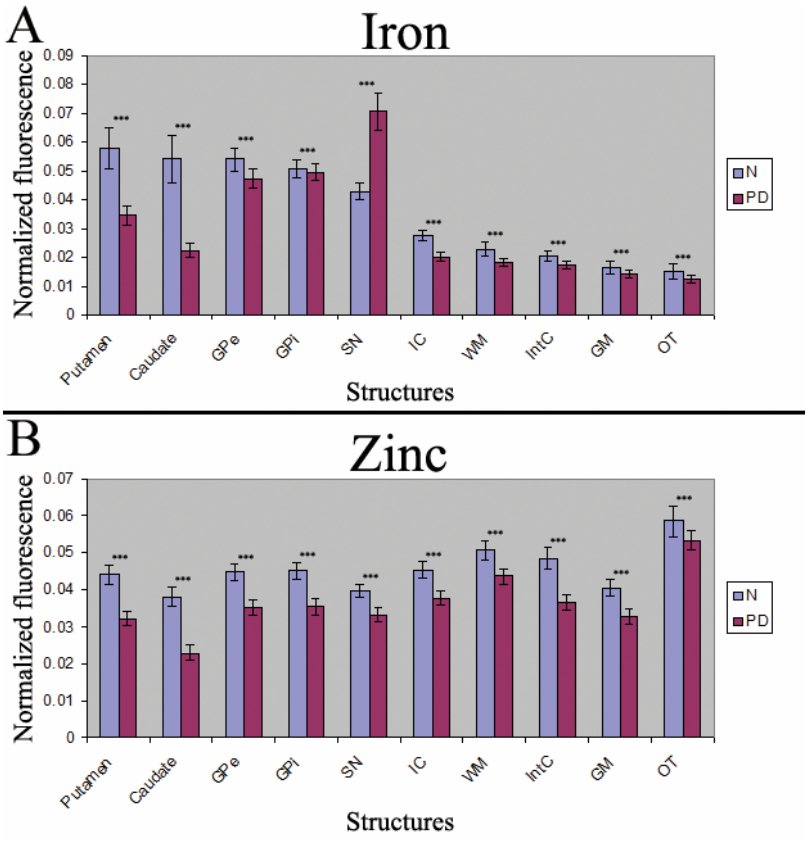

Figure 12. Metal levels are abnormal in selected regions of PD brain. Comparison of the normalized fluorescence (columns) in N (blue) and PD (magenta) by region. A. Iron fluorescence and B. zinc fluorescence. Note that the two plots do not compare Fe with Zn. The Mann–Whitney test was employed to determine if differences between N and PD metal measurements were statistically significant. Columns indicate median values of 900 individual pixels (30 × 30 square). Error bars indicate standard deviations. *** signifies extremely significant differences ($P < 0.0001$) between measurements. More extensive studies are required to determine which differences are disease related. (Note: normalized fluorescence is the fluorescence detected from the illuminated tissue volume normalized by the combined elastic and Compton scatter from the same region. This normalized value is proportional to the amount of the fluorescing element per mass of tissue.)

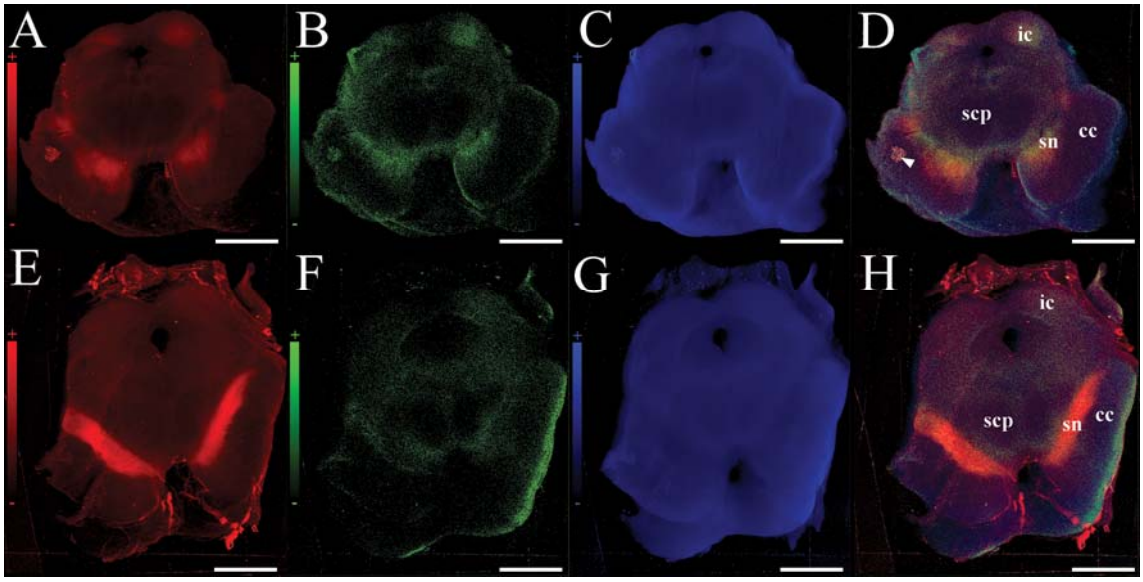

Figure 13. Metal distribution is abnormal in PD midbrain. Transverse section, normal (N) midbrain (A–D) and PD midbrain (E–H); A, E. Iron map; B, F. Copper map; C, G. Zinc map; D, H. Overlay of iron, copper and zinc; sn – substantia nigra; cc – crus cerebri; scp – spinocerebellar peduncle; ic – inferior colliculus; scan speed 22.8 ms per pixel; color scales (A, B, C, E, F, G) represent the normalized total Kα fluorescence counts, proportional to total metal present, from black (lowest) to color (highest); scale bar = 5 mm.

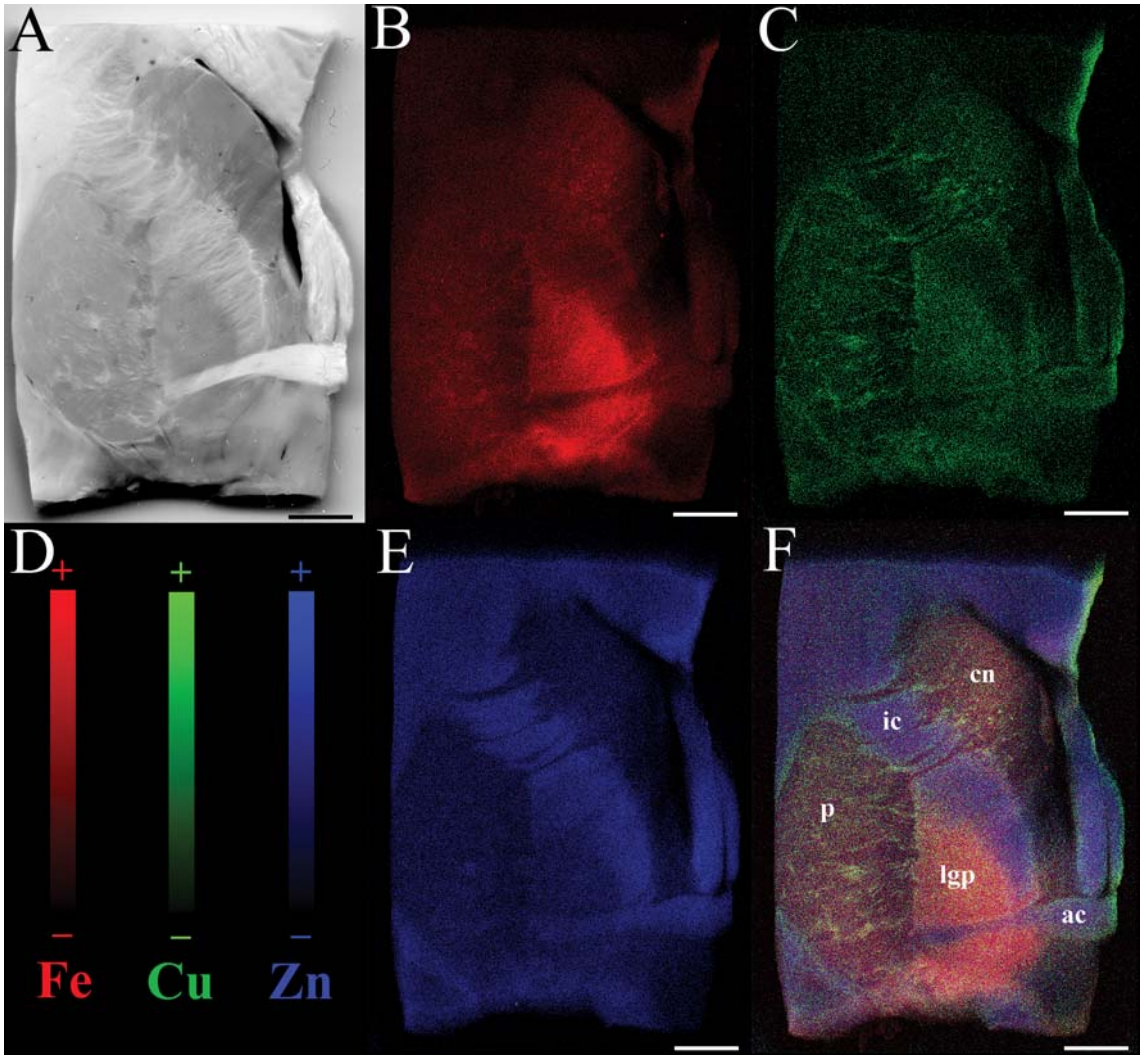

Figure 14. Increased scan speed still produces high-quality metal maps. Basal ganglia, coronal section, normal (N2) brain collected using a rapid readout system; scan speed 5.7 ms per pixel; A. Optical image; B. Iron map; C. Copper map; D. Intensity scales represent the normalized total Kα fluorescence counts, proportional to total metal present, from black (lowest) to color (highest); E Zinc map; F. Overlay of iron, copper and zinc; cn – caudate nucleus; p – putamen; lgp – lateral globus pallidus; ic – internal capsule; ac – anterior commissure; scale bar = 5 mm.

3.5 Discussion

This chapter describes results obtained using a new synchrotron approach that offers significant advantages over analytical or histological methods in localizing and quantifying brain metals. Both RS-XRF and traditional point-to-point XRF imaging can non-destructively, quantitatively and simultaneously map multiple metals with the added ability to speciate metals at points of interest. RS-XRF adds the capability of mapping large samples on a practical time scale (2005; Service 2006; Bergmann 2007).

Unlike conventional histology sections, XRF samples are not dehydrated or embedded, and therefore the same sample can be subsequently processed for histology or immunohistochemistry if desired. Formalin fixation stops post-mortem degradation and enables collection of elemental maps at room temperature. The major metals iron, copper and zinc (Chua-anusorn et al. 1997; Bush 2000) as well as nickel and chromium (Gellein et al. 2008) are well retained in fixed tissues even after long periods of storage, but substantial leaching of arsenic, cadmium, magnesium, rubidium and antimony has been measured (Gellein et al. 2008). However, post-mortem degradation, fixation and leaching of some elements could change metal chemistry making the interpretation of X-ray Absorption Near Edge Structure spectra collected from human autopsy material problematic. Animal brain, flash-frozen at the time of death, would yield spectra that better reflect *in vivo* metal chemistry. The large size of these brain maps also makes them ideal for direct comparison with magnetic resonance images (McCrea et al. 2008).

Testing hypotheses and discovering previously unrecognized metal-associated pathologies require a large sample size and/or multiple samples from different brain regions or different individuals. For example, I saw elevated perivascular iron in PD (Figure 11F and inset). To appreciate the extent and generality of this finding, large brain maps from multiple subjects would be needed and such studies are now feasible with RS-XRF.

Another advantage of RS-XRF over other methods is that multiple metals can be easily co-localized and linked to known brain structures, as exemplified by the localization of copper in the midbrain (Figure 13B, F). In a larger analytical study, Dexter (Dexter et al. 1989; Dexter et al. 1991) found that the substantia nigra copper content in PD was lower than normal. My data support Dexter's analyses but also show that

copper's spatial distribution in the midbrain is complex. Subtle changes in copper distribution would be extremely difficult if not impossible to detect by other means and could be important in PD pathogenesis.

PD was chosen for the validation study because iron has been shown to accumulate in dopaminergic neurons in the substantia nigra pars compacta (Jellinger et al. 1990; Sofic et al. 1991). This excess iron promotes oxidative generation of free radicals through the interaction with α-synuclein (Hsu et al. 2000; Ostrerova-Golts et al. 2000; Turnbull et al. 2001) and neuromelanin leading to neurodegeneration. RS-XRF mapping confirmed both the abnormal amount and location of excess iron in the midbrain that are characteristic of PD.

Although the setup used here did not collect full MCA spectra, rapid scanning does not preclude collecting MCA spectra for the post-mapping detection of additional or unexpected elements. A possible way of collecting full spectra might include the use of a buffered memory option using digital electronics from XIA.

RS-XRF is a new and powerful tool that makes systematic studies of brain metals practical. It can be applied to any human or animal tissue and I foresee important applications in testing whether a metal chelator designed to remove a particular metal disrupts the levels of others. Using animal models, RS-XRF also has great potential to improve our understanding of global metal metabolism and the inter-relationships between metals. With rapidly advancing beamline technology at third-generation synchrotrons, it should be possible to map very large sections in a matter of a few minutes, making systematic RS-XRF studies on serial slices of whole organs practical.

RS-XRF is the ideal tool to interrogate the possible involvement of metals in FRDA pathology, not only in neurodegeneration but also in cardiac degeneration. However, since the disease is examined at a very advanced stage in the case of post-mortem formalin-fixed human specimens RS-XRF will not be able to demonstrate whether the metals are the cause or the consequence of the degenerative process. Metal maps of brains and hearts from FRDA mouse models at various stages of the disease will likely answer this dilemma.

CHAPTER IV

Iron, Copper and Zinc Distribution of the Cerebellum

4.1 Introduction

Spinocerebellar ataxias (SCA) are a group of progressive ataxias in which degeneration of the spinal cord tracts is associated with cerebellar degeneration (Greenfield 1954). FRDA is the most common autosomal recessive ataxia accounting for up to half of the all hereditary ataxias (Pandolfo 1998). The neuropathological hallmark of FRDA is the degeneration of the posterior columns and loss of the large myelinated axons in the dorsal roots as a consequence of the degeneration of large neurons in the dorsal root ganglia (Greenfield 1954; Hughes et al. 1968; Oppenheimer 1979; Lamarche et al. 1984). Degeneration of the dorsal nuclei of Clarke, cuneate and gracile nuclei and spinocerebellar tracts completes the sensory neuropathy (Greenfield 1954; Oppenheimer 1979; Lamarche et al. 1984). Ataxia in FRDA is the consequence not only of this sensory neuropathy but also of the cerebellar degeneration. Severe neuronal loss in the dentate nuclei, marked atrophy of the superior cerebellar peduncles and moderate Purkinje cell loss in the cerebellar cortex (Greenfield 1954; Oppenheimer 1979; Lamarche et al. 1984) show that the cerebellum is a major site involved in the FRDA neuropathology. Although Magnetic Resonance *in vivo* studies have shown increased iron in the dentate nucleus of FRDA patients (Waldvogel et al. 1999; Boddaert et al. 2007), biochemical studies of post-mortem tissues have failed to reveal an increase in iron (Koeppen et al. 2007). Thus the involvement of iron and oxidative stress in FRDA cerebellar neurodegeneration remains controversial.

The cerebellum serves as a major integrative center for the coordination of muscular activity, facilitation of movement, and motor planning. Cerebellar lesions result in ataxia, dysmetria, dysarthria, and oculomotor impairment (Klockgether 2000). Complex connections between the dentate nucleus, thalamus, basal ganglia, and prefrontal cortex support the hypothesis that the cerebellum is also involved in cognitive functions (Middleton and Strick 1994; Dum and Strick 2003), and indeed, cognitive impairment is associated with cerebellar pathology (Corben et al. 2006). Many disorders presenting with cerebellar degeneration are members of the continually growing family of neurodegenerative diseases involving excess central nervous system accumulation of metals. These include not only Friedreich's ataxia, but also Wilson's disease, Huntington's disease and aceruloplasminemia (Byers et al. 1973; Starosta-Rubinstein et

al. 1987; Okamoto et al. 1996; Bartzokis et al. 1999; Koeppen et al. 2007). Metal deficiency can also lead to neurodegeneration involving the cerebellum, as exemplified by Menkes' disease (Williams et al. 1978).

Although an active area of research, many questions remain about how metal imbalance contributes to neurodegeneration (Cuajungco and Lees 1997; Zecca et al. 2004; Madsen and Gitlin 2007). Knowing the macroscopic metal distribution of the normal cerebellum is an important step towards better understanding the role metals play in the pathogenesis of cerebellar degeneration and how neurodegenerative diseases change cerebellar metal distribution and metabolism.

Histochemistry has long been the gold standard for localizing metals in brain slices. However, Perls' and Turnbull's methods are not able to detect heme iron (Gomori 1936; Meguro et al. 2007), copper histochemistry lacks sensitivity and specificity (Pilloni et al. 1998; Henwood 2003), and zinc histochemistry detects only part of the tissue zinc pool (Danscher et al. 1985; Lopez-Garcia et al. 2002).

In contrast, RS-XRF has been successfully employed to non-destructively and simultaneously map multiple metals in all chemical forms and oxidation states, whether protein-bound or free, or intracellular or extracellular in large samples on a practical time scale (McCrea et al. 2008; Gh Popescu et al. 2009).

In this chapter RS-XRF is used to study the macroscopic distribution of iron, copper, and zinc in sagittal and axial views of the normal cerebellum in both a young subject with no neurodegenerative disease and an older subject with PD but without identifiable cerebellar pathology.

4.2 Hypothesis and Research Objectives

4.2.1 Hypothesis

Simultaneously-collected metal XRF maps of the cerebellum allow anatomical structures to be observed due to the different distribution and regional variation in the iron, copper and zinc content.

4.2.2 Research Objectives

Map the distribution of iron, copper and zinc in the cerebellar cortex, cerebellar white matter and dentate nucleus in fixed slices of cerebellum with no identifiable pathology using RS-XRF.

4.3 Materials and Methods

4.3.1 Tissue Samples, Clinical and Neuropathological Information

Frozen sagittal slices of normal cerebellum at the level of the dentate nucleus from a Caucasian woman were obtained from National Institute of Child Health and Human Development (NICHD) Brain and Tissue Bank for Developmental Disorders at the University of Maryland, Baltimore, Maryland, under contracts N01-HD-3-3368 and N01-HD-4-3383 with ethics approval from the University of Saskatchewan (#BioReb 07-75). Prior to mapping, they were fixed in buffered formalin. The patient died of oxycodone intoxication at the age of 23. Formalin-fixed axial slices through the cerebellum at the level of the dentate nucleus from a Caucasian man were obtained from the Saskatoon Health Region Movement Disorders Clinic (ethics approval # BioReb 06-250). The patient died from renal failure at age 70. Clinical and pathological examinations confirmed a diagnosis of PD. The post-mortem interval collection times (PMI) were 19 and 10 hours, respectively.

Gross examination of the cerebella of both patients was unremarkable. Microscopic examination of hematoxylin and eosin (HE) (Thompson and Hunt 1966), luxol fast blue/HE (Thompson and Hunt 1966) and modified Bielschowsky (Yamamoto and Hirano 1986) stained 5 μm thick paraffin sections of the dentate nucleus, cerebellar deep white matter and cerebellar cortex revealed no pathological abnormalities in either case.

4.3.2 Rapid-Scanning X-ray Fluorescence Mapping

RS-XRF imaging was performed at wiggler beam line 10-2 at the Stanford Synchrotron Radiation Lightsource (SSRL). The incident X-ray beam was set to an energy of 13 keV using a Si(111) double crystal monochromator in order to excite the K-shell of the first transition row and lighter elements. Formalin-fixed brain slices 2 mm thick were cut with a commercial meat slicer (Hobart, circular, non-serrated blade with a

diameter of 30 cm), sealed in metal-free plastic sheet protectors (Itoya) and mounted vertically at 45° to the incident X-ray beam and 45° to the detector. The sample was translated rapidly in the beam in a raster pattern with continuous motor motion. Data was collected on the fly in both horizontal directions at a rate corresponding to a travel distance of 40 μm per readout, with count times of ~6 ms per 40 μm horizontal raster. A single-element Vortex-EX® silicon drift X-ray detector (SII NanoTechnology USA) was placed at a 90° angle to the beam to minimize signal due to scatter. Energy windows were set so as to resolve the Kα from the Kβ fluorescence lines of adjacent elements. Details of the imaging setup have been previously described (Gh Popescu et al. 2009).

Image analysis was performed using Interactive Data Language™ (ITT Visual Information Systems) as previously described (Gh Popescu et al. 2009). Fluorescence was normalized to take into account fluctuations in the intensity of the incoming X-ray beam.

4.4 Results

4.4.1 Metal Maps of the Dentate Nucleus and Surrounding White Matter

Although iron and zinc are more abundant than copper overall, they are distributed in a similar way in the central and subcortical white matter of the cerebellum in both the young and older brains. While copper is evenly distributed (Figures 15B and 16B), iron and zinc levels increase towards the subcortical white matter (Figures 15A, C and 16A, C).

Within the cerebellum, the metal maps (Figures 15 and 16) show the characteristic convoluted shape of the dentate nucleus, seen most clearly in the sagittal slice (Figure 16). The dentate nucleus is rich in iron and copper (Figures 15A–C and 16A–C). Some copper colocalizes with iron (Figure 15D) and with iron and zinc (Figure 16D). However, the tricolor maps (Figures 15D and 16D) show that copper is distributed in the periphery of the dentate nucleus, while iron and zinc are situated at its interior. The dentate nucleus is not as easily resolved in the zinc map of the axial slice because it has a similar or lower zinc content than the surrounding white matter (Figure 15C).

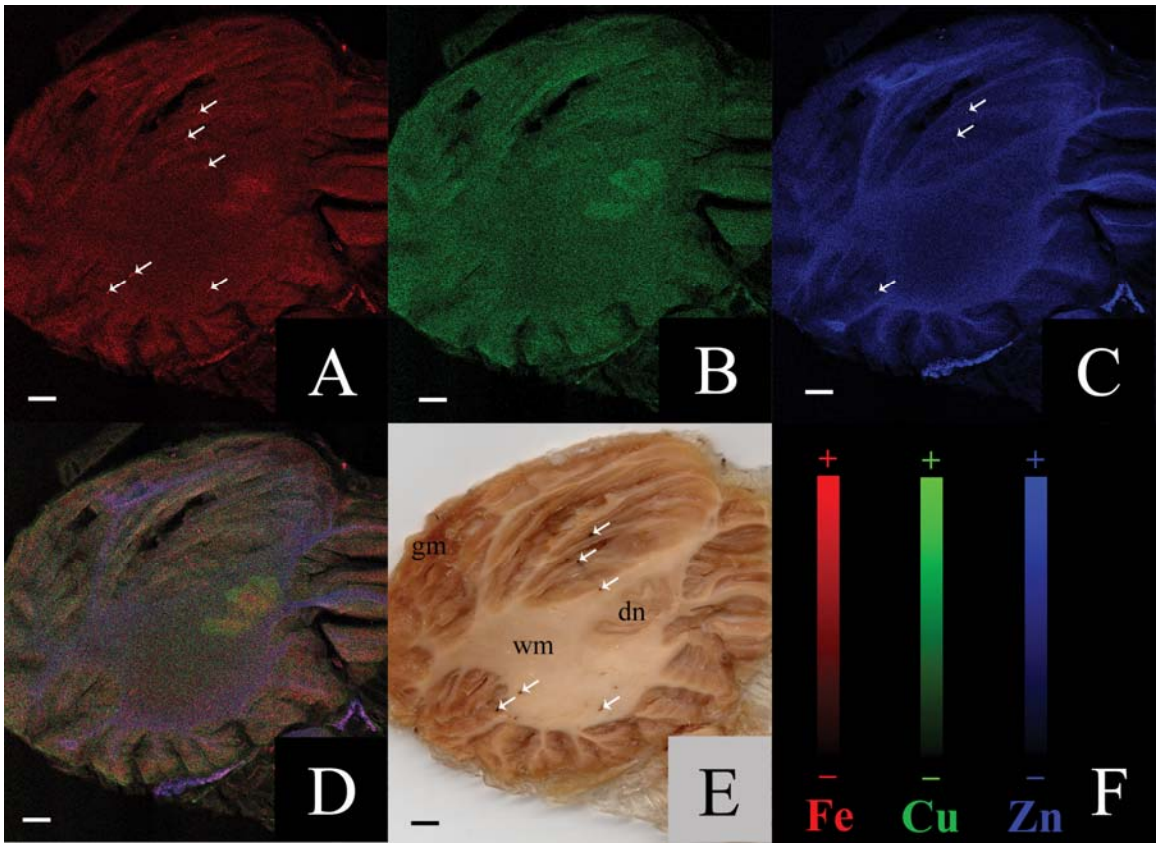

Figure 15. Iron and copper are most abundant in the dentate nucleus, while zinc is the richest in the cortical white matter of the cerebellum; cerebellum, axial section, Parkinson's disease without identifiable cerebellar pathology; A. Iron map; B. Copper map; C. Zinc map; D. Overlay of iron (red), copper (green), and zinc (blue); E. Gross axial section of the cerebellum; F. Color scales representing the normalized total Kα fluorescence, proportional to total metal present, from black (lowest) to color (highest); dn – dentate nucleus, gm – gray matter, wm – white matter, arrows blood vessels; scale bar = 5 mm.

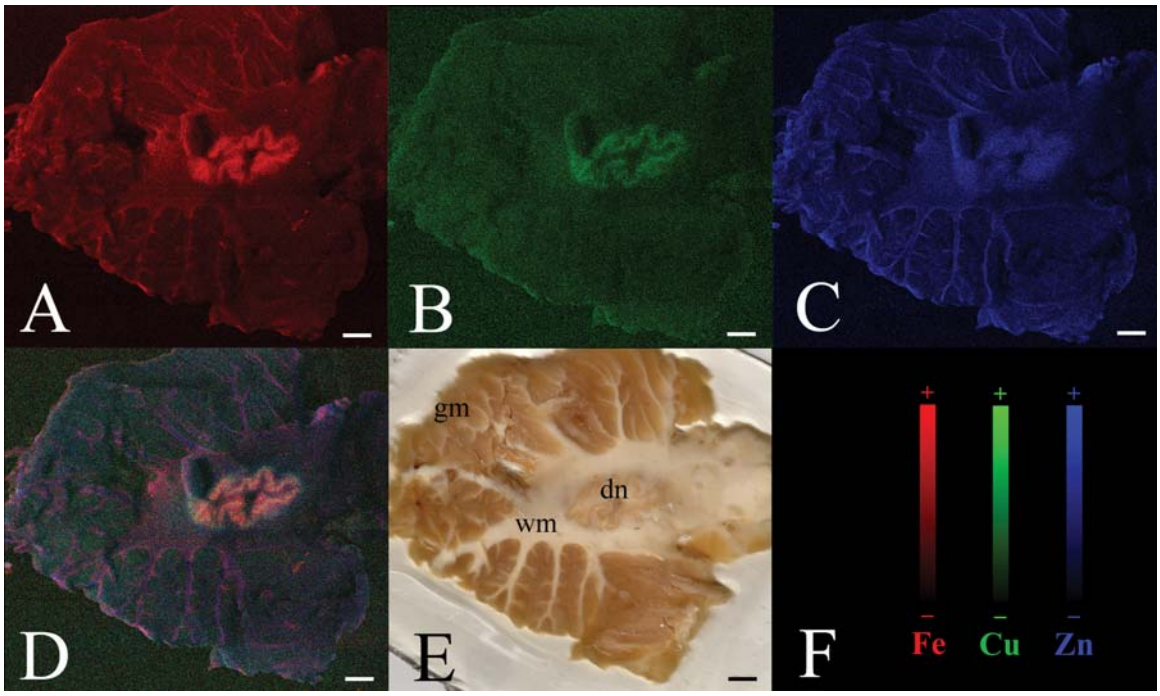

Figure 16. Metal maps show a complex distribution of iron, copper, and zinc in the cerebellum; cerebellum, sagittal section, oxycodone intoxication; A. Iron map; B. Copper map; C. Zinc map; D. Overlay of iron (red), copper (green), and zinc (blue); E. Gross sagittal section of the cerebellum; F. Color scales representing the normalized total Kα fluorescence, proportional to total metal present, from black (lowest) to color (highest); dn – dentate nucleus, gm – gray matter, wm – white matter, scale bar = 5 mm.

4.4.2 Metal Maps of the Cerebellar Cortex

In the cerebellar cortex, the high iron and zinc levels of the white matter are in sharp contrast with the low metal content of the gray matter (Figures 15A, C and 16A, C). The striking branching pattern of the cerebellar white matter (arbor vitae) is clearly resolved on the basis of metal content in the sagittal slice (Figure 16A, C). In contrast, copper is more evenly distributed (Figures 15B and 16B), with the subcortical white matter slightly richer than the central white matter (Figure 15B). The gray matter of the cerebellar cortex cannot be readily distinguished from the white matter on the basis of copper content (Figures 15B and 16B).

Blood vessels filled with iron and zinc-rich material are clearly seen traversing the white and gray matter of the cerebellum (Figure 15A, C, E, arrows).

4.5 Discussion

RS-XRF is uniquely suited for mapping brain metals. It is the only technique that permits quantitative simultaneous mapping of multiple metals in the same tissue slice, and it detects all chemical forms of each metal (Gh Popescu et al. 2009). Used as a tool for elemental analysis, RS-XRF provides spatial resolution that is far superior to conventional methods in which excised cubes of tissue are dissolved for bulk analytical analysis. Used as an imaging method, RS-XRF shows all metals simultaneously without damaging the sample, thus surpassing all conventional "single-metal" staining methods. This capability to see how the dysregulation of one metal affects others in adjacent tissues may prove to be the key to understanding global metal regulatory pathways in the brain. RS-XRF is a powerful tool that makes systematic studies of metals in whole cerebellum and/or multiple samples or different individuals practical and sets the stage for further investigations of neurodegenerative diseases.

This study focuses upon the normal cerebellum from a young patient and an older individual to provide a baseline for future studies. Despite the different age, sex, and PMI of the two patients and different planes of section, the metal distribution of the two cerebella is very similar. RS-XRF metal maps provide new information about the relative amount and location of iron, copper, and zinc in the cerebellum which is known as one of the brain structures richest in iron (Hock et al. 1975; Morris et al. 1992), copper (Warren

et al. 1960; Dexter et al. 1989; Duflou et al. 1989; Rajan et al. 1997), and zinc (Dexter et al. 1989; Rajan et al. 1997).

Our results agree with previously published quantitative (Warren et al. 1960; Hock et al. 1975; Duflou et al. 1989) and histochemical (Morris et al. 1992) analyses showing that dentate nucleus has the highest iron (Figures 15A and 16A) and copper (Figures 15B and 16B) content in the cerebellum and is also very rich in zinc (Figure 15C). Unlike histochemical iron stains, RS-XRF maps all chemical forms and oxidation states of iron. While the iron map of the sagittal slice (Figure 16A) closely reflects the previously described distribution of non-heme iron (Morris et al. 1992), the cerebellar cortex has a higher iron content, and iron in the normal convoluted shape of the dentate nucleus is more intense than histochemistry reveals. This may indicate that heme iron forms a larger proportion of total iron in these regions or that the processing procedures required for conventional histology leach or redistribute some iron from the dentate nucleus and cortex.

XRF maps also provide additional information about the relative location of copper and iron within the dentate nucleus (Figures 15D and 16D). The copper is situated towards the periphery of the nucleus, the iron is located towards its interior, and only part of the copper colocalizes with iron. Studies of the primate dentate nucleus reveal different size neurons arranged into zones containing different neurotransmitters (Chan-Palay 1977). This could explain metal segmentation of the dentate, but high resolution studies with X-ray microprobe are required to localize copper to specific neurons.

The dentate nucleus can be localized in the sagittal but not the axial section based on zinc content (Figure 15C). This difference may represent real differences between neuronal subpopulations that differ between the sections or could be related to PD or to age-related differences between the two. The dentate nucleus in humans has an older dorsomedial portion (paleodentate) and a newer ventrolateral portion (neodentate). Neurons in the two subdivisions of the dentate nucleus have different connections and sizes (Chan-Palay 1977; Middleton and Strick 1994; Parent 1996) and could have different zinc contents. Of the metals, free zinc is relatively abundant in some classes of neurons, especially in the presynaptic terminals (Mocchegiani et al. 2005). While it is hard to correlate the sagittal orientation of the dentate with the available unfolded

functional maps because of different planes of section, the part of dentate nucleus present in the axial section (Figure 15) corresponds to the nonmotor domain concerned with cognition and visuospatial function (Dum and Strick 2003). Thus, the different zinc content may also reflect neuronal populations belonging to different dentate output channels.

The metal segmentation of the dentate with the copper located towards the periphery and iron and zinc towards its interior (Figures 15D and 16D) is a new and very interesting observation. It is known that the dentate nucleus is affected in a wide range of neurodegenerative diseases. The presence of two neuronal populations with different metal contents in the dentate could prove to be very important since these neurons might possess different susceptibilities to neurodegeneration similar to neurons in pars compacta and pars reticulata of substantia nigra and their different susceptibility to neurodegeneration in PD. The dentate nucleus is a major site of neurodegeneration in FRDA (Greenfield 1954; Oppenheimer 1979; Lamarche et al. 1984) and involvement of iron in FRDA cerebellar degeneration is controversial. However, this might be explained by the different metal content of lesions at different stages of disease (Popescu et al. 2009a). By interrogating a potentially active site of degeneration, *in vivo* Magnetic Resonance studies show increased iron in the dentate nucleus of FRDA patients (Waldvogel et al. 1999; Boddaert et al. 2007) while biochemical studies of postmortem tissues fail to reveal an increase in iron (Koeppen et al. 2007) possibly because of addressing lesions in very advanced stages of neurodegeneration.

Compared to other areas of the brain, elemental analyses of cerebellar metals are few, and direct comparison between different methodologies is difficult (Haacke et al. 2005). However, when the increased water content of gray matter is taken into account, my results roughly agree with published elemental analyses (Duflou et al. 1989). In contrast, RS-XRF has little sampling error because all elements within a 50-μm spot are measured continuously across the entire sample to a depth of 0.55, 0.63, and 0.74 mm for iron, copper, and zinc, respectively.

I show that the iron content varies within different regions of the white matter with the subcortical white matter having more iron than the white matter surrounding the dentate nucleus. Subcortical white matter also has more iron than the cortical gray matter.

Cerebellar gray and white matter are very rich in zinc (Hock et al. 1975; Duflou et al. 1989), with the subcortical white matter containing the highest zinc levels (Figures 15C and 17C). The normal zinc status of the brain and the delicate zinc/copper balance have to be maintained since zinc toxicity has been linked to cerebellar demyelinating lesions (Prodan and Holland 2000) and even multiple sclerosis (Schiffer et al. 2001). In contrast, copper is more evenly distributed between central white matter, subcortical white matter, and cortical gray matter (Figures 15B and 16B) of the cerebellum. This could accurately reflect *in vivo* copper, but some post-mortem diffusion could occur. Of the metals, copper is entirely protein bound with little or no free copper present in cells (O'Halloran and Culotta 2000) and only trace amounts of copper leach from formalin fixed tissues even over 18 months of storage (Gellein et al. 2008). Thus, I propose that the distribution of copper in these maps reflects the distribution *in vivo*. The abundant metal presence in the white matter is not totally unexpected since iron (Ortiz et al. 2004; Todorich et al. 2008), copper (Madsen and Gitlin 2007), and zinc (Tsang et al. 1997; Kursula et al. 1999) are essential for myelin synthesis, structure, and maintenance with oligodendrocytes being the main iron repository cells in the brain (Connor and Menzies 1996).

It has been established that the major metals, iron, copper, and zinc (Bush et al. 1995; Chua-anusorn et al. 1997), as well as nickel and chromium (Gellein et al. 2008) are well retained in fixed tissues even after long periods of storage, but substantial leaching of arsenic, cadmium, magnesium, rubidium and antimony has been measured (Gellein et al. 2008). However, it is not known if distribution is affected. The sharp delineation of cerebellar structures based upon iron and zinc content indicates that there is little migration of these metals.

Abundant iron and zinc, but not copper, are associated with cerebellar blood vessels (Figure 15A, C, E, arrows). Some of this appears to be in the vessel wall and some in blood. The ability to see intravascular and perivascular metals is one of the major advantages of RS-XRF (Gh Popescu et al. 2009), since vascular changes are linked to neurodegenerative diseases (Brun and Englund 1986; Faucheux et al. 1999).

The brain is a specialized organ that metabolizes and accumulates metals as part of its normal functioning (Zecca et al. 2004; Bartzokis et al. 2007). Iron, copper, and zinc function as cofactors in essential metalloproteins and are required for oxidative

phosphorylation, neurotransmitter biosynthesis, modulation of neurotransmission, antioxidant defense, nitric oxide metabolism, oxygen transport, and synthesis of proteins, DNA, and RNA (Cuajungco and Lees 1997; Ponka 1999; Madsen and Gitlin 2007). The cerebellum is a major metal repository (Hock et al. 1975; Dexter et al. 1989; Duflou et al. 1989; Morris et al. 1992; Rajan et al. 1997) where large amounts of iron, copper, and zinc coexist and colocalize. The high metal content of the dentate nucleus and cerebellar white matter makes them particularly susceptible to metal-catalyzed oxidative damage, protein aggregation, neurotoxicity, and neurodegeneration (Cuajungco and Lees 1997; Zecca et al. 2004; Madsen and Gitlin 2007). In a rich metal environment, loss of function of metalloproteins and loss of defense against oxidative stress caused by deficiency of one or more metals (Madsen and Gitlin 2007) could also be responsible for neurodegeneration.

CHAPTER V

Synchrotron X-ray Fluorescence Reveals Abnormal Metal Distributions in Brain and Spinal Cord in a Case of Spinocerebellar Ataxia

5.1 Introduction

Degenerative disorders of the cerebellum, its afferent and/or efferent connections result in a characteristic type of irregular, uncoordinated movement called ataxia, which represents the core clinical feature of these conditions. SCA are a group of progressive cerebellar ataxias in which cerebellar degeneration is associated with clearly identifiable involvement of the spinal cord, with degeneration of the spinal tracts leading to sensory loss, diminished / absent tendon reflexes or hyperreflexia and Babinski sign. FRDA (Lamarche et al. 1980; Babcock et al. 1997; Adamec et al. 2000), ataxia with isolated vitamin E deficiency (AVED) (Kaplan 2002), X-linked sideroblastic anemia with ataxia (XLSA/A) (Allikmets et al. 1999; Napier et al. 2005), ataxia-telangiectasia (A-T) (Shackelford et al. 2003; Shackelford et al. 2004) and infantile-onset spinocerebellar ataxia (IOSCA) (Bottomley and Muller-Eberhard 1988; Lönnqvist et al. 2000) are examples of SCA which are caused by or lead to disturbances in iron homeostasis with oxidative damage as a common biochemical feature. Moreover, even though early work suggested a possible dysregulation of copper and zinc metabolism in some SCA, especially FRDA (Barbeau et al. 1984; Huxtable et al. 1984; Shapcott et al. 1984), the involvement of other metals in SCA neurodegeneration has not yet been investigated.

In this chapter, RS-XRF is used to compare the relative amounts and distribution of metals in the brain and spinal cord from a patient with a long history of SCA (type undefined) with a sex and age matched control. My data indicate that not only iron, but also copper and zinc may play a role in SCA physiopathology.

5.2 Hypothesis and Research Objectives

5.2.1 Hypothesis

Metal distribution is abnormal in brain and spinal cord in SCA.

5.2.2 Research Objectives

a. Map the distribution of iron, copper and zinc in fixed slices of brain and spinal cord in SCA and compare it to that of control tissues.

b. Compare the relative amounts of metals in SCA and control brain and spinal cord slices.

5.3 Materials and Methods

5.3.1 Tissue Samples, Clinical and Neuropathology Information

Formalin fixed SCA and control human tissue, clinical information and neuropathology reports were obtained from the NICHD Brain and Tissue Bank for Developmental Disorders at the University of Maryland, Baltimore, Maryland, under contracts N01-HD-3-3368 and N01-HD-4-3383. Ethics approval (# Bio 07-75) was obtained from the University of Saskatchewan.

The SCA patient was a 44 year old Caucasian female whose cause of death was cardiopulmonary arrest. The control patient was a 42 year old Caucasian female who died of hypertensive atherosclerotic cardiovascular disease. The post-mortem interval collection times were 3 and 4 hours, respectively.

The SCA and control spinal cord slices were axial sections at the cervical level. The SCA medulla was an axial section through the sensory decussation, hypoglossal, principal olivary and medial accessory olivary nuclei, while the control section was taken slightly rostral at the level of the reticular formation, solitary, principal olivary and posterior accessory olivary nuclei. Both the SCA and control cerebellum slices were axial sections at the level of the dentate nucleus. Both forebrain slices were coronal sections at the level of the caudate head, ventral pallidum, putamen, globus pallidus pars externa, genu of the internal capsule and anterior commissure, with the SCA section being at a slightly rostral level.

Following RS-XRF mapping, spinal cord and medulla slices and representative cerebellar and forebrain structures (dentate nucleus, caudate, putamen, globus pallidus, internal capsule, cerebellar and cerebral cortex) were embedded in paraffin using a Tissue-Tek ® VIP tissue processor (Miles Scientific). Sections, 5 μm thick, were cut on a water bath using a Spencer microtome (American Optical Co.), air dried and then baked in a 37ºC oven overnight. Since the escape depth for iron, copper and zinc fluorescence is 550, 630 and 740 μm respectively, I collected sections only from the top 100 μm of the face of the tissue slice from which fluorescence counts were collected. Sections were collected on Superfrost Plus micro slides (VWR), dried, deparaffinized and rehydrated by sequential immersion in xylene, xylene:ethanol (1:1), ethanol (absolute, 95%, and 70%)

and distilled water. For Luxol fast blue (LFB) staining the rehydration was stopped at 95% ethanol and for Sudan black at 70% ethanol. Sections were stained with:

a. hematoxylin (BDH Ltd.)/eosin (Aldrich) (HE) (Mallory 1938; Ibanez et al. 1960; McManus and Mowry 1960; Pathology 1960; Thompson and Hunt 1966) for demonstration of morphological components of tissues and cells

b. Luxol fast blue (JT Baker Chemical Co.) (LFB) and Luxol fast blue /cresyl violet (Fisher) (LFB/CV), Klüver and Barrera modified, for demonstration of myelin (Kluver and Barrera 1953; Thompson and Hunt 1966) and Nissl substance (Thompson and Hunt 1966).

c. Sudan black (Sudan B black, MCB Reagents) (Chiffelle and Putt 1951; Pathology 1957; Thompson and Hunt 1966) and periodic acid-Schiff (periodic acid, GFS Chemical Co.; basic fuchsin, Fisher) counterstained with Luxol fast blue (PAS/LFB) (Margolis and Pickett 1956; Margolis 1959) for demonstration of lipofuscin (Gray and Woulfe 2005).

d. phosphotungstic acid (Ted Pella Inc.)/hematoxylin/nuclear fast red (Sigma) (PTA/H/NFR) for demonstration of glial fibres (Linder 1949; Thompson and Hunt 1966).

Staining was followed by standard dehydration through distilled water, ethanol (70%, 95%, absolute), xylene:ethanol (1:1) and xylene. Coverslips (VWR) were applied to the sections with Cytoseal mounting medium (Richard-Allen Scientific).

Sudan black stained sections were not dehydrated after staining. They were washed in distilled water and immediately mounted using Kaiser's glycerol jelly aqueous mordant (Hemason 1967).

Slides were viewed under a Leitz DMRB light microscope (Carl Zeiss) and pictures were taken with a Sony Cybershot DSC-V3 digital camera.

5.3.2 Alpha-synuclein Immunohistochemistry

Alpha-synuclein immunohistochemistry was performed by the Department of Pathology and Laboratory Medicine, University of Saskatchewan. Sections cut on a distilled water bath were air dried and then baked in a 50º oven overnight. Sections were dewaxed and hydrated through xylene and decreasing concentrations of alcohol and then to distilled water. Antigen retrieval was performed in a microwave using EDTA pH 9.0 and allowed to cool again at room temperature. Sections were then loaded on Dako

Autostainer Plus for staining. Novocastra anti α-synuclein mouse monoclonal antibodies (Leica Microsytems) were used at a dilution of 1/25. Staining was completed using EnVision™ G/2 System/Alkaline Phosphatase, Rabbit/Mouse Permanent Red (Dako). A light hematoxylin counterstain was applied and then sections were dehydrated and mounted. Sections from a patient with a pathologically confirmed α-synucleopathy were used as a positive control.

5.3.3 Rapid-scanning X-ray Fluorescence Mapping

RS-XRF imaging was performed at wiggler beam line 10-2 at the Stanford Synchrotron Radiation Lightsource (SSRL). The incident X-ray beam was set to an energy of 13 keV using a Si(111) double crystal monochromator in order to excite the K-shell of the first transition row and lighter elements. The imaging setup and methodology is described in section 3.3.1 and has been published (Gh Popescu et al. 2009; Popescu et al. 2009b). In brief, 2 mm thick tissue slices were sealed in metal-free plastic sheet protectors and mounted vertically at 45º to the incident X-ray beam and 45º to the detector. The sample was translated rapidly in the beam in a raster pattern with continuous motor motion. Data was collected on the fly in both horizontal directions at a rate corresponding to a travel distance of 40 μm per readout, with count times of ~6 ms per 40 μm horizontal raster. A single element Vortex-EX® silicon drift X-ray detector (SII NanoTechnology USA Inc.) was placed at a 90º angle to the beam to minimize signal due to scatter. Energy windows were set so as to resolve the Kα from the Kβ fluorescence lines of adjacent elements.

Fluorescence was normalized to take into account fluctuations in the intensity of the incoming X-ray beam. Image analysis and relative quantification of each metal was performed using Interactive Data Language ™ (ITT Visual Information Systems) as previously described in section 3.3.2 (Gh Popescu et al. 2009). Since the escape depth and the fluorescence yield differ for each element, different metals were not compared. Rather the amount of the same element, as determined by pixel intensity was compared between similar regions in the SCA and control. Normalized fluorescence for each metal was calculated within a standard 30 x 30 pixels box (n=900). The Mann-Whitney test was employed to determine if differences in pixel intensity between control and SCA were

statistically significant (Gh Popescu et al. 2009). Since only one SCA and one control were used I cannot generalize this statistical analysis to all SCA.

5.4 Control Clinical History

The control patient was a 42 year old obese Caucasian patient who lived in the state of Maryland, USA. She was a smoker, had a history of high blood pressure and diabetes. Prior to her death, she complained of tingling and pain in her left arm and she was found unresponsive in bed. The pathology report found severe coronary atherosclerosis with acute plaque rupture and thrombotic occlusion of the right coronary artery and established hypertensive atherosclerotic cardiovascular disease as the cause of death. There was no evidence of trauma and blood tests showed that the patient did not consume alcohol or drugs prior to death.

5.5 Case Report

5.5.1 Clinical History

The patient was a 44 year old Caucasian woman whose cause of death was a cardiopulmonary arrest. The patient was an obese woman who worked as a secretary and lived at home in the state of Maryland, USA together with her husband and son. She did not smoke and consumed alcohol only occasionally. She had a long history of progressive bilateral SCA, diagnosed as FRDA when she was 25 years old based on clinical findings and electrophysiological testing. However, genetic tests for FRDA and other SCA failed to reveal any specific defect. Early development was normal but during her high school years she was thought to be “clumsy”, as she had trouble walking and sometimes needed to walk along the walls for support. This progressed to the point where she lost her balance with eye closure (i.e. a positive Romberg sign), followed by development of gait ataxia, confinement to a wheelchair, and development of appendicular ataxia and scanning dysarthria. She had no family history of a similar disorder and her 14 year old son appeared neurologically normal. Neurological examination also revealed absent deep tendon reflexes, bilaterally mute plantar responses, absent proprioception at ankles and barely perceptible at knees, barely perceptible vibration at knees and elbows and absent pinprick sensation in the legs and distal to mid forearms. The rest of the neurological

examination was normal, including full extraocular movements, normal pupillary function and optic discs, intact visual fields and no nystagmus. She had a history of depression, panic attacks, insomnia and stress urinary incontinence. Late in the disease she started to have visual hallucinations unrelated to her medication. She had no cardiomyopathy, other cardiac abnormalities, diabetes mellitus or skeletal deformities.

On the night of her death, she was admitted to the hospital for visual hallucinations and sleep deprivation. During the night, she was found unresponsive in bed. She had no blood pressure and was asystolic. A code was called but the resuscitation was unsuccessful. Although the physical examination of the cardiovascular system, electrocardiogram and echocardiography were normal and she did not have a history of cardiac problems, the pathology revealed that the cardiopulmonary arrest was due to an acute congestive heart failure, presumably secondary to an arrhythmia.

5.5.2 Neuropathology (a neuropathology report was provided by NICHD Brain and Tissue Bank for Developmental Disorders and further analysis on available tissues was performed in the Department of Anatomy and Cell Biology, University of Saskatchewan)

The gross examination of the brain and spinal cord was unremarkable, except for a slight decrease in the pigmentation of the substantia nigra (unavailable for my examination and metal mapping) and flattening of the dorsal aspects of the spinal cord at cervical levels.

Microscopic examination of spinal cord sections revealed a profound loss of myelinated axons in the dorsal columns, especially in the graciles fasciculi and the adjacent dorsal nerve roots (Figure 17B; Figure 18B). White matter vacuolation (Figure 17Q-asterisks) and gliosis were also present (Figure 17Q-arrow heads). Lower levels of the spinal cord (not available for my examination and metal mapping) also showed loss of myelinated axons in the spinocerebellar tracts and neuronal loss and gliosis in the dorsal nuclei of Clarke. LFB staining showed moderate myelin pallor in the ventral columns while the ventral horns and nerve roots were unremarkable.

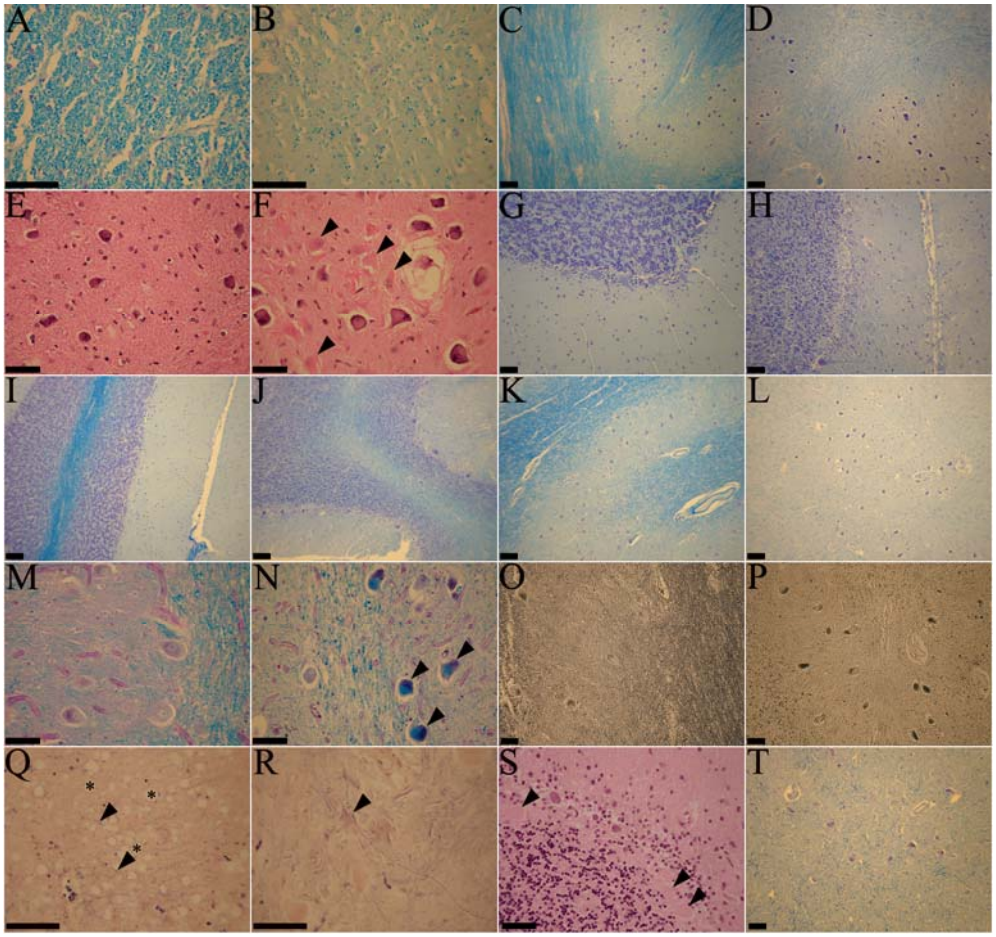
A
B
C
D
E
F
G
H
I
J
K
L
M
N
O
P
Q
R
S
T

Figure 17. Neuropathological changes seen in a case of SCA type undefined. A. Normal appearance of myelinated axons in the control dorsal columns (LFB/CV); B. Degeneration of the SCA dorsal columns, with a dramatic decrease in the number of myelinated axons (LFB/CV); C. Normal appearance of the inferior olivary nucleus and olivocerebellar fibres in the control medulla (LFB/CV); D. Degeneration of the olivocerebellar fibres in the SCA medulla (LFB/CV); E. Normal appearance of neurons and glial cells in the control inferior olivary nucleus (H/E); F. Increased number of enlarged cells (indicated by arrows) exhibiting a homogeneous, eosinophilic cytoplasm and eccentric, normal-looking nuclei consistent with reactive astrocytosis in SCA inferior olivary nucleus (H/E); G. Normal appearance of the control cerebellar cortex (LFB/CV); H. Disappearance of Purkinje cells and mild gliosis in the SCA cerebellar cortex (LFB/CV); I. Normal appearance of the subcortical white matter of the control cerebellum (LFB/CV); J. Degeneration of the subcortical white matter of the SCA cerebellum (LFB/CV); K. Normal appearance of the control cerebellar white matter in the dentate hilum and around the dentate nucleus (LFB/CV); L. Severe loss of myelinated axons in the dentate hilum and in the white matter surrounding the dentate nucleus of the SCA patient (LFB/CV); M. Normal appearance of neurons in the control dentate nucleus (LFB/PAS); N. SCA dentate nucleus neurons containing abundant PAS positive lipofuscin inclusions (arrows) (LFB/PAS); O. Normal appearance of neurons in the control dentate nucleus (Sudan black); P. SCA dentate nucleus neurons containing abundant Sudan black positive lipofuscin inclusions (Sudan black); Q. Presence of vacuoles (asterisks) and increased glial fibres (arrows) in the SCA degenerated dorsal columns (PTA/H/NFR); R. Reactive astrocytosis in the SCA inferior olivary nucleus (PTA/H/NFR); S. Purkinje cells axonal swellings in the SCA cerebellar cortex; T. Normal appearance of the globus pallidus pars externa in the SCA patient; scale bar = 50 μm, except C,D,I-L where scale bar = 100 μm.

Examination of the brainstem showed moderate neuronal loss and reactive astrocytosis in the inferior olivary nuclei (Figure 17D, F-arrow heads, R-arrow head) and loss of myelinated axons in the olivocerebellar fibres and amiculum olivae (Figure 17D; Figure 19B). Other microscopic findings in the brainstem included neuronal loss and gliosis in the accessory cuneate nuclei and substantia nigra bilaterally, pallor of the medullary pyramids and atrophy of the superior cerebellar peduncles.

Sections of the cerebellum revealed areas of Purkinje cell loss with mild Bergmann gliosis and occasional axonal swellings (Figure 17H, S-arrow heads), while other cerebellar cortical regions, including the vermis were spared. There was moderate neuronal loss and gliosis in the dentate nucleus (Figure 17L) with the remaining neurons containing heavy PAS positive (Figure 17N) and Sudan black positive (Figure 17P) inclusions consistent with lipofuscin. There was severe loss of myelinated axons in the dentate hilum (Figure 17L), in the white matter surrounding the dentate nucleus (Figure 17L) and in the subcortical white matter (Figure 17J).

Sections of the cerebral cortex, white matter and deep gray structures were unremarkable (globus pallidus pars externa shown in Figure 17T).

5.5.3 Differential Diagnosis

Many of the clinical features and neuropathological findings in this case are consistent with the diagnosis of FRDA. The majority of FRDA patients are homozygotes for two GAA repeats in the first intron of the frataxin gene (Campuzano et al. 1996; Durr et al. 1996; Pandolfo 1998), while a small percentage are compound heterozygotes for one GAA repeat and one point mutation (Durr et al. 1996; Pandolfo 1998). Since no instance of a FRDA patient carrying two frataxin point mutations has yet been described and homozygous deletions in the FRDA gene cause embryonic lethality in mice (Cossee et al. 2000), the failure of the genetic test to identify the presence of the GAA repeats on either of the two alleles of the FRDA gene makes this diagnosis unlikely.

There was no evidence of occupational exposure to excess metals since the woman worked as a secretary. While domestic exposure to metals cannot be ruled out, her husband and son with whom she shared a domicile appeared neurologically normal.

The woman was obese and apparently well nourished and so there was no evidence of metal deficiency.

Although the absence of a family history of a similar disorder suggests an autosomal recessive inheritance, a *de novo* mutation or false parenthood can not be excluded. I cannot rule out an autosomal dominant SCA or AVED because available data on this patient did not include vitamin E levels or the specific SCA for which genetic tests were negative. SCA autosomal dominant types 1 (Genis et al. 1995), 2 (Durr et al. 1995; Estrada et al. 1999) and 7 (Gouw et al. 1994; Martin et al. 1994) also present with posterior column and olivopontocerebellar degeneration and a neurological phenotype similar to FRDA. Patients with AVED present with a neurological phenotype sometimes indistinguishable from FRDA (Hammans and Kennedy 1998) and neuropathological changes similar to FRDA (Larnaout et al. 1997; Yokota et al. 2000). However, the patient presented here did not show any of the oculomotor abnormalities seen in SCA1 (Orr and Klockgether 2000) and SCA2 (Bürk and Dichgans 2000), the macular degeneration characteristic to SCA7 (Stevanin et al. 2000) or the retinal abnormalities encountered in AVED (Koenig 2000).

The absence of immunoreactivity to anti-α-synuclein antibodies (Dickson et al. 1999) (Figure 20) rules out multiple system atrophy, an idiopathic neurodegenerative disorder that can present with olivopontocerebellar atrophy and cerebellar ataxia (Papp et al. 1989).

Clioquinol-induced subacute myelo-optic-neuropathy presents with a panel of neuropathological changes almost identical to the SCA case I present, but the exact mechanism of clioquinol intoxication in not yet known (Koga et al. 1997). Clioquinol is known for its ability to chelate iron, copper and zinc (Schaumburg and Herskovitz 2008) and it is currently used in clinical trials for chelation therapy of Alzheimer's disease (Finefrock et al. 2003).

This case does not perfectly match the clinical and neuropathological features of a single clearly identifiable SCA, although a rare or aberrant presentation or more overlaying aetiologies should not be disregarded.

5.6 Results

5.6.1 Areas of Degeneration Have Low Metal Content

The dorsal columns, especially the graciles fasciculi, show the most striking loss of myelinated fibres in the SCA spinal cord (Figure 17B; Figure 18B). The degenerated dorsal columns of the SCA cervical cord have a lower metal content than the other white matter columns (Figure 18E, G, I, K) and also lower (35% less iron, 32% less copper, 19% less zinc, $p<0.0001$, Table 5) than the corresponding regions of the control spinal cord (Figure 18D, F, H, J).

A very interesting copper distribution was found in the region of the inferior olivary nucleus (Figure 19F). The inferior olivary nucleus of the control medulla is poor in copper but its convoluted shape is visible due to the contrast with the high copper content of the olivocerebellar fibres and afferent fibres that surround it (amiculum olivae) (Figure 19F). I believe that this is the first description of high copper content in this region of the normal medulla. Similar high copper content was also found in the olives of other disease controls (Figure 21). The neuropathological examination shows the degeneration of the SCA olivocerebellar fibres and amiculum olivae (Figure 17D, F; Figure 19B) and the copper XRF map shows loss of copper (57% less than the control, $p<0.0001$, Table 5) in these structures (Figure 19G). Iron (20% less, $p<0.0001$, Table 5) and zinc (34% less, $p<0.0001$, Table 5) are also lost in the olivary region (Figure 19E, I).

Neuronal loss in the dentate nucleus and loss of myelinated fibres in the dentate hilum, around the dentate nucleus and in the subcortical white matter are seen in the SCA cerebellum (Figure 17J, L, N, P). The metal content of the normal dentate nucleus has been described previously (Popescu et al. 2009b). Iron XRF maps of the cerebellum show the iron rich control dentate region (Figure 22D) and almost complete loss of iron in the SCA dentate nucleus and the adjacent white matter (51% less, $p<0.0001$, Table 5) (Figure 22E). The branching pattern of the cerebellar white matter (*arbor vitae*) is clearly resolved on the basis of metal content (Figure 22D, E, F, G, J, K) as previously described (Popescu et al. 2009b). However, the contrast between the metal rich white matter and metal poor grey matter decreases in the case of the SCA cerebellum, especially for iron (Figure 22E) and zinc (Figure 22I) because of the lower metal content of the SCA white matter (23% less iron, 11% less copper, 21% less zinc, $p<0.0001$, Table 5).

Table 5. SCA metal quantification relative to control.

	Metal	SCA (fluorescence/scatter[a])	CTRL (fluorescence/scatter[a])	Decrease (%)	Increase (%)
Dorsal columns	Fe	0.0044	0.0068	35	
	Cu	0.0058	0.0085	32	
	Zn	0.0095	0.018	19	
Olive	Fe	0.0044	0.0055	20	
	Cu	0.0074	0.0172	57	
	Zn	0.0076	0.0116	34	
Dentate nucleus	Fe	0.0073	0.0149	51	
Cerebellar white matter	Fe	0.0049	0.0064	23	
	Cu	0.0032	0.0036	11	
	Zn	0.0027	0.0034	21	
Ventral columns	Fe	0.103	0.0052		98
	Cu	0.0103	0.0063		63
	Zn	0.0184	0.0105		75
Globus pallidus pars externa	Fe	0.0903	0.0515		80
	Zn	0.0258	0.0188		37

[a] Normalized fluorescence (fluorescence counts/scatter counts). Normalized fluorescence is the fluorescence detected from the illuminated tissue volume normalized by the combined elastic and Compton scatter from the same region. This normalized value is proportional to the amount of the fluorescing element per mass of tissue.

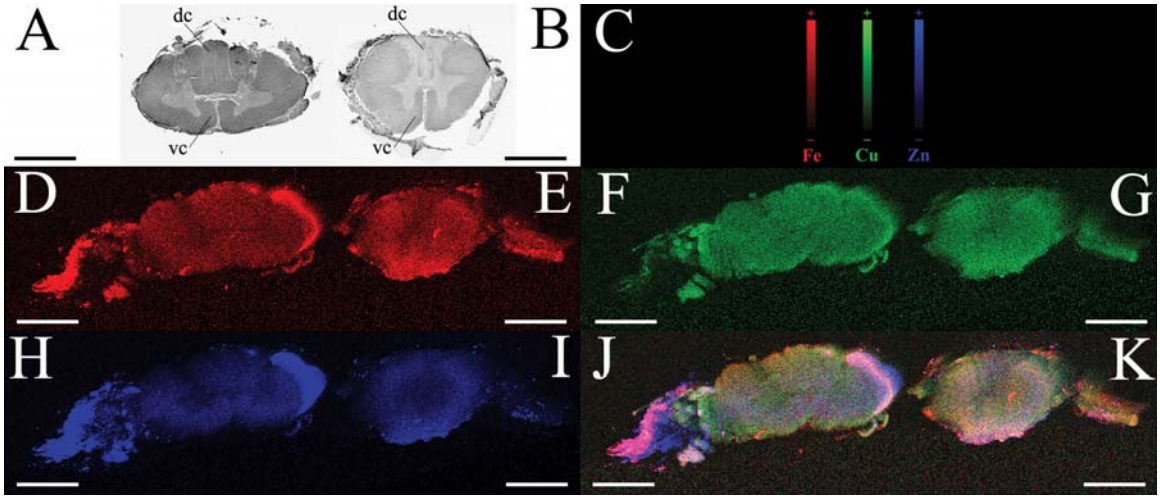

Figure 18. Metals are decreased in the degenerated posterior columns and increased in the least affected ventral columns of the SCA patient. Spinal cord, axial section, control (A,D,F,H,J) and SCA (B,E,G,I,K). A. Normal appearance of the control spinal cord (LFB/CV); B. Degenerated posterior columns and myelin pallor of the SCA spinal cord (LFB/CV); C. Color scales represent the normalized total Kα fluorescence counts, proportional to total metal present, from black (lowest) to color (highest); D,E. Iron maps; F,G. Copper maps; H,I. Zinc maps; J,K. Overlay of iron, copper and zinc; dc-dorsal columns; vc-ventral columns; scale bar = 5 mm.

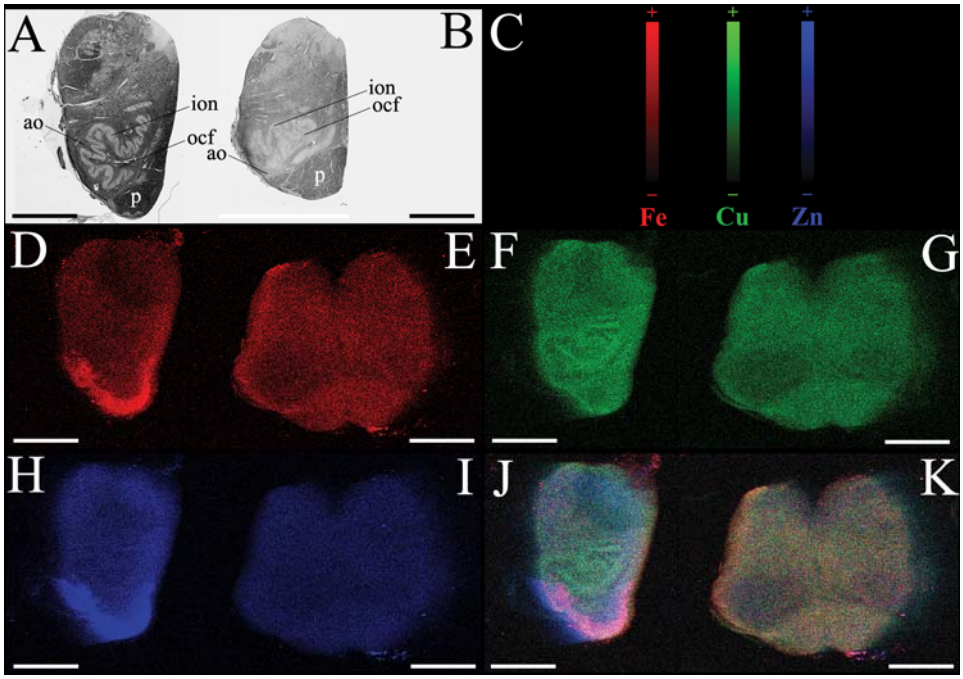

Figure 19. Metals are decreased in the degenerated olivocerebellar fibres and amiculum olivae of the SCA patient. Medulla, axial section, control (A,D,F,H,J) and SCA (B,E,G,I,K). A. Normal appearance of the control medulla (LFB/CV); B. Degenerated olivocerebellar fibres and amiculum olivae in the SCA spinal cord (LFB/CV); C. Color scales represent the normalized total Kα fluorescence counts, proportional to total metal present, from black (lowest) to color (highest); D,E. Iron maps; F,G. Copper maps; H,I. Zinc maps; J,K. Overlay of iron, copper and zinc; ion-inferior olivary nucleus; ocf-olivocerebellar fibres; ao-amiculum olivae; p-pyramid; scale bar = 5 mm.

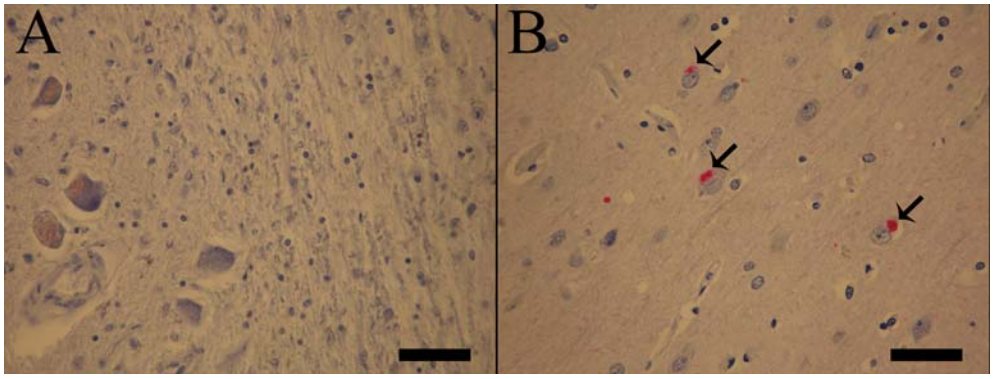

Figure 20. SCA tissue shows a negative immunohistochemistry staining reaction to α-synuclein. A. SCA tissue; B. Positive control tissue from a patient with a neuropathologically diagnosed α-synucleopathy; arrows-immunohistochemistry positive staining indicates intracytoplasmic α-synuclein accumulations; scale bar = 50 μm.

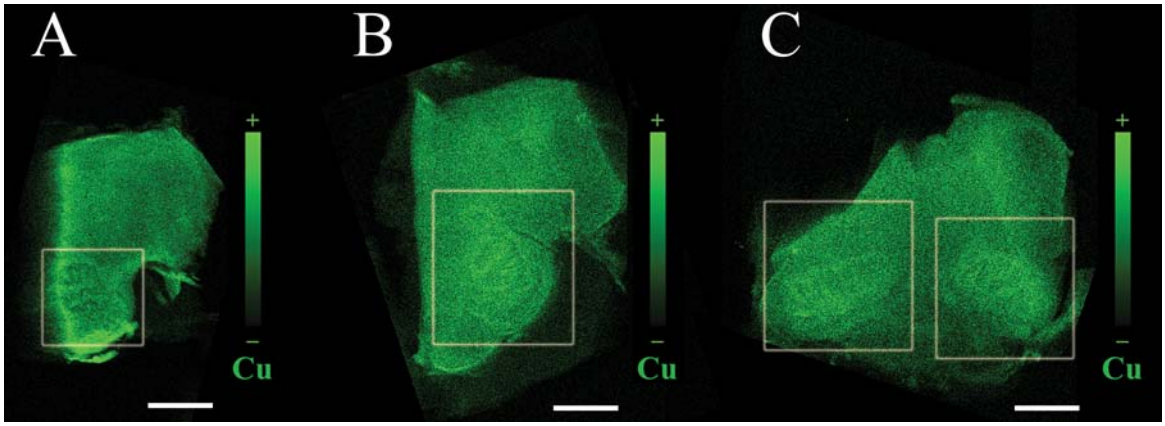

Figure 21. Olivocerebellar fibres have a high copper content in medullae (indicated by rectangles) from control patients and patients diagnosed with neurodegenerative diseases but without olivary involvement. A. Medulla from a patient with a pathologically diagnosed progressive supranuclear palsy; B. Medulla from a patient with a pathologically diagnosed progressive muscular atrophy; C. Medulla from a control patient who died as a result of multiple traumatic craniocerebral injuries; Green color scales represent the normalized total Cu Kα fluorescence counts, proportional to total metal present, from black (lowest) to green (highest); scale bar = 5 mm.

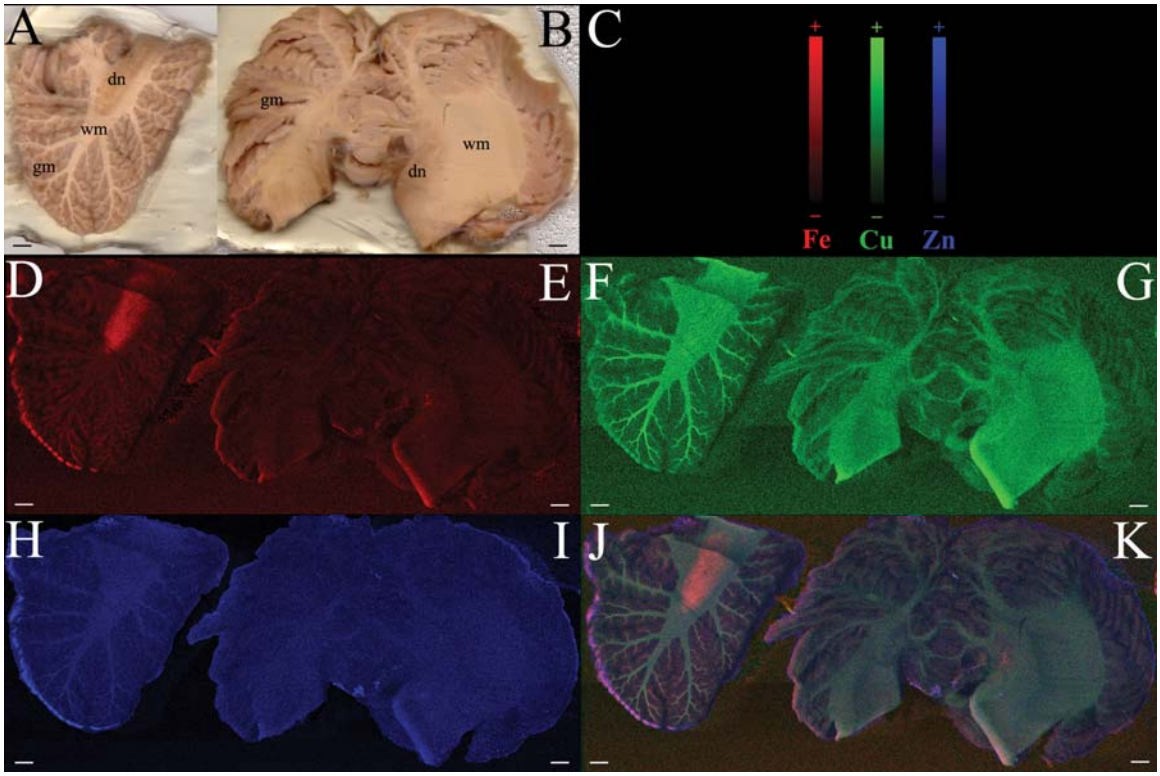

Figure 22. Iron is decreased in the degenerated dentate nucleus and metals are decreased in the cerebellar white matter of the SCA patient. Cerebellum, axial section, control (A,D,F,H,J) and SCA (B,E,G,I,K). A. Gross section of the control cerebellum; B. Gross section of the SCA cerebellum; C. Color scales represent the normalized total Kα fluorescence counts, proportional to total metal present, from black (lowest) to color (highest); D,E. Iron maps; F,G. Copper maps; H,I. Zinc maps; J,K. Overlay of iron, copper and zinc; dn-dentate nucleus; wm-white matter; gm-cortical gray matter; scale bar = 5 mm.

5.6.2 Ventral Columns of the Spinal Cord and Globus Pallidus Pars Externa of the SCA Patient Have Abnormally High Metals

The ventral columns show only moderate myelin pallor (Figure 18B). Iron, copper and zinc content are higher in the ventral columns of the SCA (98% more iron, 63% more copper, 75% more zinc, $p<0.0001$, Table 5) than the control spinal cord (Figure 18E, G, I, K). Within the SCA, the ventral columns have higher iron content than the rest of the spinal cord.

The metal distribution of the forebrain is complex (Figure 23). I have previously shown large variations in metal content between white and gray matter and between brain regions such as basal ganglia (Gh Popescu et al. 2009; Popescu et al. 2009a) that are consistent between brains and that arise from differential cellular deposition of metals. Although the microscopic examination of the cerebral hemispheres and basal ganglia is unremarkable, the metal maps show an increase in the iron (80% more iron, $p<0.0001$, Table 5; Figure 23E) and zinc (37% more zinc, $p<0.0001$, Table 5; Figure 23I) content of the SCA globus pallidus pars externa.

5.6.3 Metals are High in the Cerebral Blood Vessels of the SCA Patient

Upon gross inspection of both the SCA and control forebrain coronal sections blood vessels can be seen (Figure 23A, B-arrows). However, while the control blood vessels are barely visible in the iron and zinc maps (Figure 23A-arrows and corresponding regions in Figure 23D, H), the SCA blood vessels are very rich in iron, copper and zinc whether caught in longitudinal or cross-section (Figure 23B-arrows and corresponding regions in Figure 23E, G, I).

The SCA metal maps also show small white matter regions that are very rich in all three metals but do not correspond to any structures identifiable on gross examination (Figure 23K-arrow heads and corresponding regions in Figure 23E, G, I).

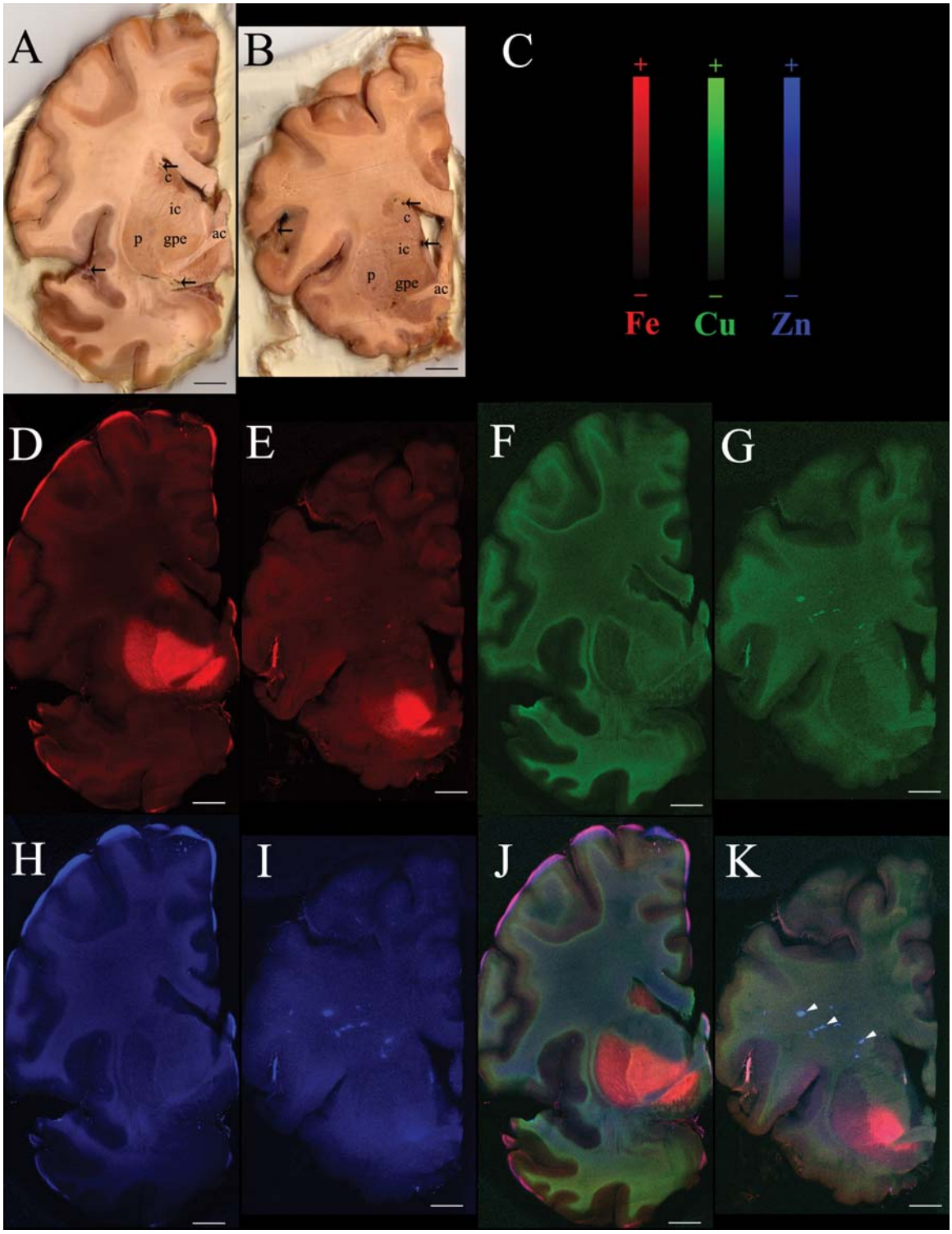
A
B
C
c
ic
p
gpe
ac
+
−
Fe
Cu
Zn
D
E
F
G
H
I
J
K

Figure 23. Metals are increased in the globus pallidus pars externa and cerebral blood vessels of the SCA patient. Forebrain, coronal section, control (A,D,F,H,J) and SCA (B,E,G,I,K). A. Gross section of the control forebrain; B. Gross section of the SCA forebrain; C. Color scales represent the normalized total Kα fluorescence counts, proportional to total metal present, from black (lowest) to color (highest); D,E. Iron maps; F,G. Copper maps; H,I. Zinc maps; J,K. Overlay of iron, copper and zinc; c-caudate; p-putamen; gpe-globus pallidus pars externa; ic-internal capsule; ac-anterior commissure; arrows-blood vessels; arrowheads-metal rich white matter regions; scale bar = 5 mm.

5.7 Discussion

Iron, copper and zinc function as cofactors in essential metalloproteins and are required for oxidative phosphorylation, neurotransmitter biosynthesis and modulation of neurotransmission, antioxidant defence, nitric oxide metabolism, oxygen transport and synthesis of proteins, DNA and RNA (Cuajungco and Lees 1997; Ponka 1999; Madsen and Gitlin 2007). Iron (Ortiz et al. 2004; Todorich et al. 2008), copper (Madsen and Gitlin 2007) and zinc (Tsang et al. 1997; Kursula et al. 1999) are also essential for myelin synthesis, structure and maintenance. Thus, myelin degradation and replacement of dying axons by the gliotic scar in chronic lesions of patients with long-standing disease may explain why the degenerated white matter of the posterior columns (Figure 17B), olivocerebellar fibres (Figure 17D) and cerebellum (Figure 17J) of the SCA patient have lower metal content (Figure 18, Figure 19, Figure 22). Furthermore, degradation of the myelin sheath is followed by the "dying back" of oligodendrocytes (Ludwin and Johnson 1981; Rodriguez et al. 1993), the main iron repository cells in the brain (Connor and Menzies 1996), which would decrease the iron content even more in the degenerated areas.

A new and very interesting observation was the high copper content of the control olivocerebellar fibres. A similar copper distribution was found in other control medullae, as well as in medullae from patients with neurodegenerative diseases that do not involve the olivocerebellar fibres (Figure 21). At this moment, I can only speculate why the only source of cerebellar climbing fibres has a unique copper distribution but further XAS and immunohistochemistry studies are needed to identify the chemical form and role of this copper.

The dentate nucleus (Figure 22D) is one of the most iron-rich structures of the brain (Hock et al. 1975; Morris et al. 1992). Iron loss in the SCA dentate region (Figure 22E) can be explained by the mild neuronal loss and by degeneration of myelinated fibres in the dentate hilum and around the dentate nucleus (Figure 17D). The neuropathological examination also revealed SCA neurons containing heavy PAS positive (Figure 17N) and Sudan black positive (Figure 17P) inclusions consistent with lipofuscin. Lipofuscin is a "wear and tear" pigment that increases with age (Brody 1960). The heavy lipofuscin accumulations seen in the SCA (compared to the lipofuscin present in the control dentate

neurons – Figure 17M, O) are abnormal for the patient's age and, thus, they may represent a sign of premature ageing. Although lipofuscin has been reported to bind iron and copper (Terman and Brunk 2004), in this SCA case the elevated lipofuscin is not associated with similarly elevated metals.

The brain is a major metal repository that not only accumulates, but also metabolizes metals as part of its normal functioning (Zecca et al. 2004; Bartzokis et al. 2007). This makes it particularly susceptible to metal-catalyzed oxidative damage, protein aggregation and neurotoxicity (Cuajungco and Lees 1997; Zecca et al. 2004; Madsen and Gitlin 2007). Metals have been also involved in the induction and subsequent aggregation of defective protein structures such as ataxin-3, the protein that causes spinocerebellar ataxia type 3 (Ricchelli et al. 2007). I found increased metal levels in the SCA ventral columns of the spinal cord (Figure 18) and globus pallidus pars externa (Figure 23), despite the lack of overt pathological changes other than a decrease in myelin stain (Figure 18B). In cerebellar ataxia associated with heteroallelic ceruloplasmin gene mutation (Miyajima et al. 2001), iron deposition has been previously reported in the globus pallidus associated with minimal or no pathological changes. Iron accumulation and myelin breakdown are known to begin before the first appearance of pathological changes in many neurodegenerative diseases (Bartzokis 2004; Bartzokis et al. 2007). While I can hypothesize that increased metals, not associated with pathological changes, represent an incipient stage of neurodegeneration, my results do not clarify if the excess metals are the cause or the result of this process. Indeed, the ability of iron (Zecca et al. 2004; Madsen and Gitlin 2007), copper (Madsen and Gitlin 2007) and zinc (Cuajungco and Lees 1997) to promote ROS formation and neurotoxicity is well known. Alternatively, the iron increase could be the result of an upregulation of iron intake necessary for axonal repair and remyelination (Graeber et al. 1989; Raivich et al. 1991). The same could be true for copper and zinc that are also essential for proper cellular functioning and myelin regeneration. Increased oxidative stress leading to demyelination and axonal damage can also lead to upregulation of metallothionein (Penkowa et al. 2003; Penkowa and Hidalgo 2003) and copper-zinc SOD (Bowling et al. 1993; Maier and Chan 2002), protective proteins that employ copper and zinc as essential cofactors. However the lack of these metals in areas of degeneration indicates that these

metalloproteins are no longer abundant or present but not metallated once the pathology is severe.

Iron, copper and zinc are abundant within the walls and perivascular spaces of SCA cerebral blood vessels (Figure 23B-arrows and corresponding regions in Figure 23E, G, I, K), but not within the control blood vessels (Figure 23A-arrows and corresponding regions in Figure 23D, F, H, J). The ability to see intravascular and perivascular metals is one of the major advantages of RS-XRF (Gh Popescu et al. 2009; Popescu et al. 2009a), since vascular changes are linked to neurodegenerative diseases (Brun and Englund 1986; Faucheux et al. 1999). The metal-rich white matter regions seen in the forebrain (Figure 23K-arrow heads and corresponding regions in Figure 23E, G, I) might also represent deep blood vessels or small haemorrhages.

In conclusion, iron, copper and zinc are low in areas where degeneration is very advanced and more abundant in areas where degeneration is potentially at an early stage. The different metal content of lesions at different stages of disease might explain for example, the contradictory results regarding the iron content of the dentate nucleus in FRDA. By interrogating a potentially active site of degeneration, *in vivo* Magnetic Resonance studies show increased iron in the dentate nucleus of FRDA patients (Waldvogel et al. 1999; Boddaert et al. 2007) while biochemical studies of post-mortem tissues fail to reveal an increase in iron (Koeppen et al. 2007). My results suggest that iron levels might be correlated with disease progression.

Using RS-XRF mapping, I have shown that not only iron, but also copper and zinc may play a role in the physiopathology of the SCA case I present. Thus, my study suggests that abnormalities of all three metals should be investigated in SCA of both known and unknown aetiologies to identify possible new therapeutic targets.

CHAPTER VI

General Discussion

Frataxin is an essential mitochondrial protein involved in iron metabolism. Its deficiency causes FRDA characterized by a wide range of metabolic disturbances including deficiency of ISC and heme synthesis, mitochondrial iron accumulation and increased oxidative stress.

Iron's toxicity, reactivity and bioavailability are linked to its chemical form (Ponka 1999; Halliwell 2001; Arosio et al. 2008). The cell has multiple mechanisms to control the uptake and metabolism of iron in different forms. The body uses ferrous iron in many molecules but only stores iron as ferric oxide/hydroxides, like ferrihydrite (Ponka 1999).

One of the "unknowns" of FRDA has been the chemical form of mitochondrial iron. It has been hypothesized that it should be possible to slow the progression of both the neurodegeneration and cardiomyopathy that characterize FRDA by reducing the iron damage. Treatment strategies have focused on either reducing the amount of iron in mitochondria through iron chelation or reducing the effects of iron-catalyzed Fenton chemistry with antioxidants reviewed in (Marmolino and Acquaviva 2009).

Using XAS I have shown that most of the mitochondrial iron in both the FRDA and control fibroblasts is stored as ferrihydrite (Popescu et al. 2007a). I have also shown that in FRDA fibroblasts most of the mitochondrial iron is stored as the non-toxic, but also poorly bioavailable ferrihydrite of MtFt and little ferrous redox-active iron is present (Popescu et al. 2007a). My data supports the new concept that once MtFt is upregulated in FRDA (by whatever means) it competes for and sequesters the available mitochondrial iron. Since MtFt mineralizes this iron but does not readily release it, my work suggests that lack of iron available for heme and ISC synthesis contributes to FRDA pathophisiology.

Yeast has no ferritin gene, but expression of either MtFt (Campanella et al. 2004) or cytosolic L type ferritin (Desmyter et al. 2004) rescues the respiratory defect, prevents the mitochondrial iron accumulation, mitochondrial DNA damage and the formation of ROS and lengthens the lifespan of frataxin knock-out yeast. Similar findings were reported when MtFt is over-expressed in FRDA fibroblasts (Campanella et al. 2009). This indicates that iron mineralization by whatever means, has some beneficial effect on iron overloaded mitochondria.

While only frataxin is able to chaperone iron to both ISC and heme proteins, both frataxin (Cavadini et al. 2002) and MtFt (Levi et al. 2001; Bou-Abdallah et al. 2005) can polymerize and detoxify redox-active iron by sequestering it in a non-toxic but bioavailable form in a protein-protected compartment at the expense of the cytosolic iron (Corsi et al. 2002; Li et al. 2008; Campanella et al. 2009). Human heart contains frataxin species of increasing molecular mass, ranging from monomers to polymers >1MDa (Cavadini et al. 2002; O'Neill et al. 2005) and I have also observed that high molecular mass frataxin polymers are present in unaffected human fibroblasts (Popescu et al. 2007a). However, in frataxin deficient fibroblasts, mitochondria might attempt to compensate for the imbalance between iron uptake and egress by storing iron as ferrihydrite in MtFt (Popescu et al. 2007a).

Since most of the iron in FRDA mitochondria is already stored as relatively non-toxic, but poorly bioavailable ferrihydrite in MtFt, chelation strategies should take into account that at least in cells that are able to synthesize MtFt, chelating the small non-ferrihydrite iron pool could prevent mitochondria from carrying out even minimal functions. Moreover, the cytosolic iron depletion that already exists in FRDA could be worsened by non-specific chelators (Li et al. 2008).

Fibroblasts, like cardiomyocytes and neurons, synthesize both frataxin and ferritins but the relative importance of each protein in iron homeostasis is poorly understood. They could serve different, but complementary roles in iron detoxification. One of frataxin's unique roles in the mitochondria may be to protect DNA from hydrogen peroxide (Karthikeyan et al. 2003), while MtFt seems to provide a redundant mechanism to store iron and control ROS formation primarily through regulation of mitochondrial iron availability (Campanella et al. 2009). Since MtFt has been detected in heart tissue from FRDA patients (Michael et al. 2006), it is possible that the lack of iron availability is also involved in the cardiodegeneration associated with FRDA. By understanding how fibroblasts regulate MtFt synthesis we may better understand how to upregulate this protective protein in cardiac and neuronal cells of FRDA patients.

In humans, iron deposits have been demonstrated in cardiomyocytes (Sanchez-Casis et al. 1976; Lamarche et al. 1980; Bradley et al. 2000; Michael et al. 2006), hepatocytes and spleen cells (Bradley et al. 2000) from FRDA patients and in FRDA

fibroblast cultures (Delatycki et al. 1999) using Perls' stain and electron microscopy. Magnetic Resonance *in vivo* studies show increased iron in the dentate nucleus of FRDA patients (Waldvogel et al. 1999; Boddaert et al. 2007) but these findings have been challenged by biochemical studies of post-mortem tissues that failed to reveal an increase in iron (Koeppen et al. 2007). However, there are no human studies linking the nervous system neurodegeneration in FRDA to iron accumulation. Moreover, even though early work suggested a possible dysregulation of copper and zinc metabolism in FRDA patients (Barbeau et al. 1984; Huxtable et al. 1984; Shapcott et al. 1984), the possible involvement of copper and zinc in FRDA neurodegeneration has not been investigated.

Lack of such data could be partially explained by the absence of an appropriate tool necessary to map the global distribution of metals in the brain and spinal cord. Although there is tremendous interest in human brain metal metabolism, complete maps from individuals have not been available (Zecca et al. 2004). Such baseline data is required if we are to fully understand how FRDA and other neurodegenerative disease change global metal distribution and metabolism.

While destructive analytic techniques such as atomic absorption and inductively coupled mass spectrometry have been used to quantify metals in selected brain regions (Hock et al. 1975; Dexter et al. 1987; Dexter et al. 1989; Duflou et al. 1989; Dexter et al. 1991; Dexter et al. 1992; Dexter et al. 1993; Rajan et al. 1997; Becker et al. 2005) and some magnetic resonance imaging sequences are used to image iron *in vivo* (Haacke et al. 2005), histochemistry has long been the gold standard to localize metals in brain slices. However Perls' and Turnbull's methods detect only nonheme iron (Perls 1867; Zaleski 1887; Gomori 1936; Meguro et al. 2007), copper histochemistry lacks sensitivity and specificity (Pilloni et al. 1998; Henwood 2003; Ferenci et al. 2005) and complex techniques are required to distinguish protein-bound from ionic zinc (Danscher et al. 1985; Lopez-Garcia et al. 2002). Because each of these methods employs a different chemistry, they cannot be combined or used sequentially on the same tissue section. Therefore, easy and quantitative assessment of interrelationships between metals has been lacking.

Since XRF is element specific and can simultaneously map multiple metals in all chemical forms, I have applied RS-XRF to map the global metal distribution of both

normal and diseased brain and spinal cord (Gh Popescu et al. 2009; Popescu et al. 2009a; Popescu et al. 2009b). Traditional point-to-point X-ray microprobe has previously been successfully employed to map multiple metals in small areas of brain tissue sections at high resolution (Yoshida et al. 2001; Ishihara et al. 2002; Collingwood and Dobson 2006; Miller et al. 2006; Linkous et al. 2007) but the time required to map large areas of the brain in this way is prohibitive. Unlike X-ray microprobe which achieves cellular or subcellular resolution, RS-XRF gives a global anatomic view of metals in whole organ slices. As with electron microscopy, very high resolution limits what can be imaged within a reasonable time and this reduces the sample size. Cell biologists recognize the futility of moving to transmission electron microscopy until precise areas of interest have been identified at the anatomic and light microscopic level. This is why I have proposed RS-XRF could be used for examining the global metal distribution of the brain and finding pathological accumulations of metals (Gh Popescu et al. 2009).

Since FRDA human tissues are not readily available, the new method has initially been validated by comparing the metal distribution in normal and PD brain (Gh Popescu et al. 2009). Then, it has been applied to study the macroscopic distribution of iron, copper, and zinc in normal cerebellum (Popescu et al. 2009b) and to compare the relative amounts and distribution of metals in the brain and spinal cord from a patient with a long history of SCA (type undefined) with a sex and age matched control (Popescu et al. 2009a). The motivation for this work was the prospect of doing future systematic studies on metal pathology in neurodegenerative diseases in general with future direct application to FRDA.

The cerebellum is an active site of neurodegeneration in FRDA (Greenfield 1954; Oppenheimer 1979; Lamarche et al. 1984) with the dentate nucleus showing the most severe neuronal loss (Oppenheimer 1979; Lamarche et al. 1984; Koeppen et al. 2007). I have shown that the dentate nucleus is extremely rich in iron, copper and zinc and that the cerebellar white matter has a high iron and zinc content (Popescu et al. 2009b) in the normal brain. There are other areas of brain that are also very rich in metals. The basal ganglia are rich in iron (Gh Popescu et al. 2009; Popescu et al. 2009a), the subcortical white matter is rich in zinc (Gh Popescu et al. 2009; Popescu et al. 2009a) and the substantia nigra is rich in both iron and copper (Gh Popescu et al. 2009).

Moreover, RS-XRF has provided us with new and very interesting findings. The dentate nucleus shows a characteristic metal segmentation with the copper located towards the periphery and iron and zinc towards its interior (Popescu et al. 2009b). The presence of two neuronal populations with different metal contents in the dentate could prove to be very important since these neurons might possess different susceptibilities to neurodegeneration. Another new observation is the high copper content of the olivary region of the normal brain (Popescu et al. 2009a). At this moment, I can only speculate why the only source of cerebellar climbing fibers has a unique copper distribution but further study is needed to identify the chemical form and role of this copper. Also, the ability to see intravascular and perivascular metals is one of the major advantages of RS-XRF (Gh Popescu et al. 2009; Popescu et al. 2009a; Popescu et al. 2009b), since vascular changes are linked to neurodegenerative diseases (Brun and Englund 1986; Faucheux et al. 1999).

The brain is a major metal repository (Hock et al. 1975; Dexter et al. 1989; Duflou et al. 1989; Morris et al. 1992; Rajan et al. 1997) where large amounts of iron, copper, and zinc coexist and colocalize. The high metal content of certain brain structures makes them particularly susceptible to metal-catalyzed oxidative damage, protein aggregation, neurotoxicity, and neurodegeneration (Cuajungco and Lees 1997; Zecca et al. 2004; Madsen and Gitlin 2007). In a rich metal environment, loss of function of metalloproteins and loss of defense against oxidative stress caused by deficiency of one or more metals (Madsen and Gitlin 2007) could also be responsible for neurodegeneration.

The very interesting SCA case I have studied has provided us with clues about how metal distribution is affected in neurodegeneration (Popescu et al. 2009a), although my findings can not be generalized. Regions with neuronal loss and gliosis in the cerebellar cortex, inferior olivary, and dentate nuclei and areas showing loss of myelinated fibers in the posterior columns, cerebellar white matter and olivocerebellar fibers were all low in all metals in SCA compared to control. In contrast, the ventral columns of the spinal cord that exhibited only moderate myelin pallor had increased metal levels. Iron and zinc were also elevated in the globus pallidus pars externa in SCA relative to control (Popescu et al. 2009a). In conclusion, iron, copper and zinc are low in

areas where degeneration is very advanced and more abundant in areas where degeneration is potentially at an early stage. The different metal content of lesions at different stages of disease might explain for example, the contradictory results regarding the iron content of the dentate nucleus in FRDA. By interrogating a potentially active site of degeneration, *in vivo* Magnetic Resonance studies show increased iron in the dentate nucleus of FRDA patients (Waldvogel et al. 1999; Boddaert et al. 2007) while biochemical studies of post-mortem tissues fail to reveal an increase in iron (Koeppen et al. 2007). My results suggest that iron levels might be correlated with disease progression.

Using XAS and RS-XRF, I have been able to identify the chemical form of iron in FRDA mitochondria and to show that not only iron, but also copper and zinc may play a role in the physiopathology of at least some SCA cases. Thus, this study suggests that abnormalities of all three metals should be investigated in FRDA and other SCA of both known and unknown aetiologies to identify possible new therapeutic targets.

CHAPTER VII

Conclusions, Impact and Future Work

7.1 FRDA Mitochondria Store the Majority of Iron as Ferrihydrite in MtFt

Since iron's toxicity, reactivity and bioavailability are linked to its chemical form (Ponka 1999; Halliwell 2001; Arosio et al. 2008), it has been hypothesized that it should be possible to slow the progression of both the FRDA associated neurodegeneration and cardiac degeneration by reducing the iron damage. However, the chemical form of mitochondrial iron in FRDA has remained an unanswered question. While previous studies performed by our laboratory have used XAS to determine the structure of frataxin's iron core *in vitro* (Nichol et al. 2003), this is the first study that applies synchrotron technology to FRDA and uses XAS to characterize the chemical form of mitochondrial iron in FRDA *in vivo* (chapter II and (Popescu et al. 2007a). I have found that, while both FRDA and control mitochondria store most of the iron as ferrihydrite, the mitochondrial iron is associated with MtFt only in FRDA. This suggests that little redox-active iron is present and that the lack of iron availability is more important than the ROS production in the pathogenesis of FRDA. Since most of the iron in FRDA mitochondria is already stored as relatively non-toxic ferrihydrite, chelation strategies should take into account that at least in cells that are able to synthesize MtF, chelating the small non-ferrihydrite iron pool could prevent mitochondria from carrying out even minimal functions. Moreover, the cytosolic iron depletion that already exists in FRDA could be worsened by non-specific chelators (Li et al. 2008).

I have performed this study using fibroblast cell cultures and further work is needed to see if my findings can be extended to those cells most affected in FRDA: neurons and cardiomyocytes. Since mature neurons and cardiomyocytes do not multiply in culture, this would be done by applying the same techniques I have used to tissues from FRDA patients collected immediately after death and flash frozen for storage. Possible difficulties would be represented by the poor availability of FRDA tissues, inevitable post-mortem changes and advanced stage of the disease at the time of the patients' death.

An alternative is the use of the mouse models, especially of the knockin/knockout mice (Miranda et al. 2002) that mimic the genetic and biochemical features of the human disease. The ease of sample collection and increased sample size represent definite advantages over human tissues. However, the main benefit that the use of mouse models

brings, is the ability to sample tissues at every stage of FRDA, not only in terminal states and to examine MtFt mRNA levels.

7.2 RS-XRF is an Ideal Synchrotron Technique to Localize Metals in Tissue Slices and Characterize Disease Induced Disturbances in Metal Distribution and Quantity

Not only iron, but also copper and zinc can cause metal-catalyzed oxidative damage, protein aggregation, neurotoxicity, and neurodegeneration (Cuajungco and Lees 1997; Zecca et al. 2004; Madsen and Gitlin 2007). This study is the first one to apply RS-XRF to mapping the global distribution of metals in brain and spinal cord slices. RS-XRF is a novel synchrotron technique developed and exclusively available at SSRL that can non-destructively, quantitatively and simultaneously map multiple metals in large samples on a practical time scale. I validated the use of RS-XRF to large pathology slices and demonstrated its significant advantages over analytical or histological methods in localizing and quantifying brain metals (chapter III and (Gh Popescu et al. 2009)). Unlike conventional histology sections, XRF samples do not have to be dehydrated or embedded, and therefore the same sample can be subsequently processed for histology or immunohistochemistry if desired.

I have used this technique to localize metals in the human cerebellum (chapter IV and (Popescu et al. 2009b)), a major site of neurodegeneration in FRDA and to localize and quantify metals in a case of SCA of unknown aetiology (chapter V and (Popescu et al. 2009a)). Some new and very interesting findings are the metal segmentation of the dentate nucleus, the high copper content of the olivary region and the different metal content of lesions at different stages of disease that might explain some of the contradictory results regarding the iron content of areas of FRDA neurodegeneration. Regarding the high copper content of the olivocerebellar fibres and amiculum olivae of the normal medullae, a study that employs RS-XRF, EXAFS and immunohistochemistry is underway trying to elucidate the role, the chemical form and cellular location of this copper.

Our results suggest that not only iron, but also copper and zinc may play a role in the physiopathology of neurodegeneration. In future work abnormalities of all three metals should be investigated in FRDA and other SCA of both known and unknown

aetiologies to identify possible new therapeutic targets. I have been able to map metals in a coronal section of the forebrain from a FRDA patient. This also is an ongoing study that will need more than one sample in order to obtain useful data.

RS-XRF is a new and powerful tool that makes systematic studies of brain metals practical. It can be applied to any human or animal tissue and I foresee important applications in testing whether a metal chelator designed to remove a particular metal disrupts the levels of others. Using animal models, RS-XRF also has great potential to improve our understanding of global metal metabolism and the inter-relationships between metals.

Some additional features have been or will be implemented in RS-XRF at SSRL's beamline 10-2. The ability to collect full MCA spectra, the ability to image frozen tissue slices and collect XANES spectra will promote RS-XRF as the tool of choice in mapping and speciating brain metals in situ. With rapidly advancing beamline technology at third-generation synchrotrons, it should be possible to map very large sections in a matter of a few minutes, making systematic RS-XRF studies on serial slices of whole organs practical.

RS-XRF is the ideal tool to interrogate the possible involvement of metals in FRDA pathology, not only in neurodegeneration but also in cardiac degeneration. However, since the disease is examined at a very advanced stage in the case of post-mortem formalin-fixed human specimens RS-XRF will not be able to demonstrate whether the metals are the cause or the consequence of the degenerative process. Metal maps of brains and hearts from FRDA mouse models at various stages of the disease will likely answer this dilemma.

REFERENCES

Anonymous (2005). "Snapshot: Eureka moment as X-rays slice through forgery." *Nature* 435(7040): 257.

Acquaviva, F., Castaldo, I., Filla, A., Giacchetti, M., Marmolino, D., Monticelli, A., Pinelli, M., Sacca, F. and Cocozza, S. (2008). "Recombinant human erythropoietin increases frataxin protein expression without increasing mRNA expression." *Cerebellum* 7(3): 360-5.

Acquaviva, F., De Biase, I., Nezi, L., Ruggiero, G., Tatangelo, F., Pisano, C., Monticelli, A., Garbi, C., Acquaviva, A. M. and Cocozza, S. (2005). "Extra-mitochondrial localisation of frataxin and its association with IscU1 during enterocyte-like differentiation of the human colon adenocarcinoma cell line Caco-2." *J Cell Sci* 118(Pt 17): 3917-24.

Adamec, J., Rusnak, F., Owen, W. G., Naylor, S., Benson, L. M., Gacy, A. M. and Isaya, G. (2000). "Iron-dependent self-assembly of recombinant yeast frataxin: implications for Friedreich ataxia." *Am J Hum Genet* 67(3): 549-62.

Agid, Y., Cervera, P., Hirsch, E., Javoy-Agid, F., Lehericy, S., Raisman, R. and Ruberg, M. (1989). "Biochemistry of Parkinson's disease 28 years later: a critical review." *Mov Disord* 4 Suppl 1: S126-44.

Allikmets, R., Raskind, W. H., Hutchinson, A., Schueck, N. D., Dean, M. and Koeller, D. M. (1999). "Mutation of a putative mitochondrial iron transporter gene (ABC7) in X-linked sideroblastic anemia and ataxia (XLSA/A)." *Hum Mol Genet* 8(5): 743-9.

Al-Mahdawi, S., Pinto, R. M., Ismail, O., Varshney, D., Lymperi, S., Sandi, C., Trabzuni, D. and Pook, M. (2008). "The Friedreich ataxia GAA repeat expansion mutation induces comparable epigenetic changes in human and transgenic mouse brain and heart tissues." *Hum Mol Genet* 17(5): 735-46.

Al-Mahdawi, S., Pinto, R. M., Varshney, D., Lawrence, L., Lowrie, M. B., Hughes, S., Webster, Z., Blake, J., Cooper, J. M., King, R. and Pook, M. A. (2006). "GAA repeat expansion mutation mouse models of Friedreich ataxia exhibit oxidative stress leading to progressive neuronal and cardiac pathology." *Genomics* 88(5): 580-90.

Anderson, P. R., Kirby, K., Hilliker, A. J. and Phillips, J. P. (2005). "RNAi-mediated suppression of the mitochondrial iron chaperone, frataxin, in Drosophila." *Hum Mol Genet* 14(22): 3397-405.

Arosio, P., Ingrassia, R. and Cavadini, P. (2008). "Ferritins: A family of molecules for iron storage, antioxidation and more." *Biochim Biophys Acta*.

Babcock, M., de Silva, D., Oaks, R., Davis-Kaplan, S., Jiralerspong, S., Montermini, L., Pandolfo, M. and Kaplan, J. (1997). "Regulation of mitochondrial iron accumulation by Yfh1p, a putative homolog of frataxin." *Science* 276(5319): 1709-12.

Baralle, M., Pastor, T., Bussani, E. and Pagani, F. (2008). "Influence of Friedreich ataxia GAA noncoding repeat expansions on pre-mRNA processing." *Am J Hum Genet* 83(1): 77-88.

Barbeau, A., Roy, M. and Paris, S. (1984). "Hair trace elements in Friedreich's disease." *Can J Neurol Sci* 11(4 Suppl): 620-2.

Bartzokis, G. (2004). "Age-related myelin breakdown: a developmental model of cognitive decline and Alzheimer's disease." *Neurobiol Aging* 25(1): 5-18; author reply 49-62.

Bartzokis, G., Beckson, M., Hance, D. B., Marx, P., Foster, J. A. and Marder, S. R. (1997). "MR evaluation of age-related increase of brain iron in young adult and older normal males." *Magn Reson Imaging* 15(1): 29-35.

Bartzokis, G., Cummings, J., Perlman, S., Hance, D. B. and Mintz, J. (1999). "Increased basal ganglia iron levels in Huntington disease." *Arch Neurol* 56(5): 569-74.

Bartzokis, G., Lu, P. H., Tishler, T. A., Fong, S. M., Oluwadara, B., Finn, J. P., Huang, D., Bordelon, Y., Mintz, J. and Perlman, S. (2007). "Myelin breakdown and iron changes in Huntington's disease: pathogenesis and treatment implications." *Neurochem Res* 32(10): 1655-64.

Bartzokis, G., Tishler, T. A., Lu, P. H., Villablanca, P., Altshuler, L. L., Carter, M., Huang, D., Edwards, N. and Mintz, J. (2007). "Brain ferritin iron may influence age- and gender-related risks of neurodegeneration." *Neurobiol Aging* 28(3): 414-23.

Becker, E. M., Greer, J. M., Ponka, P. and Richardson, D. R. (2002). "Erythroid differentiation and protoporphyrin IX down-regulate frataxin expression in Friend cells: characterization of frataxin expression compared to molecules involved in iron metabolism and hemoglobinization." *Blood* 99(10): 3813-22.

Becker, J. S., Zoriy, M. V., Pickhardt, C., Palomero-Gallagher, N. and Zilles, K. (2005). "Imaging of copper, zinc, and other elements in thin section of human brain samples (hippocampus) by laser ablation inductively coupled plasma mass spectrometry." *Anal Chem* 77(10): 3208-16.

Bencze, K. Z., Kondapalli, K. C., Cook, J. D., McMahon, S., Millan-Pacheco, C., Pastor, N. and Stemmler, T. L. (2006). "The structure and function of frataxin." *Crit Rev Biochem Mol Biol* 41(5): 269-91.

Bencze, K. Z., Yoon, T., Millan-Pacheco, C., Bradley, P. B., Pastor, N., Cowan, J. A. and Stemmler, T. L. (2007). "Human frataxin: iron and ferrochelatase binding surface." *Chem Commun (Camb)*(18): 1798-800.

Berciano, J., Pascual, J. and Polo, J. M. (2000). History of Ataxia Research. Handbook of Ataxia Disorder. Klockgether, T. New York, *Marcel Dekker, INC.*: 77-100.

Bergmann, U. (2007). "Archimedes brought to light." *Physics World* 20: 39-42.

Bhidayasiri, R., Perlman, S. L., Pulst, S. M. and Geschwind, D. H. (2005). "Late-onset Friedreich ataxia: phenotypic analysis, magnetic resonance imaging findings, and review of the literature." *Arch Neurol* 62(12): 1865-9.

Bidichandani, S. I., Ashizawa, T. and Patel, P. I. (1998). "The GAA triplet-repeat expansion in Friedreich ataxia interferes with transcription and may be associated with an unusual DNA structure." *Am J Hum Genet* 62(1): 111-21.

Blumenfeld, H. (2002). Cerebellum. Neuroanatmy Through Clinical Cases. Sunderland, *Sinauer Associates, Inc.*: 652-687.

Blumenfeld, H. (2002). Corticospinal Tract and Other Motor Pathways. Neuroanatomy Through Clinical Cases. Sunderland, *Sinauer Associates, Inc.*: 212-261.

Blumenfeld, H. (2002). Somatosensory Pathways. Neuroanatomy Through Clinical Cases. Sunderlan, *Sinauer Associates, Inc.*: 262-301.

Boddaert, N., Le Quan Sang, K. H., Rotig, A., Leroy-Willig, A., Gallet, S., Brunelle, F., Sidi, D., Thalabard, J. C., Munnich, A. and Cabantchik, Z. I. (2007). "Selective

iron chelation in Friedreich ataxia: biologic and clinical implications." *Blood* 110(1): 401-8.

Boesch, S., Sturm, B., Hering, S., Goldenberg, H., Poewe, W. and Scheiber-Mojdehkar, B. (2007). "Friedreich's ataxia: clinical pilot trial with recombinant human erythropoietin." *Ann Neurol* 62(5): 521-4.

Bottomley, S. S. and Muller-Eberhard, U. (1988). "Pathophysiology of heme synthesis." *Semin Hematol* 25(4): 282-302.

Bou-Abdallah, F., Santambrogio, P., Levi, S., Arosio, P. and Chasteen, N. D. (2005). "Unique iron binding and oxidation properties of human mitochondrial ferritin: a comparative analysis with Human H-chain ferritin." *J Mol Biol* 347(3): 543-54.

Bowling, A. C., Schulz, J. B., Brown, R. H., Jr. and Beal, M. F. (1993). "Superoxide dismutase activity, oxidative damage, and mitochondrial energy metabolism in familial and sporadic amyotrophic lateral sclerosis." *J Neurochem* 61(6): 2322-5.

Bradford, M. M. (1976). "A rapid and sensitive method for the quantitation of microgram quantities of protein utilizing the principle of protein-dye binding." *Anal Biochem* 72: 248-54.

Bradley, J. L., Blake, J. C., Chamberlain, S., Thomas, P. K., Cooper, J. M. and Schapira, A. H. (2000). "Clinical, biochemical and molecular genetic correlations in Friedreich's ataxia." *Hum Mol Genet* 9(2): 275-82.

Branda, S. S., Cavadini, P., Adamec, J., Kalousek, F., Taroni, F. and Isaya, G. (1999). "Yeast and human frataxin are processed to mature form in two sequential steps by the mitochondrial processing peptidase." *J Biol Chem* 274(32): 22763-9.

Brody, H. (1960). "The deposition of aging pigment in the human cerebral cortex." *J Gerontol* 15: 258-61.

Brun, A. and Englund, E. (1986). "A white matter disorder in dementia of the Alzheimer type: a pathoanatomical study." *Ann Neurol* 19(3): 253-62.

Bürk, K. and Dichgans, J. (2000). Spinocerebellar Ataxia Type 2. Handbook of Ataxia Disorders. Klockgether, T. New York, *Marcel Dekker, Inc.*: 363-384.

Bulteau, A. L., Lundberg, K. C., Ikeda-Saito, M., Isaya, G. and Szweda, L. I. (2005). "Reversible redox-dependent modulation of mitochondrial aconitase and

proteolytic activity during *in vivo* cardiac ischemia/reperfusion." *Proc Natl Acad Sci U S A* 102(17): 5987-91.

Bulteau, A. L., O'Neill, H. A., Kennedy, M. C., Ikeda-Saito, M., Isaya, G. and Szweda, L. I. (2004). "Frataxin acts as an iron chaperone protein to modulate mitochondrial aconitase activity." *Science* 305(5681): 242-5.

Bush, A. I. (2000). "Metals and neuroscience." *Curr Opin Chem Biol* 4(2): 184-91.

Bush, V. J., Moyer, T. P., Batts, K. P. and Parisi, J. E. (1995). "Essential and toxic element concentrations in fresh and formalin-fixed human autopsy tissues." *Clin Chem* 41(2): 284-94.

Byers, R. K., Gilles, F. H. and Fung, C. (1973). "Huntington's disease in children. Neuropathologic study of four cases." *Neurology* 23(6): 561-9.

Campanella, A., Isaya, G., O'Neill, H. A., Santambrogio, P., Cozzi, A., Arosio, P. and Levi, S. (2004). "The expression of human mitochondrial ferritin rescues respiratory function in frataxin-deficient yeast." *Hum Mol Genet* 13(19): 2279-88.

Campanella, A., Rovelli, E., Santambrogio, P., Cozzi, A., Taroni, F. and Levi, S. (2009). "Mitochondrial ferritin limits oxidative damage regulating mitochondrial iron availability: hypothesis for a protective role in Friedreich ataxia." *Hum Mol Genet* 18(1): 1-11.

Campuzano, V., Montermini, L., Lutz, Y., Cova, L., Hindelang, C., Jiralerspong, S., Trottier, Y., Kish, S. J., Faucheux, B., Trouillas, P., Authier, F. J., Durr, A., Mandel, J. L., Vescovi, A., Pandolfo, M. and Koenig, M. (1997). "Frataxin is reduced in Friedreich ataxia patients and is associated with mitochondrial membranes." *Hum Mol Genet* 6(11): 1771-80.

Campuzano, V., Montermini, L., Molto, M. D., Pianese, L., Cossee, M., Cavalcanti, F., Monros, E., Rodius, F., Duclos, F., Monticelli, A., Zara, F., Canizares, J., Koutnikova, H., Bidichandani, S. I., Gellera, C., Brice, A., Trouillas, P., De Michele, G., Filla, A., De Frutos, R., Palau, F., Patel, P. I., Di Donato, S., Mandel, J. L., Cocozza, S., Koenig, M. and Pandolfo, M. (1996). "Friedreich's ataxia: autosomal recessive disease caused by an intronic GAA triplet repeat expansion." *Science* 271(5254): 1423-7.

Castaldo, I., Pinelli, M., Monticelli, A., Acquaviva, F., Giacchetti, M., Filla, A., Sacchetti, S., Keller, S., Avvedimento, V. E., Chiariotti, L. and Cocozza, S. (2008). "DNA methylation in intron 1 of the frataxin gene is related to GAA repeat length and age of onset in Friedreich ataxia patients." *J Med Genet* 45(12): 808-12.

Cavadini, P., Adamec, J., Taroni, F., Gakh, O. and Isaya, G. (2000). "Two-step processing of human frataxin by mitochondrial processing peptidase. Precursor and intermediate forms are cleaved at different rates." *J Biol Chem* 275(52): 41469-75.

Cavadini, P., O'Neill, H. A., Benada, O. and Isaya, G. (2002). "Assembly and iron-binding properties of human frataxin, the protein deficient in Friedreich ataxia." *Hum Mol Genet* 11(3): 217-27.

Cazzola, M., Invernizzi, R., Bergamaschi, G., Levi, S., Corsi, B., Travaglino, E., Rolandi, V., Biasiotto, G., Drysdale, J. and Arosio, P. (2003). "Mitochondrial ferritin expression in erythroid cells from patients with sideroblastic anemia." *Blood* 101(5): 1996-2000.

Chamberlain, S., Shaw, J., Rowland, A., Wallis, J., South, S., Nakamura, Y., von Gabain, A., Farrall, M. and Williamson, R. (1988). "Mapping of mutation causing Friedreich's ataxia to human chromosome 9." *Nature* 334(6179): 248-50.

Chandramouli, K., Unciuleac, M. C., Naik, S., Dean, D. R., Huynh, B. H. and Johnson, M. K. (2007). "Formation and properties of [4Fe-4S] clusters on the IscU scaffold protein." *Biochemistry* 46(23): 6804-11.

Chan-Palay, V. (1977). Cerebellar Dentate Nucleus: Organization, Cytology and Transmitters. Berlin, Springer-Verlag.

Chantrel-Groussard, K., Geromel, V., Puccio, H., Koenig, M., Munnich, A., Rotig, A. and Rustin, P. (2001). "Disabled early recruitment of antioxidant defenses in Friedreich's ataxia." *Hum Mol Genet* 10(19): 2061-7.

Chen, O. S., Crisp, R. J., Valachovic, M., Bard, M., Winge, D. R. and Kaplan, J. (2004). "Transcription of the yeast iron regulon does not respond directly to iron but rather to iron-sulfur cluster biosynthesis." *J Biol Chem* 279(28): 29513-8.

Chen, O. S., Hemenway, S. and Kaplan, J. (2002). "Genetic analysis of iron citrate toxicity in yeast: implications for mammalian iron homeostasis." *Proc Natl Acad Sci U S A* 99(26): 16922-7.

Chen, O. S., Hemenway, S. and Kaplan, J. (2002). "Inhibition of Fe-S cluster biosynthesis decreases mitochondrial iron export: evidence that Yfh1p affects Fe-S cluster synthesis." *Proc Natl Acad Sci U S A* 99(19): 12321-6.

Chiffelle, T. L. and Putt, F. A. (1951). "Propylene and ethylene glycol as solvents for Sudan IV and Sudan black B." *Stain Technol* 26(1): 51-6.

Chua-anusorn, W., Webb, J., Macey, D. J., Pootrakul, P. and St Pierre, T. G. (1997). "The effect of histological processing on the form of iron in iron-loaded human tissues." *Biochim Biophys Acta* 1360(3): 255-61.

Chung, M. C. (1985). "A specific iron stain for iron-binding proteins in polyacrylamide gels: application to transferrin and lactoferrin." *Anal Biochem* 148(2): 498-502.

Clark, R. M., De Biase, I., Malykhina, A. P., Al-Mahdawi, S., Pook, M. and Bidichandani, S. I. (2007). "The GAA triplet-repeat is unstable in the context of the human FXN locus and displays age-dependent expansions in cerebellum and DRG in a transgenic mouse model." *Hum Genet* 120(5): 633-40.

Collingwood, J. and Dobson, J. (2006). "Mapping and characterization of iron compounds in Alzheimer's tissue." *J Alzheimers Dis* 10(2-3): 215-22.

Collingwood, J. F., Mikhaylova, A., Davidson, M., Batich, C., Streit, W. J., Terry, J. and Dobson, J. (2005). "In situ characterization and mapping of iron compounds in Alzheimer's disease tissue." *J Alzheimers Dis* 7(4): 267-72.

Condo, I., Ventura, N., Malisan, F., Tomassini, B. and Testi, R. (2006). "A pool of extramitochondrial frataxin that promotes cell survival." *J Biol Chem* 281(24): 16750-6.

Connor, J. R. and Menzies, S. L. (1996). "Relationship of iron to oligodendrocytes and myelination." *Glia* 17(2): 83-93.

Coppola, G., De Michele, G., Cavalcanti, F., Pianese, L., Perretti, A., Santoro, L., Vita, G., Toscano, A., Amboni, M., Grimaldi, G., Salvatore, E., Caruso, G. and Filla, A. (1999). "Why do some Friedreich's ataxia patients retain tendon reflexes? A clinical, neurophysiological and molecular study." *J Neurol* 246(5): 353-7.

Corben, L. A., Georgiou-Karistianis, N., Fahey, M. C., Storey, E., Churchyard, A., Horne, M., Bradshaw, J. L. and Delatycki, M. B. (2006). "Towards an understanding of cognitive function in Friedreich ataxia." *Brain Res Bull* 70(3): 197-202.

Corsi, B., Cozzi, A., Arosio, P., Drysdale, J., Santambrogio, P., Campanella, A., Biasiotto, G., Albertini, A. and Levi, S. (2002). "Human mitochondrial ferritin expressed in HeLa cells incorporates iron and affects cellular iron metabolism." *J Biol Chem* 277(25): 22430-7.

Cossee, M., Campuzano, V., Koutnikova, H., Fischbeck, K., Mandel, J. L., Koenig, M., Bidichandani, S. I., Patel, P. I., Molte, M. D., Canizares, J., De Frutos, R., Pianese, L., Cavalcanti, F., Monticelli, A., Cocozza, S., Montermini, L. and Pandolfo, M. (1997). "Frataxin fracas." *Nat Genet* 15(4): 337-8.

Cossee, M., Durr, A., Schmitt, M., Dahl, N., Trouillas, P., Allinson, P., Kostrzewa, M., Nivelon-Chevallier, A., Gustavson, K. H., Kohlschutter, A., Muller, U., Mandel, J. L., Brice, A., Koenig, M., Cavalcanti, F., Tammaro, A., De Michele, G., Filla, A., Cocozza, S., Labuda, M., Montermini, L., Poirier, J. and Pandolfo, M. (1999). "Friedreich's ataxia: point mutations and clinical presentation of compound heterozygotes." *Ann Neurol* 45(2): 200-6.

Cossee, M., Puccio, H., Gansmuller, A., Koutnikova, H., Dierich, A., LeMeur, M., Fischbeck, K., Dolle, P. and Koenig, M. (2000). "Inactivation of the Friedreich ataxia mouse gene leads to early embryonic lethality without iron accumulation." *Hum Mol Genet* 9(8): 1219-26.

Cowley, J. M., Janney, D. E., Gerkin, R. C. and Buseck, P. R. (2000). "The structure of ferritin cores determined by electron nanodiffraction." *J Struct Biol* 131(3): 210-6.

Cramer, S. P., Trench, O., Yocum, M. and George, G. N. (1988). "A 13-element Ge detector for fluorescence EXAFS." *Nucl. Instrum. Methods Phys. Red.*(266): 586-591.

Cuajungco, M. P. and Lees, G. J. (1997). "Zinc metabolism in the brain: relevance to human neurodegenerative disorders." *Neurobiol Dis* 4(3-4): 137-69.

Danscher, G., Howell, G., Perez-Clausell, J. and Hertel, N. (1985). "The dithizone, Timm's sulphide silver and the selenium methods demonstrate a chelatable pool

of zinc in CNS. A proton activation (PIXE) analysis of carbon tetrachloride extracts from rat brains and spinal cords intravitally treated with dithizone." *Histochemistry* 83(5): 419-22.

De Michele, G., Di Salle, F., Filla, A., D'Alessio, G., Ambrosio, G., Viscardi, L., Scala, R. and Campanella, G. (1995). "Magnetic resonance imaging in "typical" and "late onset" Friedreich's disease and early onset cerebellar ataxia with retained tendon reflexes." *Ital J Neurol Sci* 16(5): 303-8.

De Michele, G., Filla, A., Cavalcanti, F., Di Maio, L., Pianese, L., Castaldo, I., Calabrese, O., Monticelli, A., Varrone, S., Campanella, G. and et al. (1994). "Late onset Friedreich's disease: clinical features and mapping of mutation to the FRDA locus." *J Neurol Neurosurg Psychiatry* 57(8): 977-9.

Delatycki, M. B., Camakaris, J., Brooks, H., Evans-Whipp, T., Thorburn, D. R., Williamson, R. and Forrest, S. M. (1999). "Direct evidence that mitochondrial iron accumulation occurs in Friedreich ataxia." *Ann Neurol* 45(5): 673-5.

Desmyter, L., Dewaele, S., Reekmans, R., Nystrom, T., Contreras, R. and Chen, C. (2004). "Expression of the human ferritin light chain in a frataxin mutant yeast affects ageing and cell death." *Exp Gerontol* 39(5): 707-15.

Dexter, D. T., Carayon, A., Javoy-Agid, F., Agid, Y., Wells, F. R., Daniel, S. E., Lees, A. J., Jenner, P. and Marsden, C. D. (1991). "Alterations in the levels of iron, ferritin and other trace metals in Parkinson's disease and other neurodegenerative diseases affecting the basal ganglia." *Brain* 114 (Pt 4): 1953-75.

Dexter, D. T., Jenner, P., Schapira, A. H. and Marsden, C. D. (1992). "Alterations in levels of iron, ferritin, and other trace metals in neurodegenerative diseases affecting the basal ganglia. The Royal Kings and Queens Parkinson's Disease Research Group." *Ann Neurol* 32 Suppl: S94-100.

Dexter, D. T., Sian, J., Jenner, P. and Marsden, C. D. (1993). "Implications of alterations in trace element levels in brain in Parkinson's disease and other neurological disorders affecting the basal ganglia." *Adv Neurol* 60: 273-81.

Dexter, D. T., Wells, F. R., Agid, F., Agid, Y., Lees, A. J., Jenner, P. and Marsden, C. D. (1987). "Increased nigral iron content in postmortem parkinsonian brain." *Lancet* 2(8569): 1219-20.

Dexter, D. T., Wells, F. R., Lees, A. J., Agid, F., Agid, Y., Jenner, P. and Marsden, C. D. (1989). "Increased nigral iron content and alterations in other metal ions occurring in brain in Parkinson's disease." *J Neurochem* 52(6): 1830-6.

Dhe-Paganon, S., Shigeta, R., Chi, Y. I., Ristow, M. and Shoelson, S. E. (2000). "Crystal structure of human frataxin." *J Biol Chem* 275(40): 30753-6.

Dick, F. D., De Palma, G., Ahmadi, A., Scott, N. W., Prescott, G. J., Bennett, J., Semple, S., Dick, S., Counsell, C., Mozzoni, P., Haites, N., Wettinger, S. B., Mutti, A., Otelea, M., Seaton, A., Soderkvist, P. and Felice, A. (2007). "Environmental risk factors for Parkinson's disease and parkinsonism: the Geoparkinson study." *Occup Environ Med* 64(10): 666-72.

Dickson, D. W., Lin, W., Liu, W. K. and Yen, S. H. (1999). "Multiple system atrophy: a sporadic synucleinopathy." *Brain Pathol* 9(4): 721-32.

Dilmanian, F. A., Morris, G. M., Le Duc, G., Huang, X., Ren, B., Bacarian, T., Allen, J. C., Kalef-Ezra, J., Orion, I., Rosen, E. M., Sandhu, T., Sathe, P., Wu, X. Y., Zhong, Z. and Shivaprasad, H. L. (2001). "Response of avian embryonic brain to spatially segmented x-ray microbeams." *Cell Mol Biol (Noisy-le-grand)* 47(3): 485-93.

Drayer, B. P. (1988). "Imaging of the aging brain. Part I. Normal findings." *Radiology* 166(3): 785-96.

Drysdale, J., Arosio, P., Invernizzi, R., Cazzola, M., Volz, A., Corsi, B., Biasiotto, G. and Levi, S. (2002). "Mitochondrial ferritin: a new player in iron metabolism." *Blood Cells Mol Dis* 29(3): 376-83.

Duby, G., Foury, F., Ramazzotti, A., Herrmann, J. and Lutz, T. (2002). "A non-essential function for yeast frataxin in iron-sulfur cluster assembly." *Hum Mol Genet* 11(21): 2635-43.

Duflou, H., Maenhaut, W. and De Reuck, J. (1989). "Regional distribution of potassium, calcium, and six trace elements in normal human brain." *Neurochem Res* 14(11): 1099-112.

Dum, R. P. and Strick, P. L. (2003). "An unfolded map of the cerebellar dentate nucleus and its projections to the cerebral cortex." *J Neurophysiol* 89(1): 634-9.

Durr, A., Cossee, M., Agid, Y., Campuzano, V., Mignard, C., Penet, C., Mandel, J. L., Brice, A. and Koenig, M. (1996). "Clinical and genetic abnormalities in patients with Friedreich's ataxia." *N Engl J Med* 335(16): 1169-75.

Durr, A., Smadja, D., Cancel, G., Lezin, A., Stevanin, G., Mikol, J., Bellance, R., Buisson, G. G., Chneiweiss, H., Dellanave, J. and et al. (1995). "Autosomal dominant cerebellar ataxia type I in Martinique (French West Indies). Clinical and neuropathological analysis of 53 patients from three unrelated SCA2 families." *Brain* 118 (Pt 6): 1573-81.

Elgin, S. C. and Grewal, S. I. (2003). "Heterochromatin: silence is golden." *Curr Biol* 13(23): R895-8.

El-Osta, A. and Wolffe, A. P. (2000). "DNA methylation and histone deacetylation in the control of gene expression: basic biochemistry to human development and disease." *Gene Expr* 9(1-2): 63-75.

Emond, M., Lepage, G., Vanasse, M. and Pandolfo, M. (2000). "Increased levels of plasma malondialdehyde in Friedreich ataxia." *Neurology* 55(11): 1752-3.

Estrada, R., Galarraga, J., Orozco, G., Nodarse, A. and Auburger, G. (1999). "Spinocerebellar ataxia 2 (SCA2): morphometric analyses in 11 autopsies." *Acta Neuropathol* 97(3): 306-10.

Fatterpekar, G. M., Naidich, T. P., Delman, B. N., Aguinaldo, J. G., Gultekin, S. H., Sherwood, C. C., Hof, P. R., Drayer, B. P. and Fayad, Z. A. (2002). "Cytoarchitecture of the human cerebral cortex: MR microscopy of excised specimens at 9.4 Tesla." *AJNR Am J Neuroradiol* 23(8): 1313-21.

Faucheux, B. A., Bonnet, A. M., Agid, Y. and Hirsch, E. C. (1999). "Blood vessels change in the mesencephalon of patients with Parkinson's disease." *Lancet* 353(9157): 981-2.

Ferenci, P., Steindl-Munda, P., Vogel, W., Jessner, W., Gschwantler, M., Stauber, R., Datz, C., Hackl, F., Wrba, F., Bauer, P. and Lorenz, O. (2005). "Diagnostic value of quantitative hepatic copper determination in patients with Wilson's Disease." *Clin Gastroenterol Hepatol* 3(8): 811-8.

Filla, A., De Michele, G., Cavalcanti, F., Pianese, L., Monticelli, A., Campanella, G. and Cocozza, S. (1996). "The relationship between trinucleotide (GAA) repeat length and clinical features in Friedreich ataxia." *Am J Hum Genet* 59(3): 554-60.

Finefrock, A. E., Bush, A. I. and Doraiswamy, P. M. (2003). "Current status of metals as therapeutic targets in Alzheimer's disease." *J Am Geriatr Soc* 51(8): 1143-8.

Fleming, J., Spinoulas, A., Zheng, M., Cunningham, S. C., Ginn, S. L., McQuilty, R. C., Rowe, P. B. and Alexander, I. E. (2005). "Partial correction of sensitivity to oxidant stress in Friedreich ataxia patient fibroblasts by frataxin-encoding adeno-associated virus and lentivirus vectors." *Hum Gene Ther* 16(8): 947-56.

Foury, F. and Cazzalini, O. (1997). "Deletion of the yeast homologue of the human gene associated with Friedreich's ataxia elicits iron accumulation in mitochondria." *FEBS Lett* 411(2-3): 373-7.

Foury, F. and Talibi, D. (2001). "Mitochondrial control of iron homeostasis. A genome wide analysis of gene expression in a yeast frataxin-deficient strain." *J Biol Chem* 276(11): 7762-8.

Frazzini, V., Rockabrand, E., Mocchegiani, E. and Sensi, S. L. (2006). "Oxidative stress and brain aging: is zinc the link?" *Biogerontology* 7(5-6): 307-14.

Frederickson, C. J. and Cuajungco, M. P. (2005). "Is zinc the link between compromises of brain perfusion (excitotoxicity) and Alzheimer's disease?" *J Alzheimers Dis* 8(2): 155-60; discussion 209-15.

Fujita, R., Agid, Y., Trouillas, P., Seck, A., Tommasi-Davenas, C., Driesel, A. J., Olek, K., Grzeschik, K. H., Nakamura, Y., Mandel, J. L. and et al. (1989). "Confirmation of linkage of Friedreich ataxia to chromosome 9 and identification of a new closely linked marker." *Genomics* 4(1): 110-1.

Gakh, O., Adamec, J., Gacy, A. M., Twesten, R. D., Owen, W. G. and Isaya, G. (2002). "Physical evidence that yeast frataxin is an iron storage protein." *Biochemistry* 41(21): 6798-804.

Gakh, O., Park, S., Liu, G., Macomber, L., Imlay, J. A., Ferreira, G. C. and Isaya, G. (2006). "Mitochondrial iron detoxification is a primary function of frataxin that limits oxidative damage and preserves cell longevity." *Hum Mol Genet* 15(3): 467-79.

Gakh, O., Smith, D. Y. t. and Isaya, G. (2008). "Assembly of the iron-binding protein frataxin in Saccharomyces cerevisiae responds to dynamic changes in mitochondrial iron influx and stress level." *J Biol Chem* 283(46): 31500-10.

Gellein, K., Flaten, T. P., Erikson, K. M., Aschner, M. and Syversen, T. (2008). "Leaching of trace elements from biological tissue by formalin fixation." *Biol Trace Elem Res* 121(3): 221-5.

Genis, D., Matilla, T., Volpini, V., Rosell, J., Davalos, A., Ferrer, I., Molins, A. and Estivill, X. (1995). "Clinical, neuropathologic, and genetic studies of a large spinocerebellar ataxia type 1 (SCA1) kindred: (CAG)n expansion and early premonitory signs and symptoms." *Neurology* 45(1): 24-30.

Geoffroy, G., Barbeau, A., Breton, G., Lemieux, B., Aube, M., Leger, C. and Bouchard, J. P. (1976). "Clinical description and roentgenologic evaluation of patients with Friedreich's ataxia." *Can J Neurol Sci* 3(4): 279-86.

Gerber, J., Muhlenhoff, U. and Lill, R. (2003). "An interaction between frataxin and Isu1/Nfs1 that is crucial for Fe/S cluster synthesis on Isu1." *EMBO Rep* 4(9): 906-11.

Gh Popescu, B. F., George, M. J., Bergmann, U., Garachtchenko, A. V., Kelly, M. E., McCrea, R. P., Luning, K., Devon, R. M., George, G. N., Hanson, A. D., Harder, S. M., Chapman, L. D., Pickering, I. J. and Nichol, H. (2009). "Mapping metals in Parkinson's and normal brain using rapid-scanning x-ray fluorescence." *Phys Med Biol* 54(3): 651-63.

Gibson, T. J., Koonin, E. V., Musco, G., Pastore, A. and Bork, P. (1996). "Friedreich's ataxia protein: phylogenetic evidence for mitochondrial dysfunction." *Trends Neurosci* 19(11): 465-8.

Gomori, G. (1936). "Microtechnical demonstartion of iron: a criticism of its methods." *Am J Pathol* 12: 655-663.

Gonzalez-Cabo, P., Vazquez-Manrique, R. P., Garcia-Gimeno, M. A., Sanz, P. and Palau, F. (2005). "Frataxin interacts functionally with mitochondrial electron transport chain proteins." *Hum Mol Genet* 14(15): 2091-8.

Gottesfeld, J. M. (2007). "Small molecules affecting transcription in Friedreich ataxia." *Pharmacol Ther* 116(2): 236-48.

Gouw, L. G., Digre, K. B., Harris, C. P., Haines, J. H. and Ptacek, L. J. (1994). "Autosomal dominant cerebellar ataxia with retinal degeneration: clinical, neuropathologic, and genetic analysis of a large kindred." *Neurology* 44(8): 1441-7.

Grabczyk, E., Mancuso, M. and Sammarco, M. C. (2007). "A persistent RNA.DNA hybrid formed by transcription of the Friedreich ataxia triplet repeat in live bacteria, and by T7 RNAP *in vitro*." *Nucleic Acids Res* 35(16): 5351-9.

Graeber, M. B., Raivich, G. and Kreutzberg, G. W. (1989). "Increase of transferrin receptors and iron uptake in regenerating motor neurons." *J Neurosci Res* 23(3): 342-5.

Grant, R. A., Filman, D. J., Finkel, S. E., Kolter, R. and Hogle, J. M. (1998). "The crystal structure of Dps, a ferritin homolog that binds and protects DNA." *Nat Struct Biol* 5(4): 294-303.

Gray, D. A. and Woulfe, J. (2005). "Lipofuscin and aging: a matter of toxic waste." *Sci Aging Knowledge Environ* 2005(5): re1.

Greene, E., Entezam, A., Kumari, D. and Usdin, K. (2005). "Ancient repeated DNA elements and the regulation of the human frataxin promoter." *Genomics* 85(2): 221-30.

Greene, E., Mahishi, L., Entezam, A., Kumari, D. and Usdin, K. (2007). "Repeat-induced epigenetic changes in intron 1 of the frataxin gene and its consequences in Friedreich ataxia." *Nucleic Acids Res* 35(10): 3383-90.

Greenfield, J. C. (1954). Friedreich's ataxia. The spino-cerebellar degenerations. Aring, C. D. Oxford, *Blackwell Scientific Publications*: 21-34.

Greenfield, J. C. (1954). The spino-cerebellar degenerations. Oxford, Blackwell Scientific Publications.

Haacke, E. M., Cheng, N. Y., House, M. J., Liu, Q., Neelavalli, J., Ogg, R. J., Khan, A., Ayaz, M., Kirsch, W. and Obenaus, A. (2005). "Imaging iron stores in the brain using magnetic resonance imaging." *Magn Reson Imaging* 23(1): 1-25.

Hallgren, B. and Sourander, P. (1958). "The effect of age on the non-haemin iron in the human brain." *J Neurochem* 3(1): 41-51.

Halliwell, B. (2001). "Role of free radicals in the neurodegenerative diseases: therapeutic implications for antioxidant treatment." *Drugs Aging* 18(9): 685-716.

Hammans, S. R. and Kennedy, C. R. (1998). "Ataxia with isolated vitamin E deficiency presenting as mutation negative Friedreich's ataxia." *J Neurol Neurosurg Psychiatry* 64(3): 368-70.

Harding, A. E. (1981). "Friedreich's ataxia: a clinical and genetic study of 90 families with an analysis of early diagnostic criteria and intrafamilial clustering of clinical features." *Brain* 104(3): 589-620.

Harrison, P. M. and Arosio, P. (1996). "The ferritins: molecular properties, iron storage function and cellular regulation." *Biochim Biophys Acta* 1275(3): 161-203.

He, Y., Alam, S. L., Proteasa, S. V., Zhang, Y., Lesuisse, E., Dancis, A. and Stemmler, T. L. (2004). "Yeast frataxin solution structure, iron binding, and ferrochelatase interaction." *Biochemistry* 43(51): 16254-62.

Hemason, G. L. (1967). Staining Procedures. Animal Tissue Techniques. San Francisco, *W. H. Freeman & Company*: 125-35.

Henderson, R. and Schertler, G. F. (1990). "The structure of bacteriorhodopsin and its relevance to the visual opsins and other seven-helix G-protein coupled receptors." *Philos Trans R Soc Lond B Biol Sci* 326(1236): 379-89.

Henwood, A. (2003). "Current applications of orcein in histochemistry. A brief review with some new observations concerning influence of dye batch variation and aging of dye solutions on staining." *Biotech Histochem* 78(6): 303-8.

Herman, D., Jenssen, K., Burnett, R., Soragni, E., Perlman, S. L. and Gottesfeld, J. M. (2006). "Histone deacetylase inhibitors reverse gene silencing in Friedreich's ataxia." *Nat Chem Biol* 2(10): 551-8.

Hewer, R. L. (1968). "Study of fatal cases of Friedreich's ataxia." *Br Med J* 3(5619): 649-52.

Hewer, R. L. and Robinson, N. (1968). "Diabetes mellitus in Friedreich's ataxia." *J Neurol Neurosurg Psychiatry* 31(3): 226-31.

Hock, A., Demmel, U., Schicha, H., Kasperek, K. and Feinendegen, L. E. (1975). "Trace element concentration in human brain. Activation analysis of cobalt, iron,

rubidium, selenium, zinc, chromium, silver, cesium, antimony and scandium." *Brain* 98(1): 49-64.

Hsu, L. J., Sagara, Y., Arroyo, A., Rockenstein, E., Sisk, A., Mallory, M., Wong, J., Takenouchi, T., Hashimoto, M. and Masliah, E. (2000). "alpha-synuclein promotes mitochondrial deficit and oxidative stress." *Am J Pathol* 157(2): 401-10.

Hughes, J. T., Brownell, B. and Hewer, R. L. (1968). "The peripheral sensory pathway in friedreich's ataxia. An examination by light and electron microscopy of the posterior nerve roots, posterior root ganglia, and peripheral sensory nerves in cases of friedreich's ataxia." *Brain* 91(4): 803-18.

Huxtable, R. J., Johnson, P. and Lippincott, S. E. (1984). "Free amino acids and calcium, magnesium and zinc levels in Friedreich's ataxia." *Can J Neurol Sci* 11(4 Suppl): 616-9.

Ibanez, M. L., Russell, W. O., Chang, J. P. and Speece, A. J. (1960). "Cold chamber frozen sections for operating room diagnosis and routine surgical pathology." *Lab Invest* 9: 98-109.

Ilari, A., Latella, M. C., Ceci, P., Ribacchi, F., Su, M., Giangiacomo, L., Stefanini, S., Chasteen, N. D. and Chiancone, E. (2005). "The unusual intersubunit ferroxidase center of Listeria innocua Dps is required for hydrogen peroxide detoxification but not for iron uptake. A study with site-specific mutants." *Biochemistry* 44(15): 5579-87.

Isaya, G., O'Neill, H. A., Gakh, O., Park, S., Mantcheva, R. and Mooney, S. M. (2004). "Functional studies of frataxin." *Acta Paediatr Suppl* 93(445): 68-71; discussion 72-3.

Ishihara, R., Ide-Ektessabi, A., Ikeda, K., Mizuno, Y., Fujisawa, S., Takeuchi, T. and Ohta, T. (2002). "Investigation of cellular metallic elements in single neurons of human brain tissues." *Neuroreport* 13(14): 1817-20.

Jauslin, M. L., Meier, T., Smith, R. A. and Murphy, M. P. (2003). "Mitochondria-targeted antioxidants protect Friedreich Ataxia fibroblasts from endogenous oxidative stress more effectively than untargeted antioxidants." *Faseb J* 17(13): 1972-4.

Javoy-Agid, F., Ruberg, M., Taquet, H., Bokobza, B., Agid, Y., Gaspar, P., Berger, B., N'Guyen-Legros, J., Alvarez, C., Gray, F. and et al. (1984). "Biochemical neuropathology of Parkinson's disease." *Adv Neurol* 40: 189-98.

Jellinger, K., Paulus, W., Grundke-Iqbal, I., Riederer, P. and Youdim, M. B. (1990). "Brain iron and ferritin in Parkinson's and Alzheimer's diseases." *J Neural Transm Park Dis Dement Sect* 2(4): 327-40.

Jiralerspong, S., Ge, B., Hudson, T. J. and Pandolfo, M. (2001). "Manganese superoxide dismutase induction by iron is impaired in Friedreich ataxia cells." *FEBS Lett* 509(1): 101-5.

Jiralerspong, S., Liu, Y., Montermini, L., Stifani, S. and Pandolfo, M. (1997). "Frataxin shows developmentally regulated tissue-specific expression in the mouse embryo." *Neurobiol Dis* 4(2): 103-13.

Johnson, D. C., Dean, D. R., Smith, A. D. and Johnson, M. K. (2005). "Structure, function, and formation of biological iron-sulfur clusters." *Annu Rev Biochem* 74: 247-81.

Kaplan, J. (2002). "Spinocerebellar ataxias due to mitochondrial defects." *Neurochem Int* 40(6): 553-7.

Karlberg, T., Schagerlof, U., Gakh, O., Park, S., Ryde, U., Lindahl, M., Leath, K., Garman, E., Isaya, G. and Al-Karadaghi, S. (2006). "The structures of frataxin oligomers reveal the mechanism for the delivery and detoxification of iron." *Structure* 14(10): 1535-46.

Karthikeyan, G., Santos, J. H., Graziewicz, M. A., Copeland, W. C., Isaya, G., Van Houten, B. and Resnick, M. A. (2003). "Reduction in frataxin causes progressive accumulation of mitochondrial damage." *Hum Mol Genet* 12(24): 3331-42.

Kawas, C. H. and Brookmeyer, R. (2001). "Aging and the public health effects of dementia." *N Engl J Med* 344(15): 1160-1.

Klausner, R. D. and Rouault, T. A. (1993). "A double life: cytosolic aconitase as a regulatory RNA binding protein." *Mol Biol Cell* 4(1): 1-5.

Klockgether, T. (2000). "Recent advances in degenerative ataxias." *Curr Opin Neurol* 13(4): 451-5.

Klockgether, T., Petersen, D., Grodd, W. and Dichgans, J. (1991). "Early onset cerebellar ataxia with retained tendon reflexes. Clinical, electrophysiological and MRI observations in comparison with Friedreich's ataxia." *Brain* 114 (Pt 4): 1559-73.

Kluver, H. and Barrera, E. (1953). "A method for the combined staining of cells and fibers in the nervous system." *J Neuropathol Exp Neurol* 12(4): 400-3.

Koenig, M. (2000). Ataxia with Isolated Vitamin E Deficiency. Handbook of Ataxia Disorders. Klockgether, T. New york, *Marcel Dekker, Inc.*: 223-234.

Koeppen, A. H., Michael, S. C., Knutson, M. D., Haile, D. J., Qian, J., Levi, S., Santambrogio, P., Garrick, M. D. and Lamarche, J. B. (2007). "The dentate nucleus in Friedreich's ataxia: the role of iron-responsive proteins." *Acta Neuropathol* 114(2): 163-73.

Koga, M., Tsutsumi, A. and Shirabe, T. (1997). "The pathogenesis of olivary changes in clioquinol intoxication." *Neuropathology* 17: 290-294.

Koutnikova, H., Campuzano, V., Foury, F., Dolle, P., Cazzalini, O. and Koenig, M. (1997). "Studies of human, mouse and yeast homologues indicate a mitochondrial function for frataxin." *Nat Genet* 16(4): 345-51.

Kratz, A., Pesce, M. A. and Fink, D. J. (2008). Appendix: Clinical Chemistry and Immunology. Harrison's Principles of Internal Medicine. Fauci, A. S., Braunwald, E., Kasper, D. L.et al. New York, *McGraw Hill Medicine*: A1-A16.

Kursula, P., Merilainen, G., Lehto, V. P. and Heape, A. M. (1999). "The small myelin-associated glycoprotein is a zinc-binding protein." *J Neurochem* 73(5): 2110-8.

Laemmli, U. K. (1970). "Cleavage of structural proteins during the assembly of the head of bacteriophage T4." *Nature* 227(5259): 680-5.

Lamarche, J. B., Cote, M. and Lemieux, B. (1980). "The cardiomyopathy of Friedreich's ataxia morphological observations in 3 cases." *Can J Neurol Sci* 7(4): 389-96.

Lamarche, J. B., Lemieux, B. and Lieu, H. B. (1984). "The neuropathology of "typical" Friedreich's ataxia in Quebec." *Can J Neurol Sci* 11(4 Suppl): 592-600.

Larnaout, A., Belal, S., Zouari, M., Feki, M., Ben Hamida, C., Goebel, H. H., Ben Hamida, M. and Hentati, F. (1997). "Friedreich's ataxia with isolated vitamin E deficiency: a neuropathological study of a Tunisian patient." *Acta Neuropathol* 8: 416-425.

Lesuisse, E., Santos, R., Matzanke, B. F., Knight, S. A., Camadro, J. M. and Dancis, A. (2003). "Iron use for haeme synthesis is under control of the yeast frataxin homologue (Yfh1)." *Hum Mol Genet* 12(8): 879-89.

Levi, S. and Arosio, P. (2004). "Mitochondrial ferritin." *Int J Biochem Cell Biol* 36(10): 1887-9.

Levi, S., Corsi, B., Bosisio, M., Invernizzi, R., Volz, A., Sanford, D., Arosio, P. and Drysdale, J. (2001). "A human mitochondrial ferritin encoded by an intronless gene." *J Biol Chem* 276(27): 24437-40.

Li, K., Besse, E. K., Ha, D., Kovtunovych, G. and Rouault, T. A. (2008). "Iron-dependent regulation of frataxin expression: implications for treatment of Friedreich ataxia." *Hum Mol Genet* 17(15): 2265-73.

Lill, R. and Muhlenhoff, U. (2005). "Iron-sulfur-protein biogenesis in eukaryotes." *Trends Biochem Sci* 30(3): 133-41.

Lill, R. and Muhlenhoff, U. (2008). "Maturation of iron-sulfur proteins in eukaryotes: mechanisms, connected processes, and diseases." *Annu Rev Biochem* 77: 669-700.

Lin, J. J. (1981). "Monoclonal antibodies against myofibrillar components of rat skeletal muscle decorate the intermediate filaments of cultured cells." *Proc Natl Acad Sci U S A* 78(4): 2335-9.

Linder, J. E. (1949). "A Simple Method of Staining the Basement Membrane of Glomerular Capillaries." *Quarterly Journal Microscopical Science, Vol.* 90(4): 427-29.

Linkous, D. H., Flinn, J. M., Koh, J. Y., Lanzirotti, A., Bertsch, P., Jones, B. F., Giblin, L. J. and Frederickson, C. J. (2007). "Evidence That the ZNT-3 Protein Controls the Total Amount of Elemental Zinc in Synaptic Vesicles." *J Histochem Cytochem*.

Llorens, J. V., Navarro, J. A., Martinez-Sebastian, M. J., Baylies, M. K., Schneuwly, S., Botella, J. A. and Molto, M. D. (2007). "Causative role of oxidative stress in a Drosophila model of Friedreich ataxia." *Faseb J* 21(2): 333-44.

Lobmayr, L., Brooks, D. G. and Wilson, R. B. (2005). "Increased IRP1 activity in Friedreich ataxia." *Gene* 354: 157-61.

Locke, M. and Huie, P. (1980). Cuticle techniques in arthropods. Ultrastructure methods in cuticle research. Miller, T. A. New York, *Springer*: 91-144.

Lodi, R., Cooper, J. M., Bradley, J. L., Manners, D., Styles, P., Taylor, D. J. and Schapira, A. H. (1999). "Deficit of *in vivo* mitochondrial ATP production in patients with Friedreich ataxia." *Proc Natl Acad Sci U S A* 96(20): 11492-5.

Lönnqvist, T., Paetau, A., Pihko, H. and Nikali, K. (2000). Infantile-Onset Spinocerebellar Ataxia. Handbook of Ataxia Disorders. Klockgether, T. New York, *Marcel Dekker, Inc.*: 293-309.

Lopez-Garcia, C., Varea, E., Palop, J. J., Nacher, J., Ramirez, C., Ponsoda, X. and Molowny, A. (2002). "Cytochemical techniques for zinc and heavy metals localization in nerve cells." *Microsc Res Tech* 56(5): 318-31.

Lu, C. and Cortopassi, G. (2007). "Frataxin knockdown causes loss of cytoplasmic iron-sulfur cluster functions, redox alterations and induction of heme transcripts." *Arch Biochem Biophys* 457(1): 111-22.

Lu, Z., Nie, G., Li, Y., Soe-Lin, S., Tao, Y., Cao, Y., Zhang, Z., Liu, N., Ponka, P. and Zhao, B. (2009). "Overexpression of Mitochondrial Ferritin Sensitizes Cells to Oxidative Stress Via an Iron-Mediated Mechanism." *Antioxid Redox Signal*.

Ludwin, S. K. and Johnson, E. S. (1981). "Evidence for a "dying-back" gliopathy in demyelinating disease." *Ann Neurol* 9(3): 301-5.

MacDonald, B. K., Cockerell, O. C., Sander, J. W. and Shorvon, S. D. (2000). "The incidence and lifetime prevalence of neurological disorders in a prospective community-based study in the UK." *Brain* 123 (Pt 4): 665-76.

Madsen, E. and Gitlin, J. D. (2007). "Copper and iron disorders of the brain." *Annu Rev Neurosci* 30: 317-37.

Maier, C. M. and Chan, P. H. (2002). "Role of superoxide dismutases in oxidative damage and neurodegenerative disorders." *Neuroscientist* 8(4): 323-34.

Mallory, F. B. (1938). Pathological Technique. Philadelphia, W. B. Saunders Company.

Margolis, G. (1959). "Senile cerebral disease: a critical survey of traditional concepts based upon observations with newer technics." *Laboratory investigation; a journal of technical methods and pathology* 8(2): 335-70.

Margolis, G. and Pickett, J. P. (1956). "New applications of the Luxol fast blue myelin stain." *Lab Invest* 5(6): 459-74.

Marmolino, D. and Acquaviva, F. (2009). "Friedreich's Ataxia: From the (GAA)(n) Repeat Mediated Silencing to New Promising Molecules for Therapy." *Cerebellum*.

Martelli, A., Wattenhofer-Donze, M., Schmucker, S., Bouvet, S., Reutenauer, L. and Puccio, H. (2007). "Frataxin is essential for extramitochondrial Fe-S cluster proteins in mammalian tissues." *Hum Mol Genet* 16(22): 2651-8.

Martin, J. J., Van Regemorter, N., Krols, L., Brucher, J. M., de Barsy, T., Szliwowski, H., Evrard, P., Ceuterick, C., Tassignon, M. J., Smet-Dieleman, H. and et al. (1994). "On an autosomal dominant form of retinal-cerebellar degeneration: an autopsy study of five patients in one family." *Acta Neuropathol* 88(4): 277-86.

Martin, W. R., Ye, F. Q. and Allen, P. S. (1998). "Increasing striatal iron content associated with normal aging." *Mov Disord* 13(2): 281-6.

Mascalchi, M., Salvi, F., Piacentini, S. and Bartolozzi, C. (1994). "Friedreich's ataxia: MR findings involving the cervical portion of the spinal cord." *AJR Am J Roentgenol* 163(1): 187-91.

McCrea, R. P., Harder, S. L., Martin, M., Buist, R. and Nichol, H. (2008). "A comparison of rapid-scanning X-ray fluorescence mapping and magnetic resonance imaging to localize brain iron distribution." *Eur J Radiol*.

McManus, J. F. A. and Mowry, R. W. (1960). Staining Methods, Histological and Histochemical. New York, Paul B. Hoebner, Inc.

Meguro, R., Asano, Y., Odagiri, S., Li, C., Iwatsuki, H. and Shoumura, K. (2007). "Nonheme-iron histochemistry for light and electron microscopy: a historical, theoretical and technical review." *Arch Histol Cytol* 70(1): 1-19.

Michael, S., Petrocine, S. V., Qian, J., Lamarche, J. B., Knutson, M. D., Garrick, M. D. and Koeppen, A. H. (2006). "Iron and iron-responsive proteins in the cardiomyopathy of Friedreich's ataxia." *Cerebellum* 5(4): 257-67.

Middleton, F. A. and Strick, P. L. (1994). "Anatomical evidence for cerebellar and basal ganglia involvement in higher cognitive function." *Science* 266(5184): 458-61.

Miller, L. M., Wang, Q., Telivala, T. P., Smith, R. J., Lanzirotti, A. and Miklossy, J. (2006). "Synchrotron-based infrared and X-ray imaging shows focalized accumulation of Cu and Zn co-localized with beta-amyloid deposits in Alzheimer's disease." *J Struct Biol* 155(1): 30-7.

Miranda, C. J., Santos, M. M., Ohshima, K., Smith, J., Li, L., Bunting, M., Cossee, M., Koenig, M., Sequeiros, J., Kaplan, J. and Pandolfo, M. (2002). "Frataxin knockin mouse." *FEBS Lett* 512(1-3): 291-7.

Miranda, C. J., Santos, M. M., Ohshima, K., Tessaro, M., Sequeiros, J. and Pandolfo, M. (2004). "Frataxin overexpressing mice." *FEBS Lett* 572(1-3): 281-8.

Miyajima, H., Kono, S., Takahashi, Y., Sugimoto, M., Sakamoto, M. and Sakai, N. (2001). "Cerebellar ataxia associated with heteroallelic ceruloplasmin gene mutation." *Neurology* 57(12): 2205-10.

Mocchegiani, E., Bertoni-Freddari, C., Marcellini, F. and Malavolta, M. (2005). "Brain, aging and neurodegeneration: role of zinc ion availability." *Prog Neurobiol* 75(6): 367-90.

Molina-Holgado, F., Hider, R. C., Gaeta, A., Williams, R. and Francis, P. (2007). "Metals ions and neurodegeneration." *Biometals* 20(3-4): 639-54.

Montermini, L., Richter, A., Morgan, K., Justice, C. M., Julien, D., Castellotti, B., Mercier, J., Poirier, J., Capozzoli, F., Bouchard, J. P., Lemieux, B., Mathieu, J., Vanasse, M., Seni, M. H., Graham, G., Andermann, F., Andermann, E., Melancon, S. B., Keats, B. J., Di Donato, S. and Pandolfo, M. (1997). "Phenotypic variability in Friedreich ataxia: role of the associated GAA triplet repeat expansion." *Ann Neurol* 41(5): 675-82.

Morgan, R. O., Naglie, G., Horrobin, D. F. and Barbeau, A. (1979). "Erythrocyte protoporphyrin levels in patients with Friedreich's and other ataxias." *Can J Neurol Sci* 6(2): 227-32.

Morris, C. M., Candy, J. M., Keith, A. B., Oakley, A. E., Taylor, G. A., Pullen, R. G., Bloxham, C. A., Gocht, A. and Edwardson, J. A. (1992). "Brain iron homeostasis." *J Inorg Biochem* 47(3-4): 257-65.

Morris, C. M., Candy, J. M., Oakley, A. E., Bloxham, C. A. and Edwardson, J. A. (1992). "Histochemical distribution of non-haem iron in the human brain." *Acta Anat (Basel)* 144(3): 235-57.

Morris, C. M. and Edwardson, J. A. (1994). "Iron histochemistry of the substantia nigra in Parkinson's disease." *Neurodegeneration* 3(4): 277-82.

Muhlenhoff, U., Gerber, J., Richhardt, N. and Lill, R. (2003). "Components involved in assembly and dislocation of iron-sulfur clusters on the scaffold protein Isu1p." *Embo J* 22(18): 4815-25.

Napier, I., Ponka, P. and Richardson, D. R. (2005). "Iron trafficking in the mitochondrion: novel pathways revealed by disease." *Blood* 105(5): 1867-74.

Nichol, H., Gakh, O., O'Neill, H. A., Pickering, I. J., Isaya, G. and George, G. N. (2003). "Structure of frataxin iron cores: an X-ray absorption spectroscopic study." *Biochemistry* 42(20): 5971-6.

Nie, G., Sheftel, A. D., Kim, S. F. and Ponka, P. (2005). "Overexpression of mitochondrial ferritin causes cytosolic iron depletion and changes cellular iron homeostasis." *Blood* 105(5): 2161-7.

Ogg, R. J., Langston, J. W., Haacke, E. M., Steen, R. G. and Taylor, J. S. (1999). "The correlation between phase shifts in gradient-echo MR images and regional brain iron concentration." *Magn Reson Imaging* 17(8): 1141-8.

O'Halloran, T. V. (1993). "Transition metals in control of gene expression." *Science* 261(5122): 715-25.

O'Halloran, T. V. and Culotta, V. C. (2000). "Metallochaperones, an intracellular shuttle service for metal ions." *J Biol Chem* 275(33): 25057-60.

Ohshima, K., Montermini, L., Wells, R. D. and Pandolfo, M. (1998). "Inhibitory effects of expanded GAA.TTC triplet repeats from intron I of the Friedreich ataxia gene on transcription and replication *in vivo*." *J Biol Chem* 273(23): 14588-95.

Okamoto, N., Wada, S., Oga, T., Kawabata, Y., Baba, Y., Habu, D., Takeda, Z. and Wada, Y. (1996). "Hereditary ceruloplasmin deficiency with hemosiderosis." *Hum Genet* 97(6): 755-8.

O'Neill, H. A., Gakh, O. and Isaya, G. (2005). "Supramolecular assemblies of human frataxin are formed via subunit-subunit interactions mediated by a non-conserved amino-terminal region." *J Mol Biol* 345(3): 433-9.

O'Neill, H. A., Gakh, O., Park, S., Cui, J., Mooney, S. M., Sampson, M., Ferreira, G. C. and Isaya, G. (2005). "Assembly of human frataxin is a mechanism for detoxifying redox-active iron." *Biochemistry* 44(2): 537-45.

Oppenheimer, D. R. (1979). "Brain lesions in Friedreich's ataxia." *Can J Neurol Sci* 6(2): 173-6.

Ornstein, L. (1964). "Disc Electrophoresis. I. Background and Theory." *Ann N Y Acad Sci* 121: 321-49.

Orr, H. T. and Klockgether, T. (2000). Spinocerebellar Ataxia 1. Handbook of Ataxia Disorders. Klockgether, T. New York, *Marcel Dekker, Inc.*: 343-361.

Ortiz, E., Pasquini, J. M., Thompson, K., Felt, B., Butkus, G., Beard, J. and Connor, J. R. (2004). "Effect of manipulation of iron storage, transport, or availability on myelin composition and brain iron content in three different animal models." *J Neurosci Res* 77(5): 681-9.

Ostrerova-Golts, N., Petrucelli, L., Hardy, J., Lee, J. M., Farer, M. and Wolozin, B. (2000). "The A53T alpha-synuclein mutation increases iron-dependent aggregation and toxicity." *J Neurosci* 20(16): 6048-54.

Pandolfo, M. (1998). "Molecular genetics and pathogenesis of Friedreich ataxia." *Neuromuscul Disord* 8(6): 409-15.

Papp, M. I., Kahn, J. E. and Lantos, P. L. (1989). "Glial cytoplasmic inclusions in the CNS of patients with multiple system atrophy (striatonigral degeneration, olivopontocerebellar atrophy and Shy-Drager syndrome)." *J Neurol Sci* 94(1-3): 79-100.

Parent, A. (1996). Cerebellum. Carpenter's human neuroanatomy. Coryell, P. Media, *Williams & Wilkins*: 583-629.

Park, S., Gakh, O., Mooney, S. M. and Isaya, G. (2002). "The ferroxidase activity of yeast frataxin." *J Biol Chem* 277(41): 38589-95.

Park, S., Gakh, O., O'Neill, H. A., Mangravita, A., Nichol, H., Ferreira, G. C. and Isaya, G. (2003). "Yeast frataxin sequentially chaperones and stores iron by coupling protein assembly with iron oxidation." *J Biol Chem* 278(33): 31340-51.

Pathology, A. F. I. o. (1957). Manual of Histologic and Special Staining Technics. Washington.

Pathology, A. F. I. o. (1960). Manual of Histologic and Special Staining Technics. New York, McGraw-Hill, Blakiston Division.

Pearce, J. M. (2004). "Friedreich's ataxia." *J Neurol Neurosurg Psychiatry* 75(5): 688.

Penkowa, M., Espejo, C., Martinez-Caceres, E. M., Montalban, X. and Hidalgo, J. (2003). "Increased demyelination and axonal damage in metallothionein I+II-deficient mice during experimental autoimmune encephalomyelitis." *Cell Mol Life Sci* 60(1): 185-97.

Penkowa, M. and Hidalgo, J. (2003). "Treatment with metallothionein prevents demyelination and axonal damage and increases oligodendrocyte precursors and tissue repair during experimental autoimmune encephalomyelitis." *J Neurosci Res* 72(5): 574-86.

Perls, M. (1867). "Nachweis von Eisenoxyd in gewissen Pigmenten." *Virchows Arch Path Anat* 39: 42-48.

Pickering, I. J., Prince, R. C., Divers, T. and George, G. N. (1998). "Sulfur K-edge X-ray absorption spectroscopy for determining the chemical speciation of sulfur in biological systems." *FEBS Lett* 441(1): 11-4.

Piemonte, F., Pastore, A., Tozzi, G., Tagliacozzi, D., Santorelli, F. M., Carrozzo, R., Casali, C., Damiano, M., Federici, G. and Bertini, E. (2001). "Glutathione in blood of patients with Friedreich's ataxia." *Eur J Clin Invest* 31(11): 1007-11.

Pilloni, L., Lecca, S., Van Eyken, P., Flore, C., Demelia, L., Pilleri, G., Nurchi, A. M., Farci, A. M., Ambu, R., Callea, F. and Faa, G. (1998). "Value of histochemical stains for copper in the diagnosis of Wilson's disease." *Histopathology* 33(1): 28-33.

Pomplun, D., Voigt, A., Schulz, T. J., Thierbach, R., Pfeiffer, A. F. and Ristow, M. (2007). "Reduced expression of mitochondrial frataxin in mice exacerbates diet-induced obesity." *Proc Natl Acad Sci U S A* 104(15): 6377-81.

Ponka, P. (1999). "Cellular iron metabolism." *Kidney Int Suppl* 69: S2-11.

Pook, M. A., Al-Mahdawi, S., Carroll, C. J., Cossee, M., Puccio, H., Lawrence, L., Clark, P., Lowrie, M. B., Bradley, J. L., Cooper, J. M., Koenig, M. and Chamberlain, S. (2001). "Rescue of the Friedreich's ataxia knockout mouse by human YAC transgenesis." *Neurogenetics* 3(4): 185-93.

Popescu, B. F., Pickering, I. J., George, G. N. and Nichol, H. (2007a). "The chemical form of mitochondrial iron in Friedreich's ataxia." *J Inorg Biochem* 101(6): 957-66.

Popescu, B. F., Belak, Z. R., Ignatyev, K., Ovsenek, N. and Nichol, H. (2007b). "Asymmetric distribution of metals in the Xenopus laevis oocyte: a synchrotron X-ray fluorescence microprobe study." *Biochem Cell Biol* 85(5): 537-42.

Popescu, B. F., Robinson, C. A., Chapman, L. D. and Nichol, H. (2009a). "Synchrotron X-ray Fluorescence Reveals Abnormal Metal Distributions in Brain and Spinal Cord in Spinocerebellar Ataxia: A Case Report." *Cerebellum* In Press (DOI 10.1007/s12311-009-0102-z)

Popescu, B. F., Robinson, C. A., Rajput, A., Rajput, A. H., Harder, S. L. and Nichol, H. (2009b). "Iron, Copper, and Zinc Distribution of the Cerebellum." *Cerebellum* 8(2): 74-9.

Priller, J., Scherzer, C. R., Faber, P. W., MacDonald, M. E. and Young, A. B. (1997). "Frataxin gene of Friedreich's ataxia is targeted to mitochondria." *Ann Neurol* 42(2): 265-9.

Prodan, C. I. and Holland, N. R. (2000). "CNS demyelination from zinc toxicity?" *Neurology* 54(8): 1705-6.

Puccio, H., Simon, D., Cossee, M., Criqui-Filipe, P., Tiziano, F., Melki, J., Hindelang, C., Matyas, R., Rustin, P. and Koenig, M. (2001). "Mouse models for Friedreich ataxia exhibit cardiomyopathy, sensory nerve defect and Fe-S enzyme deficiency followed by intramitochondrial iron deposits." *Nat Genet* 27(2): 181-6.

Quintana, C., Bellefqih, S., Laval, J. Y., Guerquin-Kern, J. L., Wu, T. D., Avila, J., Ferrer, I., Arranz, R. and Patino, C. (2006). "Study of the localization of iron, ferritin, and hemosiderin in Alzheimer's disease hippocampus by analytical microscopy at the subcellular level." *J Struct Biol* 153(1): 42-54.

Radisky, D. C., Babcock, M. C. and Kaplan, J. (1999). "The yeast frataxin homologue mediates mitochondrial iron efflux. Evidence for a mitochondrial iron cycle." *J Biol Chem* 274(8): 4497-9.

Rai, M., Soragni, E., Jenssen, K., Burnett, R., Herman, D., Coppola, G., Geschwind, D. H., Gottesfeld, J. M. and Pandolfo, M. (2008). "HDAC inhibitors correct frataxin deficiency in a Friedreich ataxia mouse model." *PLoS ONE* 3(4): e1958.

Raivich, G., Graeber, M. B., Gehrmann, J. and Kreutzberg, G. W. (1991). "Transferrin Receptor Expression and Iron Uptake in the Injured and Regenerating Rat Sciatic Nerve." *Eur J Neurosci* 3(10): 919-927.

Rajan, M. T., Jagannatha Rao, K. S., Mamatha, B. M., Rao, R. V., Shanmugavelu, P., Menon, R. B. and Pavithran, M. V. (1997). "Quantification of trace elements in normal human brain by inductively coupled plasma atomic emission spectrometry." *J Neurol Sci* 146(2): 153-66.

Ramazzotti, A., Vanmansart, V. and Foury, F. (2004). "Mitochondrial functional interactions between frataxin and Isu1p, the iron-sulfur cluster scaffold protein, in Saccharomyces cerevisiae." *FEBS Lett* 557(1-3): 215-20.

Renaud, D. L., Nichol, H. and Locke, M. (1991). "The visualization of apoferritin in the secretory pathway of vertebrate liver cells." *J Submicrosc Cytol Pathol* 23(4): 501-7.

Ricchelli, F., Fusi, P., Tortora, P., Valtorta, M., Riva, M., Tognon, G., Chieregato, K., Bolognin, S. and Zatta, P. (2007). "Destabilization of non-pathological variants of ataxin-3 by metal ions results in aggregation/fibrillogenesis." *Int J Biochem Cell Biol* 39(5): 966-77.

Ristow, M., Mulder, H., Pomplun, D., Schulz, T. J., Muller-Schmehl, K., Krause, A., Fex, M., Puccio, H., Muller, J., Isken, F., Spranger, J., Muller-Wieland, D., Magnuson, M. A., Mohlig, M., Koenig, M. and Pfeiffer, A. F. (2003). "Frataxin deficiency in pancreatic islets causes diabetes due to loss of beta cell mass." *J Clin Invest* 112(4): 527-34.

Ristow, M., Pfister, M. F., Yee, A. J., Schubert, M., Michael, L., Zhang, C. Y., Ueki, K., Michael, M. D., 2nd, Lowell, B. B. and Kahn, C. R. (2000). "Frataxin activates

mitochondrial energy conversion and oxidative phosphorylation." *Proc Natl Acad Sci U S A* 97(22): 12239-43.

Rodriguez, M., Scheithauer, B. W., Forbes, G. and Kelly, P. J. (1993). "Oligodendrocyte injury is an early event in lesions of multiple sclerosis." *Mayo Clin Proc* 68(7): 627-36.

Rossi, L., Lombardo, M. F., Ciriolo, M. R. and Rotilio, G. (2004). "Mitochondrial dysfunction in neurodegenerative diseases associated with copper imbalance." *Neurochem Res* 29(3): 493-504.

Rotig, A., de Lonlay, P., Chretien, D., Foury, F., Koenig, M., Sidi, D., Munnich, A. and Rustin, P. (1997). "Aconitase and mitochondrial iron-sulphur protein deficiency in Friedreich ataxia." *Nat Genet* 17(2): 215-7.

Rouault, T. A. and Tong, W. H. (2008). "Iron-sulfur cluster biogenesis and human disease." *Trends Genet* 24(8): 398-407.

Sakamoto, N., Chastain, P. D., Parniewski, P., Ohshima, K., Pandolfo, M., Griffith, J. D. and Wells, R. D. (1999). "Sticky DNA: self-association properties of long GAA.TTC repeats in R.R.Y triplex structures from Friedreich's ataxia." *Mol Cell* 3(4): 465-75.

Sakamoto, N., Larson, J. E., Iyer, R. R., Montermini, L., Pandolfo, M. and Wells, R. D. (2001). "GGA*TCC-interrupted triplets in long GAA*TTC repeats inhibit the formation of triplex and sticky DNA structures, alleviate transcription inhibition, and reduce genetic instabilities." *J Biol Chem* 276(29): 27178-87.

Sakamoto, N., Ohshima, K., Montermini, L., Pandolfo, M. and Wells, R. D. (2001). "Sticky DNA, a self-associated complex formed at long GAA*TTC repeats in intron 1 of the frataxin gene, inhibits transcription." *J Biol Chem* 276(29): 27171-7.

Sanchez-Casis, G., Cote, M. and Barbeau, A. (1976). "Pathology of the heart in Friedreich's ataxia: review of the literature and report of one case." *Can J Neurol Sci* 3(4): 349-54.

Santambrogio, P., Biasiotto, G., Sanvito, F., Olivieri, S., Arosio, P. and Levi, S. (2007). "Mitochondrial ferritin expression in adult mouse tissues." *J Histochem Cytochem* 55(11): 1129-37.

Santos, R., Dancis, A., Eide, D., Camadro, J. M. and Lesuisse, E. (2003). "Zinc suppresses the iron-accumulation phenotype of Saccharomyces cerevisiae lacking the yeast frataxin homologue (Yfh1)." *Biochem J* 375(Pt 2): 247-54.

Sarsero, J. P., Holloway, T. P., Li, L., McLenachan, S., Fowler, K. J., Bertoncello, I., Voullaire, L., Gazeas, S. and Ioannou, P. A. (2005). "Evaluation of an FRDA-EGFP genomic reporter assay in transgenic mice." *Mamm Genome* 16(4): 228-41.

Sarsero, J. P., Li, L., Holloway, T. P., Voullaire, L., Gazeas, S., Fowler, K. J., Kirby, D. M., Thorburn, D. R., Galle, A., Cheema, S., Koenig, M., Williamson, R. and Ioannou, P. A. (2004). "Human BAC-mediated rescue of the Friedreich ataxia knockout mutation in transgenic mice." *Mamm Genome* 15(5): 370-82.

Saveliev, A., Everett, C., Sharpe, T., Webster, Z. and Festenstein, R. (2003). "DNA triplet repeats mediate heterochromatin-protein-1-sensitive variegated gene silencing." *Nature* 422(6934): 909-13.

Schaumburg, H. and Herskovitz, S. (2008). "Copper deficiency myeloneuropathy: a clue to clioquinol-induced subacute myelo-optic neuropathy?" *Neurology* 71(9): 622-3.

Schiffer, R. B., McDermott, M. P. and Copley, C. (2001). "A multiple sclerosis cluster associated with a small, north-central Illinois community." *Arch Environ Health* 56(5): 389-95.

Schoenfeld, R. A., Napoli, E., Wong, A., Zhan, S., Reutenauer, L., Morin, D., Buckpitt, A. R., Taroni, F., Lonnerdal, B., Ristow, M., Puccio, H. and Cortopassi, G. A. (2005). "Frataxin deficiency alters heme pathway transcripts and decreases mitochondrial heme metabolites in mammalian cells." *Hum Mol Genet* 14(24): 3787-99.

Schulz, J. B., Dehmer, T., Schols, L., Mende, H., Hardt, C., Vorgerd, M., Burk, K., Matson, W., Dichgans, J., Beal, M. F. and Bogdanov, M. B. (2000). "Oxidative stress in patients with Friedreich ataxia." *Neurology* 55(11): 1719-21.

Service, R. F. (2006). "Imaging. Brilliant X-rays reveal fruits of a brilliant mind." *Science* 313(5788): 744.

Seznec, H., Simon, D., Bouton, C., Reutenauer, L., Hertzog, A., Golik, P., Procaccio, V., Patel, M., Drapier, J. C., Koenig, M. and Puccio, H. (2005). "Friedreich ataxia: the oxidative stress paradox." *Hum Mol Genet* 14(4): 463-74.

Seznec, H., Simon, D., Monassier, L., Criqui-Filipe, P., Gansmuller, A., Rustin, P., Koenig, M. and Puccio, H. (2004). "Idebenone delays the onset of cardiac functional alteration without correction of Fe-S enzymes deficit in a mouse model for Friedreich ataxia." *Hum Mol Genet* 13(10): 1017-24.

Shackelford, R. E., Manuszak, R. P., Johnson, C. D., Hellrung, D. J., Link, C. J. and Wang, S. (2004). "Iron chelators increase the resistance of Ataxia telangeictasia cells to oxidative stress." *DNA Repair (Amst)* 3(10): 1263-72.

Shackelford, R. E., Manuszak, R. P., Johnson, C. D., Hellrung, D. J., Steele, T. A., Link, C. J. and Wang, S. (2003). "Desferrioxamine treatment increases the genomic stability of Ataxia-telangiectasia cells." *DNA Repair (Amst)* 2(9): 971-81.

Shadel, G. S. (2005). "Mitochondrial DNA, aconitase 'wraps' it up." *Trends Biochem Sci* 30(6): 294-6.

Shapcott, D., Giguere, R. and Lemieux, B. (1984). "Zinc and taurine in Friedreich's ataxia." *Can J Neurol Sci* 11(4 Suppl): 623-5.

Simon, D., Seznec, H., Gansmuller, A., Carelle, N., Weber, P., Metzger, D., Rustin, P., Koenig, M. and Puccio, H. (2004). "Friedreich ataxia mouse models with progressive cerebellar and sensory ataxia reveal autophagic neurodegeneration in dorsal root ganglia." *J Neurosci* 24(8): 1987-95.

Sofic, E., Paulus, W., Jellinger, K., Riederer, P. and Youdim, M. B. (1991). "Selective increase of iron in substantia nigra zona compacta of parkinsonian brains." *J Neurochem* 56(3): 978-82.

Starosta-Rubinstein, S., Young, A. B., Kluin, K., Hill, G., Aisen, A. M., Gabrielsen, T. and Brewer, G. J. (1987). "Clinical assessment of 31 patients with Wilson's disease. Correlations with structural changes on magnetic resonance imaging." *Arch Neurol* 44(4): 365-70.

Stevanin, G., Durr, A. and Brice, A. (2000). Spinocerebellar Ataxia Type 7. Handbook of Ataxia Disorders. Klockgether, T. New York, *Marcel Dekker, Inc.*: 469-486.

Sturm, B., Bistrich, U., Schranzhofer, M., Sarsero, J. P., Rauen, U., Scheiber-Mojdehkar, B., de Groot, H., Ioannou, P. and Petrat, F. (2005). "Friedreich's ataxia, no changes in mitochondrial labile iron in human lymphoblasts and fibroblasts: a decrease in antioxidative capacity?" *J Biol Chem* 280(8): 6701-8.

Sturm, B., Stupphann, D., Kaun, C., Boesch, S., Schranzhofer, M., Wojta, J., Goldenberg, H. and Scheiber-Mojdehkar, B. (2005). "Recombinant human erythropoietin: effects on frataxin expression *in vitro*." *Eur J Clin Invest* 35(11): 711-7.

Su, M., Cavallo, S., Stefanini, S., Chiancone, E. and Chasteen, N. D. (2005). "The so-called Listeria innocua ferritin is a Dps protein. Iron incorporation, detoxification, and DNA protection properties." *Biochemistry* 44(15): 5572-8.

Tan, G., Chen, L. S., Lonnerdal, B., Gellera, C., Taroni, F. A. and Cortopassi, G. A. (2001). "Frataxin expression rescues mitochondrial dysfunctions in FRDA cells." *Hum Mol Genet* 10(19): 2099-107.

Terman, A. and Brunk, U. T. (2004). "Lipofuscin." *Int J Biochem Cell Biol* 36(8): 1400-4.

Thierbach, R., Schulz, T. J., Isken, F., Voigt, A., Mietzner, B., Drewes, G., von Kleist-Retzow, J. C., Wiesner, R. J., Magnuson, M. A., Puccio, H., Pfeiffer, A. F., Steinberg, P. and Ristow, M. (2005). "Targeted disruption of hepatic frataxin expression causes impaired mitochondrial function, decreased life span and tumor growth in mice." *Hum Mol Genet* 14(24): 3857-64.

Thomas, M. and Jankovic, J. (2004). "Neurodegenerative disease and iron storage in the brain." *Curr Opin Neurol* 17(4): 437-42.

Thompson, S. W. and Hunt, R. D. (1966). Microscopic Demonstration of Morphologic Components of Animal Tissues. Selected Histochemical and Histopathological Methods, *Charles C Thomas Publisher*: 749-873.

Thompson, S. W. and Hunt, R. D. (1966). Microscopic Histochemical Methods for the Demonstration of Lipids. Selected Histochemical and Histopathological Methods, *Charles C Thomas Publisher*: 325-369.

Todorich, B., Pasquini, J. M., Garcia, C. I., Paez, P. M. and Connor, J. R. (2008). "Oligodendrocytes and myelination: The role of iron." *Glia*.

Towbin, H., Staehelin, T. and Gordon, J. (1979). "Electrophoretic transfer of proteins from polyacrylamide gels to nitrocellulose sheets: procedure and some applications." *Proc Natl Acad Sci U S A* 76(9): 4350-4.

Tozzi, G., Nuccetelli, M., Lo Bello, M., Bernardini, S., Bellincampi, L., Ballerini, S., Gaeta, L. M., Casali, C., Pastore, A., Federici, G., Bertini, E. and Piemonte, F. (2002). "Antioxidant enzymes in blood of patients with Friedreich's ataxia." *Arch Dis Child* 86(5): 376-9.

Tsang, D., Tsang, Y. S., Ho, W. K. and Wong, R. N. (1997). "Myelin basic protein is a zinc-binding protein in brain: possible role in myelin compaction." *Neurochem Res* 22(7): 811-9.

Turnbull, S., Tabner, B. J., El-Agnaf, O. M., Moore, S., Davies, Y. and Allsop, D. (2001). "alpha-Synuclein implicated in Parkinson's disease catalyses the formation of hydrogen peroxide *in vitro*." *Free Radic Biol Med* 30(10): 1163-70.

Vazquez-Manrique, R. P., Gonzalez-Cabo, P., Ros, S., Aziz, H., Baylis, H. A. and Palau, F. (2006). "Reduction of Caenorhabditis elegans frataxin increases sensitivity to oxidative stress, reduces lifespan, and causes lethality in a mitochondrial complex II mutant." *Faseb J* 20(1): 172-4.

Waldvogel, D., van Gelderen, P. and Hallett, M. (1999). "Increased iron in the dentate nucleus of patients with Friedrich's ataxia." *Ann Neurol* 46(1): 123-5.

Ward, R. J., Legssyer, R., Henry, C. and Crichton, R. R. (2000). "Does the haemosiderin iron core determine its potential for chelation and the development of iron-induced tissue damage?" *J Inorg Biochem* 79(1-4): 311-7.

Ward, R. J., Ramsey, M., Dickson, D. P., Hunt, C., Douglas, T., Mann, S., Aquad, F., Peters, T. J. and Crichton, R. R. (1994). "Further characterisation of forms of haemosiderin in iron-overloaded tissues." *Eur J Biochem* 225(1): 187-94.

Warren, P. J., Earl, C. J. and Thompson, R. H. (1960). "The distribution of copper in human brain." *Brain* 83: 709-17.

Wessel, K., Schroth, G., Diener, H. C., Muller-Forell, W. and Dichgans, J. (1989). "Significance of MRI-confirmed atrophy of the cranial spinal cord in Friedreich's ataxia." *Eur Arch Psychiatry Neurol Sci* 238(4): 225-30.

Whitnall, M., Rahmanto, Y. S., Sutak, R., Xu, X., Becker, E. M., Mikhael, M. R., Ponka, P. and Richardson, D. R. (2008). "The MCK mouse heart model of Friedreich's ataxia: Alterations in iron-regulated proteins and cardiac hypertrophy are limited by iron chelation." *Proc Natl Acad Sci U S A* 105(28): 9757-62.

Williams, R. S., Marshall, P. C., Lott, I. T. and Caviness, V. S., Jr. (1978). "The cellular pathology of Menkes steely hair syndrome." *Neurology* 28(6): 575-83.

Wilson, R. B., Lynch, D. R., Farmer, J. M., Brooks, D. G. and Fischbeck, K. H. (2000). "Increased serum transferrin receptor concentrations in Friedreich ataxia." *Ann Neurol* 47(5): 659-61.

Wilson, R. B. and Roof, D. M. (1997). "Respiratory deficiency due to loss of mitochondrial DNA in yeast lacking the frataxin homologue." *Nat Genet* 16(4): 352-7.

Wingert, R. A., Galloway, J. L., Barut, B., Foott, H., Fraenkel, P., Axe, J. L., Weber, G. J., Dooley, K., Davidson, A. J., Schmid, B., Paw, B. H., Shaw, G. C., Kingsley, P., Palis, J., Schubert, H., Chen, O., Kaplan, J. and Zon, L. I. (2005). "Deficiency of glutaredoxin 5 reveals Fe-S clusters are required for vertebrate haem synthesis." *Nature* 436(7053): 1035-39.

Wong, A., Yang, J., Cavadini, P., Gellera, C., Lonnerdal, B., Taroni, F. and Cortopassi, G. (1999). "The Friedreich's ataxia mutation confers cellular sensitivity to oxidant stress which is rescued by chelators of iron and calcium and inhibitors of apoptosis." *Hum Mol Genet* 8(3): 425-30.

Wong, A., Yang, J., Danielson, S., Gellera, C., Taroni, F. and Cortopassi, G. (2000). "Sensitivity of FRDA lymphoblasts to salts of transition metal ions." *Antioxid Redox Signal* 2(3): 461-5.

Wullner, U., Klockgether, T., Petersen, D., Naegele, T. and Dichgans, J. (1993). "Magnetic resonance imaging in hereditary and idiopathic ataxia." *Neurology* 43(2): 318-25.

Yabe, T., Morimoto, K., Kikuchi, S., Nishio, K., Terashima, I. and Nakai, M. (2004). "The Arabidopsis chloroplastic NifU-like protein CnfU, which can act as an iron-sulfur cluster scaffold protein, is required for biogenesis of ferredoxin and photosystem I." *Plant Cell* 16(4): 993-1007.

Yamamoto, T. and Hirano, A. (1986). "A comparative study of modified Bielschowsky, Bodian and thioflavin S stains on Alzheimer's neurofibrillary tangles." *Neuropathol Appl Neurobiol* 12(1): 3-9.

Yokota, T., Uchihara, T., Kumagai, J., Shiojiri, T., Pang, J. J., Arita, M., Arai, H., Hayashi, M., Kiyosawa, M., Okeda, R. and Mizusawa, H. (2000). "Postmortem study of ataxia with retinitis pigmentosa by mutation of the alpha-tocopherol transfer protein gene." *J Neurol Neurosurg Psychiatry* 68(4): 521-5.

Yoon, T. and Cowan, J. A. (2003). "Iron-sulfur cluster biosynthesis. Characterization of frataxin as an iron donor for assembly of [2Fe-2S] clusters in ISU-type proteins." *J Am Chem Soc* 125(20): 6078-84.

Yoon, T. and Cowan, J. A. (2004). "Frataxin-mediated iron delivery to ferrochelatase in the final step of heme biosynthesis." *J Biol Chem* 279(25): 25943-6.

Yoshida, S., Ektessabi, A. and Fujisawa, S. (2001). "XANES spectroscopy of a single neuron from a patient with Parkinson's disease." *J Synchrotron Radiat* 8(Pt 2): 998-1000.

Zaleski, S. S. (1887). "Das Eisen der Organe bei Morbus maculosus Werlhoffi." *Arch Experiment Patholol Pharmacol* 23: 77-90.

Zecca, L., Stroppolo, A., Gatti, A., Tampellini, D., Toscani, M., Gallorini, M., Giaveri, G., Arosio, P., Santambrogio, P., Fariello, R. G., Karatekin, E., Kleinman, M. H., Turro, N., Hornykiewicz, O. and Zucca, F. A. (2004). "The role of iron and copper molecules in the neuronal vulnerability of locus coeruleus and substantia nigra during aging." *Proc Natl Acad Sci U S A* 101(26): 9843-8.

Zecca, L., Youdim, M. B., Riederer, P., Connor, J. R. and Crichton, R. R. (2004). "Iron, brain ageing and neurodegenerative disorders." *Nat Rev Neurosci* 5(11): 863-73.

Zhao, G., Ceci, P., Ilari, A., Giangiacomo, L., Laue, T. M., Chiancone, E. and Chasteen, N. D. (2002). "Iron and hydrogen peroxide detoxification properties of DNA-binding protein from starved cells. A ferritin-like DNA-binding protein of Escherichia coli." *J Biol Chem* 277(31): 27689-96.

Zhu, Y., Zhang, H., Bewer, B., Popescu, B. F. G., Nichol, H. and Chapman, D. (2008). "Field flatteners fabricated with a rapid prototyper for K-edge subtraction imaging

of small animals." *Nuclear Instruments and Methods in Physics Research A* 588(3): 442-447.

Appendix

Several side projects I have been involved in during my Ph.D. are listed below. Some of them resulted in publications that are not included in my Ph.D. thesis.

The first main side project has been the mapping of metals in oocytes from *Xenopus laevis* using X-ray microprobe correlated with histology. This resulted in the publication of an article regarding the assymetrical distribution of metals in stage VI *Xenopus laevis* oocytes showing that synchrotron X-ray fluorescence microprobe would be a useful tool to examine how metals accumulate and redistribute during fertilization and embryonic development (Popescu et al. 2007b). This article has been featured on the cover of Biochemistry and Cell Biology journal. Since the publication of this paper more data has been collected to publish a more ample study regarding the metal distribution in stage III to stage VI *Xenopus laevis* oocytes.

The second main side project has been my involvement with Gene Expression Mapping using Synchrotron light (GEMS). I developed the animal model used to test the filed flattener prototype developed by Dr. Chapman's team for K-edge subtraction imaging of small animals (Zhu et al. 2008). I have also been involved in culturing the C6 glioma cells and their implantation in rats, and assisting with animal handling during GEMS experiments that took place at the Canadian Light Source.

Other main side projects that I started towards the latter period of my Ph.D. degree are the mapping of metals in brains from patients with multiple sclerosis and Huntington disease, and enough data is collected to publish these findings.

Other projects that I have been involved are the determination of the chemical form of mitochondrial zinc, the chemical form of extraterrestrial iron and the chemical form of metals in various Drosophila models of human neurodegenerative diseases, Magnetic Resonance/XRF correlation, and metal mapping in stroke and peripheral and central demyelination.